University of California
Santa Barbara

Difficulties and Opportunities for Effective Field Theories of Beyond the Standard Model Physics

A dissertation submitted in partial satisfaction
of the requirements for the degree

Doctor of Philosophy
in
Physics

by

Ian Banta

Committee in charge:

Professor Nathaniel Craig, Chair
Professor Hugh Lippincott
Professor Mark Srednicki

September 2023

The Dissertation of Ian Banta is approved.

Professor Hugh Lippincott

Professor Mark Srednicki

Professor Nathaniel Craig, Committee Chair

August 2023

Difficulties and Opportunities for Effective Field Theories of Beyond the Standard Model Physics

by

Ian Banta

Acknowledgements

Thanks first and foremost to Nathaniel Craig, who has been an exemplary mentor throughout my time in grad school. He has taught me how to think about physics, how to communicate physics, and how to create a welcoming environment. He has provided exceptional support as my interests have evolved, and I could not have asked for a better advisor.

Many faculty members and other senior academics have supported me before and during graduate school and all are much appreciated. In particular, Dave Sutherland, Tim Cohen and Xiaochuan Lu have been collaborators on a program of projects over my entire grad school career and greatly enhanced my physics knowledge. Tengiz Bibilashvili and Sathya Guruswamy have provided valuable mentorship as my interest in teaching has grown. Also, my development at Williams was invaluable to my time at graduate school, with thanks especially to Dave Tucker-Smith.

My time as a graduate student has been enriched by my peers, whether they have participated directly in my physics or in various fun activities; I would not have done as well as I have without them. Special thanks in particular to David Grabovsky, Justin Berman, and Mariam Ughrelidze.

Last but not least, thanks to my family, especially my parents David and Jennifer, for all of their support.

Curriculum Vitæ

Ian Banta

Education

2023	Ph.D. in Physics, University of California, Santa Barbara.
2021	M.A. in Physics, University of California, Santa Barbara.
2019	B.A. in Physics and Computer Science, Williams College.

Publications

"Structures of Neural Network Effective Field Theories"
Ian Banta, Tianji Cai, Nathaniel Craig, Zhengkang Zhang
In review, [arXiv:2305.02334 [hep-th]] [1]

"Effective Field Theory of the Two Higgs Doublet Model"
Ian Banta, Tim Cohen, Nathaniel Craig, Xiaochuan Lu, Dave Sutherland
JHEP 06 (2023) 150, [arXiv:2304.09884 [hep-ph]] [2]

"A Strongly First-Order Electroweak Phase Transition from Loryons"
Ian Banta
JHEP 06 (2022) 099, [arXiv:2202.04608 [hep-ph]] [3]

"Non-Decoupling New Particles"
Ian Banta, Tim Cohen, Nathaniel Craig, Xiaochuan Lu, Dave Sutherland
JHEP 02 (2022) 029, [arXiv:2110.02967 [hep-ph]] [4]

"The Muon Smasher's Guide"
Hind Al Ali et al.
Rept.Prog.Phys. 85 (2022) 8, 084201, [arXiv:2103.14043 [hep-ph]] [5]

"Wall Speed and Shape in Singlet-Assisted Strong Electroweak Phase Transitions"
Avi Friedlander, Ian Banta, James M. Cline, David Tucker-Smith
Phys.Rev.D 103 (2021) 5, 055020, [arXiv:2009.14295 [hep-ph]] [6]

Abstract

Difficulties and Opportunities for Effective Field Theories of Beyond the Standard Model Physics

by

Ian Banta

In this thesis, we study some possible extensions of the Standard Model and the insight they provide into treating the Standard Model as an effective field theory. Following an introduction highlighting the uses and difficulties of effective field theory in study of the Standard Model and physics beyond the Standard Model (BSM), we first focus on Loryons, particles which acquire most of their mass from the Higgs. We explain how BSM Loryons necessitate the use of HEFT as an effective field theory description and examine the experimental viability of scalars and vector-like fermions. We then investigate how BSM Loryons could affect the electroweak phase transition and gravitational wave background. Finally, we analyze the effective field theory of the two Higgs doublet model, demonstrating the importance of choosing an appropriate flavor basis for the two doublets and introducing a new basis particularly suited to effective field theory analysis.

Contents

Chapter 1

Introduction

Since its development in the second half of the twentieth century the Standard Model of particle physics has been enormously successful, culminating in the discovery of the Higgs boson in 2012. However, there are many outstanding experimental results which are not explained by or accounted for in the Standard Model, including, e.g., neutrino masses, dark matter, dark energy, the matter-antimatter asymmetry, and gravity. We thus know there must be additional physics beyond the Standard Model.

There are two broad ways one can imagine discovering new beyond the Standard Model (BSM) physics. The most obvious would be a "smoking gun": a direct discovery of a new particle. Alternatively, we could have some flavor of indirect detection, with the new particle(s) not explicitly seen but inferred through their effect on other, known particles. Direct detection would be the more satisfying and is what we would ultimately like to achieve in order to say that we have discovered some new physics. Indeed, we could identify experimental observation of the previously highlighted issues with the Standard Model as already being indirect detection of new physics; for example, we have indirectly detected dark matter through its gravitational effects. Despite these indirect detections, we continue to search for an explanation of what exactly this BSM physics is, and to

confirm any particular explanation we would ideally make a direct detection. However, history suggests that we are much more likely to discover new physics indirectly, with direct detection only coming later, and it is thus worthwhile to make significant efforts towards indirect detection (both in the sense of actually working towards experimentally making such a detection and understanding which indirect effects we are most likely to see and thus should look for). While any particular indirect effect will not uniquely identify a particular BSM candidate, indirect observations are still useful for narrowing the space of possibilities and providing direction as to which are the most likely candidates.

To pursue indirect detection, one could imagine taking some specific model of BSM physics (henceforth referred to as a *UV model*), calculating a number of indirect signatures it would produce (e.g. how it changes various scattering cross sections between Standard Model particles), and then searching for these indirect signatures. Unless there are reasons to consider only a handful of UV models of interest, this quickly becomes infeasible given the number of possibilities. We would prefer to proceed in a more model-independent way, which is provided by effective field theory (EFT) [7].

An EFT is a quantum field theory which is only valid up to some energy cutoff Λ. It contains an infinite series of operators with higher-dimension operators suppressed by powers of Λ; thus, at energies significantly below Λ, higher-dimension operators quickly become negligible as their mass dimension increases. From a top-down perspective, it is useful for highlighting the relevant behavior of a UV theory at some low energy scale. Suppose one has a UV theory with a particle of mass M and is running experiments at an energy scale Λ, with $M \gg \Lambda$. The particle is thus too massive to be produced and will not be seen directly; however, it can still have an effect on the interactions of other particles in the theory. In order to calculate needed amplitudes and cross sections, one could just use the UV theory. However, from a practical point of view, the physics can often be better understood by integrating out the heavy particle to produce a new, effective

theory which contains only the lighter particles as degrees of freedom and has additional tree-level interactions not present in the UV theory. The infinite tower of new operators is suppressed by appropriate powers of M, and this effective theory will thus be valid up to an energy cutoff $\Lambda \approx M$. A specific example of this is the Fermi theory of beta decay. At energies below the W mass, propagating W bosons are not observed, but they can still mediate decay of a neutron to a proton, electron, and electron antineutrino. Starting with the theory of the weak interactions and then integrating out the W/Z bosons produces an effective theory with a new four-fermion interaction in the Lagrangian, the size of which is controlled by the mass of the W boson.

One can also think about an EFT from a bottom-up perspective. In this case, instead of starting with a UV theory and integrating out heavy particles, we start with a collection of low-energy degrees of freedom and add in higher-order interactions which could be mediated by some (unknown) heavy particles. For example, if we are interested in indirect detection of BSM physics, we have

$$\mathcal{L}_{\text{EFT}} = \mathcal{L}_{\text{SM}} + \sum_i \frac{C_i}{\Lambda^{p_i}} \mathcal{O}_i \,, \tag{1.1}$$

where $\mathcal{O}_i$ are various operators with mass dimension $p_i > 4$ and C_i are dimensionless coefficients. We expect the mass scale Λ, where the EFT breaks down, to be around the mass of the (unknown) heavy particles in the underlying UV theory. On the closer-to-experiment side, one can then place bounds on the EFT coefficients C_i and scale Λ; on the closer-to-models side, one can calculate from a given UV model what the EFT coefficients C_i and scale Λ are (see, e.g., [8, 9] for recent examples).

An EFT is not, however, entirely agnostic about the UV physics. Writing down the higher-dimension operators requires not just knowing the particle content of the EFT but also knowing the symmetries of the theory. It may be that the symmetries can be

copied over from the low-energy particle content, but it may also be that not all of these are good symmetries of the EFT. For example, it could be that there are some accidental symmetries of the low-energy degrees of freedom which are not preserved in the UV theory. Assuming a symmetry persists will forbid some operators on the EFT side and *a priori* rule out some UV models. For extending the Standard Model as an EFT, there are two common choices. One is to assert that the EFT obeys the full $SU(2)_L \times U(1)_Y$ electroweak symmetry of the Standard Model (there is also the $SU(3)_C$ of the strong force, but unless otherwise mentioned this will always be along for the ride). This is known as SMEFT, for Standard Model Effective Field Theory; see [10] for a review. The other is to assert that the EFT only obeys the $U(1)_{\text{em}}$ of electromagnetism, which is the unbroken portion of the symmetry at low energies; this is known most commonly as HEFT, for Higgs Effective Field Theory [11, 12, 13, 14].

Because of its more restrictive symmetry structure, SMEFT has fewer additional operators and is less complicated, and it is thus often preferred. However, not all UV models obey the full electroweak symmetry at low energies; those models which do not require the use of HEFT rather than SMEFT. In general, those models which require the use of HEFT have either (1) new particles which acquire most of their mass from electroweak symmetry breaking and the Higgs vev; or (2) an additional source of electroweak symmetry breaking beyond the Higgs vev. For a more detailed discussion of which UV models require HEFT, see [11].

In this work, we will examine UV models which may require the use of HEFT. Such models are interesting for several reasons. First, to the extent that such models remain experimentally viable, they provide support for not considering only SMEFT in EFT analyses. Next, from the other side, such models could in fact be ruled out; to require HEFT, they must intrinsically interact with the electroweak scale, and thus could be ruled out as we push the energy frontier forwards rather than merely being shifted to

higher energies (whether fine-tuned or not). If they were to be ruled out, then SMEFT could be taken as the way of treating the Standard Model as an EFT. Such models can also produce striking experimental signatures, either through deviations which are not possible in SMEFT due to its symmetry structure or through simply having a large coupling to the Higgs. For these reasons, it is useful to understand the features of such models and the proper way to treat them using effective field theory.

This work is organized as follows. In Chap. 2, we consider the case of new scalars and vector-like fermions which receive most of their mass from the Higgs ("Loryons") and determine whether such particles remain experimentally viable. Due to receiving most of their mass from the Higgs, integrating out Loryons to produce an EFT requires the use of HEFT. Since unitarity constraints prevent the coupling to the Higgs from being too large, there is an upper bound on the mass of Loryons, and they could be experimentally ruled out. In Chap. 3, we examine the effect of experimentally viable Loryons on the electroweak phase transition. Since by definition Loryons have a sizable coupling to the Higgs, they generically have a significant effect on the electroweak phase transition and could contribute to the matter-antimatter asymmetry or a gravitational wave background. In Chap. 4, we treat the two Higgs doublet model. In particular, we consider the effect of different basis choices in the UV model and the extent to which HEFT is required as the EFT description. Supplementary calculations appear in a set of appendices.

Chapter 2

Non-Decoupling New Particles

This chapter is based on work with Timothy Cohen, Nathaniel Craig, Xiaochuan Lu, and Dave Sutherland, published as [4].

Have we discovered all of the particles that acquire most of their mass from the Higgs? Thanks to decoupling, whether we have discovered all particles that acquire *any* of their mass from the Higgs is essentially unknowable with finite experimental precision. But particles acquiring a fixed fraction of their mass from the Higgs are effectively non-decoupling as the strength of their interaction with the Higgs necessarily grows in proportion to their mass. Among these, perhaps the most interesting are particles acquiring *the majority* of their mass from the Higgs.[1] The low-energy effects of such particles must be described by the $U(1)_{\rm em}$-symmetric HEFT rather than the $SU(2)_L \times U(1)_Y$-symmetric SMEFT. The underlying reason is that the low-energy theory obtained by integrating out such particles does not admit a SMEFT-like expansion around a $SU(2)_L \times U(1)_Y$-preserving point in the EFT field space that converges at our observed vacuum [11]. In this sense,

[1] We will sharpen the notion of "majority" in what follows; the detailed criteria varies weakly depending on the quantum numbers of the new particles and the nature of their couplings to the Higgs, but in all cases it roughly corresponds to particles obtaining more than half of their mass from the Higgs.

particles acquiring most of their mass from the Higgs provide simple, perturbative UV completions of HEFT that cannot be described using SMEFT [11, 12, 13, 14]. Insofar as their masses are bounded from above by unitarity considerations to be $\lesssim 4\pi v$ (where v is the Higgs boson vacuum expectation value), these particles provide a well-defined and entirely finite target for experimental searches.

We follow in the footsteps of Gell-Mann and refer to such particles as *Loryons*.[2] Most of the fundamental particles in the Standard Model are themselves Loryons, with the exception of the photon and gluon (though the pedantic among us might argue for their inclusion as well, inasmuch as their Higgs-independent masses are not larger than their Higgs dependent-ones, both being zero). This classification is perhaps even more apt when applied to mesons and baryons, whose masses arise only in part from electroweak symmetry breaking; pions, kaons, and B mesons are Loryons, while protons and neutrons are not. Our goal here is to explore the phenomenology of BSM Loryons, with a particular eye towards the parameter space that could yield a future discovery.

The search for BSM Loryons has a long history. Perhaps the most notable example is the extension of the Standard Model (SM) that includes a chiral fourth generation, the smallest anomaly-free set of entirely chiral fermions that all carry SM charges. Famously, this model is excluded by a combination of unitarity bounds, Higgs coupling measurements, precision electroweak tests, and direct searches [16, 17]. But this leaves the door open for vector-like fermions, scalars, or vectors in various representations of $SU(3)_C \times SU(2)_L \times U(1)_Y$. In the case of vector-like fermions, even though their vector-like masses are allowed by their gauge quantum numbers, it is technically natural for them

[2]From *Finnegan's Wake*, "with Pa's new heft...see Loryon the comaleon." Note that Loryons whose masses vanish as $v \to 0$ were referred to as "Higgs descendents" in [15]. Such particles form a particularly interesting subset of Loryons, as the EFT manifold obtained by integrating them out does not contain an $SU(2)_L \times U(1)_Y$-preserving fixed point. But our interest lies in the broader class of perturbative UV completions of HEFT that cannot be described using SMEFT, for which imposing $m \to 0$ as $v \to 0$ is too strong of a requirement.

to receive the majority of their mass from electroweak symmetry breaking since these terms may still violate global symmetries. Aspects of this scenario and its implications for the EFT of the Higgs were recently studied in [18]. For scalars, there are (famously) fewer symmetries available to protect possible mass terms. So while such BSM examples are still phenomenologically interesting, justifying a small mass that is independent of electroweak symmetry is harder from a symmetry perspective.[3] In the case of vectors, gauge symmetry provides a natural way of controlling mass terms, but strong constraints exist for models where the Higgs is directly charged under the new gauge group so that it can be primarily responsible for generating the associated gauge boson masses. A more viable option is for the non-zero Higgs vacuum expectation value to induce spontaneous symmetry breaking of the BSM local symmetry via another scalar, in which case the vector bosons can acquire most of their mass from the Higgs without coupling to it via renormalizable operators. Such indirect scenarios were highlighted in [15]. For simplicity, in what follows we will focus on scalar and fermionic Loryons obtaining the majority of their mass from a direct coupling to the Higgs. As we will see, there is no shortage of such candidates, but it would also be interesting to further explore the space of Loryon candidates indirectly acquiring the majority of their mass from the Higgs.

To the extent that they remain viable, BSM Loryons provide compelling motivation to use HEFT to parameterize possible deviations in Higgs coupling measurements. Of course, it is reasonable to ask whether one should use an EFT to describe the low-energy effects of Loryons in the first place given that their masses are necessarily bounded to lie below $\sim 4\pi v$. Here it bears emphasizing that the vast majority of collisions at the LHC involve partonic energies below 1 TeV, and in particular the events most relevant to precision Higgs measurements involve partonic energies much closer to the weak scale. In

[3]But not impossible – for instance, a Goldstone boson whose coupling to the Higgs provides the leading violation of its shift symmetry can naturally acquire most of its mass from electroweak symmetry breaking.

this regime, EFTs truncated at lower orders in their derivative expansion (as is the case in the practical application of HEFT and SMEFT) are appropriate. While it is possible that some Loryons may be discovered (or excluded) predominantly by direct searches, as we will see, Higgs couplings and other Standard Model precision measurements provide a complementary (and perhaps even the best) probe of Loryon parameter space. Signals in these channels are generally well-described by an EFT, and the first signs of a deviation are likely to be presented in an EFT framework. As such, the existence of Loryons consistent with current data provides a strong motivation to use HEFT as the BSM parameterization when performing future searches for Higgs coupling deviations.

This chapter is organized as follows: In Sec. 2.1, we enumerate scalar and fermionic Loryons obtaining the majority of their mass from direct coupling to the Higgs. For simplicity, and to minimize constraints from precision electroweak measurements, we only study candidates that can be expressed as multiplets of the approximate $SU(2)_L \times SU(2)_R$ custodial symmetry of the SM. We allow for all custodially symmetric renormalizable couplings to the Higgs that respect a $\mathbb{Z}_2$ symmetry acting on the Loryons. Imposing the $\mathbb{Z}_2$ symmetry allows us to highlight the irreducible loop-level signatures of Loryons; tree-level signatures in the absence of this symmetry typically lead to stronger constraints but are not inherent to the definition of Loryons. We present a sharp criterion for determining when the local EFT obtained by integrating out these custodial irreducible representations (irreps) must be HEFT (in that it cannot be written in terms of a convergent SMEFT at our vacuum) and use this to define the parameter space of interest for Loryons. In these cases, the mass scale of weakly-coupled Loryons is bounded from above by perturbative unitarity considerations. While it is certainly possible for Loryon couplings to exceed these bounds, we use them to determine the regime in which our perturbative calculations remain under control. In Sec. 2.2, we consider constraints on the Loryon candidates coming from Higgs coupling measurements, most notably LHC bounds on

$h \to \gamma\gamma$, $h \to gg$, $h \to$ invisible, and $h \to$ untagged. We then turn to consider precision electroweak limits in Sec. 2.3, which largely stem from bounds on the S parameter given our imposition of custodial symmetry. In Sec. 2.4, we determine the current state of direct limits on the Loryon candidates that remain viable after imposing perturbative unitarity bounds, Higgs couplings, and precision electroweak measurements are taken into account. We summarize the surviving parameter space of Loryons in Sec. 2.5, finding a number of compelling candidates that are consistent with all known data, thereby providing a sharp target for future searches. We briefly sketch the future prospects for the HL-LHC in Sec. 2.6, focusing on projected improvements in Higgs coupling measurements; both $h \to Z\gamma$ and h pair production are expected to provide qualitatively new sensitivity. We present our conclusions in Sec. 2.7. The calculation of the mass spectrum and one-loop contribution to the Higgs wave function renormalization is relegated to App. A.

2.1 Loryon Catalog

Our starting point is to enumerate the BSM Loryons that have a possibility of being phenomenologically viable. Our first goal will be to specify their SM quantum numbers and to understand the implications for the allowed mass terms and couplings to the Higgs field in Sec. 2.1.1. We will then discuss the connection to HEFT in Sec. 2.1.2 by specifying the conditions under which integrating out a Loryon requires matching the resulting theory onto HEFT. In these cases, the mass of the Loryons are bounded from above by perturbative unitarity considerations, which we will explore in Sec. 2.1.3.

2.1.1 Representations and Mass Spectrum

New physics that badly violates the approximate $SU(2)_L \times SU(2)_R$ custodial symmetry of the SM is strongly constrained by precision electroweak measurements.[4] In order to focus on the candidates that are most compatible with current data, we will restrict our attention to Loryons that preserve custodial symmetry. There are, of course, viable Loryon candidates that violate custodial symmetry, albeit with parameter spaces more tightly constrained by precision electroweak data; we leave the study of this broader class of candidates to future work.

Given this assumption, we will refer to the representation of the BSM Loryons in two ways, depending on the context. One useful approach is to denote the representation under the SM gauge groups; this will be written using the notation $(C, L)_Y$ for the charges under $SU(3)_C$, $SU(2)_L$, and $U(1)_Y$. The other notation is to specify the representation under custodial symmetry; this will be written as $[L, R]_Y$, where we suppress the color information, and use the integers L/R to denote the dimensions of the representations under $SU(2)_{L/R}$. In this notation, Y denotes the hypercharge of the states *on top of* the eigenvalues of the $SU(2)_R$ generator T^3_R, so the custodial representation $[L, R]_Y$ contains SM fields $(C, L)_{-(R-1)/2+Y}$ to $(C, L)_{(R-1)/2+Y}$ in steps of unit hypercharge. We require a priori that all BSM Loryons satisfy the following three conditions:

- The color singlets have integer electromagnetic charges.
- Those possessing electromagnetic charges can promptly decay.
- Fermionic Loryons are introduced in pairs such that one can write a custodial singlet Yukawa term.

[4] In fact, the lack of evidence for additional custodial symmetry violation is often taken as a reason for preferring to interpret experimental results using SMEFT over HEFT. We caution that this is not a valid argument since both EFT frameworks admit custodially symmetric limits.

The prompt decay constraint is taken to be $c\tau \lesssim 1$ mm. A rough calculation taking a benchmark suppression scale $\Lambda \gtrsim 5$ TeV gives a conservative bound dim ≤ 9 for the decay operator, which is only logarithmically sensitive to the chosen value of Λ. This constrains the allowed color, electroweak, and hypercharge representations of BSM Loryons. In Table 2.1 and Table 2.2, we enumerate the custodial irreps considered, list their maximum allowed hypercharge, and give the labeling of the SM representations following the conventions of [19]. We do not explicitly enumerate the possible color representations; virtually all of these will be easily ruled out by constraints on the Higgs coupling to gluons parameterized by κ_g (see Sec. 2.2.3).

Scalars: We start with the case of scalar Loryons, listing their SM and custodial representations in Table 2.1. For each custodial irrep $[L, R]_Y$, we define a $L \times R$ matrix field Φ that transforms as $\Phi \to U_L \Phi U_R^\dagger$ under the chosen irrep $U_{L/R}$ of $SU(2)_{L/R}$. The custodial irrep is real iff $L + R$ is even and $Y = 0$. We can write an explicit mass term for Φ,

$$\mathcal{L} \supset -\frac{m_{\text{ex}}^2}{2^\rho} \operatorname{tr}\left(\Phi^\dagger \Phi\right) , \tag{2.1}$$

where $\rho = 0\,(1)$ for a complex (real) representation.

Arranging the components of the Higgs doublet $(\phi_+, \phi_0)^T$ into the $[2, 2]_0$ custodial representation,

$$H = \begin{pmatrix} \phi_0^* & \phi_+ \\ -\phi_- & \phi_0 \end{pmatrix} \xrightarrow{\text{unitary gauge}} \frac{v + h}{\sqrt{2}} \begin{pmatrix} 1 & 0 \\ 0 & 1 \end{pmatrix} , \tag{2.2}$$

we can also write down a Higgs portal interaction,

$$\mathcal{L} \supset -\frac{\lambda_{h\Phi}}{2^\rho} \operatorname{tr}\left(\Phi^\dagger \Phi\right) \frac{1}{2} \operatorname{tr}\left(H^\dagger H\right) , \tag{2.3}$$

SCALARS

SM Reps	$(1,1)_Y$	$(1,2)_Y$	$(1,3)_Y$	$(1,4)_Y$	$(1,L)_Y$	$(3,1)_Y$	$(3,2)_Y$
Field	S_Y	Φ_{2Y}	Ξ_Y	Θ_{2Y}	$X_{L,Y}$	$\omega_{\lvert 3Y\rvert}$	$\Pi_{\lvert 6Y\rvert}$

	$R=1$	2	3	4	5	6	7	8
$L=1$	$\lvert Y_{max}\rvert = 3$	$\frac{5}{2}$	2	$\frac{3}{2}$	1	$\frac{1}{2}$	0	$\times$
2	$\frac{7}{2}$	4	$\frac{7}{2}$	4	$\frac{9}{2}$	5	$\frac{11}{2}$	5
3	3	$\frac{7}{2}$	4	$\frac{9}{2}$	4	$\frac{9}{2}$	5	$\frac{11}{2}$
4	$\frac{7}{2}$	3	$\frac{7}{2}$	4	$\frac{9}{2}$	5	$\frac{11}{2}$	5
5	3	$\frac{7}{2}$	4	$\frac{7}{2}$	4	$\frac{9}{2}$	5	$\frac{11}{2}$
6	$\frac{5}{2}$	3	$\frac{7}{2}$	4	$\frac{9}{2}$	5	$\frac{9}{2}$	4
7	3	$\frac{7}{2}$	3	$\frac{5}{2}$	2	$\frac{3}{2}$	1	$\frac{1}{2}$
8	$\frac{3}{2}$	1	$\frac{1}{2}$	0	$\times$	$\times$	$\times$	$\times$

Table 2.1: The representations and corresponding fields for the scalar BSM Loryons considered in this work. We express "SM charges" as $(C,L)_Y$ and "custodial charges" as $[L,R]_Y$; the custodial representation $[L,R]_Y$ contains SM fields $(C,L)_{-(R-1)/2+Y}$ to $(C,L)_{(R-1)/2+Y}$ in steps of unit hypercharge. Hypercharges Y are restricted so that any new charged particles can promptly decay.

which provides a contribution $\lambda_{h\Phi}v^2/2$ to the mass for all the components of Φ. We will be interested in the Loryon parameter space where the BSM state gets the majority of its mass from electroweak symmetry breaking. To this end, it is convenient to define the dimensionless quantity $\lambda_{\rm ex} \equiv 2m_{\rm ex}^2/v^2$. Thus the explicit mass term gives a mass-squared $\lambda_{\rm ex}v^2/2$ to each component of Φ (though we emphasize that the explicit masses are independent of the Higgs vev).

Additionally, for the representations that are charged under both $SU(2)_L$ and $SU(2)_R$,

there is another contraction for the quartic term,

$$\mathcal{L} \supset -\frac{\lambda'_{h\Phi}}{2^\rho}\, 2\,\mathrm{tr}\left(\Phi^\dagger T_L^a \Phi T_R^{\dot{a}}\right) 2\,\mathrm{tr}\left(H^\dagger T_2^a H T_2^{\dot{a}}\right), \tag{2.4}$$

involving Hermitian $SU(2)$ generators $T^a_{\mathrm{dim(irrep)}}$, indexed by $a, \dot{a} = 1, 2, 3$. In our notation, these generators are canonically normalized,

$$\mathrm{tr}\left(T^a_{\mathrm{dim}} T^b_{\mathrm{dim}}\right) = \delta^{ab}\,\frac{1}{3}\,\mathrm{dim}\; C_2(\mathrm{dim})\,, \tag{2.5}$$

with the Casimir (note that $\mathrm{dim} = 2j + 1$)

$$C_2(\mathrm{dim}) = j(j+1) = \frac{1}{4}(\mathrm{dim}+1)(\mathrm{dim}-1)\,. \tag{2.6}$$

After electroweak symmetry breaking, the interaction in Eq. (2.4) leads to a mass splitting among the components of Φ. The remaining degeneracies in the mass spectrum arrange into irreps of the unbroken diagonal subgroup $SU(2)_V \subset SU(2)_L \times SU(2)_R$. Explicitly, one can collect the $L \times R$ components of the matrix Φ into a direct sum of V-dimensional vectors ϕ_V that are $SU(2)_V$ representations:

$$\Phi \to \bigoplus_{V \in \mathcal{V}} \phi_V\,, \tag{2.7}$$

with

$$\mathcal{V} = \Big\{ L+R-1\,,\; L+R-3\,,\; \cdots\,,\; |L-R|+1 \Big\}\,. \tag{2.8}$$

As a concrete example to illustrate Eq. (2.7), we consider the complex custodial irrep $\Phi \sim [2,3]_{-1/2}$. It has six components and decomposes into a quadruplet and a doublet

under $SU(2)_V$:

$$\Phi = \begin{pmatrix} \Phi_{11} & \Phi_{12} & \Phi_{13} \\ \Phi_{21} & \Phi_{22} & \Phi_{23} \end{pmatrix} \to \phi_4 \oplus \phi_2 \,. \tag{2.9}$$

Working with the T_R^3-spin basis, namely each column of the matrix Φ above has a definite T_R^3-spin of $SU(2)_R$ (or equivalently of $SU(2)_V$), respectively $-1, 0, 1$ in order, we can write out each $SU(2)_V$ irrep ϕ_V from the Φ elements using the Clebsch-Gordan coefficients,

$$\phi_4 = \begin{pmatrix} \Phi_{13} \\ \frac{1}{\sqrt{3}}\left(-\sqrt{2}\,\Phi_{12} + \Phi_{23}\right) \\ \frac{1}{\sqrt{3}}\left(\Phi_{11} - \sqrt{2}\,\Phi_{22}\right) \\ \Phi_{21} \end{pmatrix}, \qquad \phi_2 = \begin{pmatrix} \frac{1}{\sqrt{3}}\left(\Phi_{12} + \sqrt{2}\,\Phi_{23}\right) \\ \frac{1}{\sqrt{3}}\left(-\sqrt{2}\,\Phi_{11} - \Phi_{22}\right) \end{pmatrix}. \tag{2.10}$$

Then the interaction in Eq. (2.4) reads (in the unitary gauge)

$$\mathcal{L} \supset -\lambda'_{h\Phi}\, 2\,\mathrm{tr}\left(\Phi^\dagger T_L^a \Phi T_R^a\right) \frac{1}{2}(v+h)^2 = -\frac{1}{2}\lambda'_{h\Phi}(v+h)^2 \left(-\phi_4^\dagger\phi_4 + 2\phi_2^\dagger\phi_2\right) . \tag{2.11}$$

General cases are worked out systematically in App. A. In the end, we obtain the decomposition of Eq. (2.4) as

$$\mathcal{L} \supset -\frac{1}{2^\rho}\,\frac{1}{2}\lambda'_{h\Phi}(v+h)^2 \sum_{V\in\mathcal{V}} \phi_V^\dagger \Big[C_2(L) + C_2(R) - C_2(V)\Big]\phi_V \,. \tag{2.12}$$

This leads us to a convenient form of the quadratic piece of the Lagrangian for an $[L, R]_Y$

scalar Loryon:

$$\mathcal{L}_{\rm quad} = -\frac{1}{2^\rho}\sum_{V\in\mathcal{V}}\phi_V^\dagger\left[D^2+\frac{1}{2}\lambda_{\rm ex}v^2+\frac{1}{2}\lambda_V(v+h)^2\right]\phi_V\,, \tag{2.13}$$

where we have introduced the notation

$$\lambda_V \equiv \lambda_{h\Phi}+\lambda'_{h\Phi}\Big[C_2(L)+C_2(R)-C_2(V)\Big]\,. \tag{2.14}$$

Note in particular that the mass spectrum of the scalar Loryon is

$$m_V^2 = m_{\rm ex}^2+\frac{1}{2}\lambda_V v^2 = \frac{1}{2}v^2\left(\lambda_{\rm ex}+\lambda_V\right)\,, \qquad \forall\, V\in\mathcal{V}\,. \tag{2.15}$$

Here and henceforth we assume $\lambda_{\rm ex}, \lambda_{\rm ex}+\lambda_V \geq 0$ in order to ensure stability of the $\Phi = 0$ vacuum for any background value of the Higgs.

We will find it useful to scale the mass splitting by the mass common to all the components. To this end, we define

$$r_{\rm split} \equiv \frac{\lambda'_{h\Phi}}{\lambda_{\rm ex}+\lambda_{h\Phi}}\,. \tag{2.16}$$

In principle, some scalar BSM Loryons could also couple linearly to various powers of H, leading to Higgs-Loryon mixing after electroweak symmetry breaking. We assume these couplings are small, consistent with an approximate discrete symmetry acting on the BSM scalars. We further assume that the Higgs-independent potential for the new scalars is such that they are stabilized at the origin. Under these assumptions, mixing between new scalars and components of the Higgs is a subleading effect on low-energy physics.

Fermions: For fermionic Loryons, we consider vector-like fermions whose SM and custo-

dial representations are summarized in Table 2.2. As in the scalar case, for each custodial irrep $[L, R]_Y$, we define an $L \times R$ matrix field Ψ that transforms as $\Psi \to U_L \Psi U_R^\dagger$. Each element in Ψ is a Dirac field that contains both a left-handed Weyl fermion and a right-handed Weyl fermion. We can then write down an explicit mass term,

$$\mathcal{L} \supset -M_{\text{ex}} \text{ tr}\left(\overline{\Psi}\Psi\right) . \tag{2.17}$$

As before, it is convenient to define $y_{\text{ex}} \equiv \sqrt{2}M_{\text{ex}}/v$. This facilitates the comparison between the fraction of the fermions' masses that is independent of electroweak symmetry breaking and the fraction that arises from electroweak symmetry breaking. The latter comes from the Yukawa interactions that can be schematically written as

$$\mathcal{L} \supset -y_{12}\, \overline{\Psi}_1 \cdot H \cdot \Psi_2 + \text{h.c.} . \tag{2.18}$$

The representations $[L_1, R_1]_Y$ and $[L_2, R_2]_Y$ (of Ψ_1 and Ψ_2 respectively) are chosen such that contracting their indices with the $[2, 2]_0$ Higgs representation (as schematically denoted by the dot products above) can yield a custodial singlet. This enforces the equality of the hypercharges of two representations and means that $L_1 = L_2 \pm 1$ and $R_1 = R_2 \pm 1$. Henceforth we refer to such a pairing as $[L_1, R_1]_Y \oplus [L_2, R_2]_Y$.

Upon electroweak symmetry breaking, the Yukawa interaction in Eq. (2.18) leads to mass splitting among the components of Ψ_1 and Ψ_2. To keep track of this, we decompose each of them into their respective irreps under the diagonal subgroup $SU(2)_V \subset SU(2)_L \times SU(2)_R$, similar to the scalar case in Eq. (2.7):

$$\Psi_1 \to \bigoplus_{V_1 \in \mathcal{V}_1} \psi_{1,V_1} , \qquad \Psi_2 \to \bigoplus_{V_2 \in \mathcal{V}_2} \psi_{2,V_2} , \tag{2.19}$$

Vector-like Fermions

SM Reps	$(1,1)_Y$	$(1,2)_Y$	$(1,3)_Y$	$(1,L)_Y$	$(3,1)_Y$
Field	E_Y	Δ_{2Y}	Σ_Y	$K_{L,Y}$	$P_{\lvert 3Y\rvert}$

	$R=1$	2	3	4	5	6	7	8
$L=1$	$\lvert Y_{max}\rvert = 3$	$\frac{5}{2}$	2	$\frac{3}{2}$	1	$\frac{1}{2}$	0	$\times$
2	$\frac{7}{2}$	3	$\frac{7}{2}$	4	$\frac{9}{2}$	5	$\frac{11}{2}$	5
3	3	$\frac{7}{2}$	3	$\frac{7}{2}$	4	$\frac{9}{2}$	5	$\frac{11}{2}$
4	$\frac{5}{2}$	3	$\frac{7}{2}$	4	$\frac{7}{2}$	4	$\frac{9}{2}$	5
5	3	$\frac{5}{2}$	3	$\frac{7}{2}$	4	$\frac{9}{2}$	5	$\frac{9}{2}$
6	$\frac{5}{2}$	3	$\frac{7}{2}$	3	$\frac{5}{2}$	2	$\frac{3}{2}$	1
7	2	$\frac{3}{2}$	1	$\frac{1}{2}$	0	$\times$	$\times$	$\times$
8	$\times$	$\times$	$\times$	$\times$	$\times$	$\times$	$\times$	$\times$

Table 2.2: The representations and corresponding fields for the vector-like fermionic BSM Loryons considered in this work. We express "SM charges" as $(C,L)_Y$ and "custodial charges" as $[L,R]_Y$; the custodial representation $[L,R]_Y$ contains SM fields $(C,L)_{-(R-1)/2+Y}$ to $(C,L)_{(R-1)/2+Y}$ in steps of unit hypercharge. Hypercharges Y are restricted so that any new charged particles can promptly decay and so that the Yukawa terms with the Higgs are gauge singlets.

with

$$\mathcal{V}_1 = \Big\{ L_1 + R_1 - 1\ ,\ L_1 + R_1 - 3\ ,\ \cdots\ ,\ |L_1 - R_1| + 1 \Big\}\,, \tag{2.20a}$$

$$\mathcal{V}_2 = \Big\{ L_2 + R_2 - 1\ ,\ L_2 + R_2 - 3\ ,\ \cdots\ ,\ |L_2 - R_2| + 1 \Big\}\,. \tag{2.20b}$$

In the overlap of these two sets $V = V_1 = V_2$, the two fermions ψ_{1,V_1} and ψ_{2,V_2} get mass mixings through the interaction in Eq. (2.18).

As a concrete example to illustrate this mass mixing, we consider the pair of custodial

irreps $\Psi_1 \sim [2,3]_{-1/2}$ and $\Psi_2 \sim [1,2]_{-1/2}$. The contraction of indices in Eq. (2.18) can be written out as

$$\mathcal{L} \supset -y_{12}\,\overline{\Psi}_{1,\alpha\dot{a}}\,H_{\alpha\dot{\alpha}}\,\frac{1}{\sqrt{2}}\sigma^{\dot{a}}_{\dot{\gamma}\dot{\alpha}}\epsilon_{\dot{\gamma}\dot{\beta}}\,\Psi_{2,1\dot{\beta}} + \text{h.c.}\,, \tag{2.21}$$

where undotted (dotted) indices are for $SU(2)_L$ ($SU(2)_R$) and Greek (Latin) indices are used to denote fundamental (adjoint) representations. Upon electroweak symmetry breaking, we have $H_{\alpha\dot{\alpha}} = \frac{1}{\sqrt{2}}(v+h)\delta_{\alpha\dot{\alpha}}$ and hence (dropping dots on indices)

$$\mathcal{L} \supset -\frac{1}{2}\,y_{12}\,\overline{\Psi}_{1,\alpha a}\,\sigma^{a}_{\gamma\alpha}\epsilon_{\gamma\beta}\,\Psi_{2,1\dot{\beta}} + \text{h.c.} = -\frac{1}{\sqrt{2}}\sqrt{\frac{3}{2}}\,y_{12}(v+h)\,\overline{\psi}_{1,2}\,\psi_{2,2} + \text{h.c.}\,, \tag{2.22}$$

from which we can make the identification

$$(\psi_{1,2})_\beta = \frac{1}{\sqrt{3}}\,\sigma^{a}_{\alpha\beta}\Psi_{1,\alpha a}\,, \qquad (\psi_{2,2})_\beta = \epsilon_{\beta\alpha}\Psi_{2,1\alpha}\,. \tag{2.23}$$

As expected from Eq. (2.20), Ψ_2 in this example has a single $SU(2)_V$ irrep with $V_2 \in \{2\}$. On the other hand, Ψ_1 has two $SU(2)_V$ irreps with $V_1 \in \{4,2\}$. The interaction in Eq. (2.18) gives a mass mixing between the components in the overlap of the two sets $V_1 = V_2 = 2$.[5]

The general cases of a pair of custodial irreps $[L_1,R_1]_Y \oplus [L_2,R_2]_Y$ have been worked out systematically in App. A. This leads us to the following general form of the Lagrangian that is quadratic in the fermions,

$$\mathcal{L}_{\text{quad}} = \sum_{V\in\mathcal{V}_1-\mathcal{V}_2} \overline{\psi}_{1,V}\left(i\not{D} - M_1\right)\psi_{1,V} + \sum_{V\in\mathcal{V}_2-\mathcal{V}_1} \overline{\psi}_{2,V}\left(i\not{D} - M_2\right)\psi_{2,V}$$

[5]The expression for $\psi_{1,2}$ in Eq. (2.23) appears to be different from its scalar counterpart (namely ϕ_2 in Eq. (2.10)). This is because in Eq. (2.21) we used the adjoint basis for the columns of Ψ_1, as opposed to the T^3_R-spin basis used for Φ in Eq. (2.9). Carrying out the basis change, one can verify that they are the same linear combination.

$$+\sum_{V\in\mathcal{V}_1\cap\mathcal{V}_2}\begin{pmatrix}\overline{\psi}_{1,V} & \overline{\psi}_{2,V}\end{pmatrix}\left[i\not{D}-\begin{pmatrix}M_1 & \frac{1}{\sqrt{2}}y_V(v+h)\\ \frac{1}{\sqrt{2}}y_V^*(v+h) & M_2\end{pmatrix}\right]\begin{pmatrix}\psi_{1,V}\\ \psi_{2,V}\end{pmatrix}, \quad (2.24)$$

with

$$y_V=(-1)^{j_1+r_1+l_2+\frac{1}{2}}\,y_{12}\times\sqrt{L_1R_1}\times\begin{Bmatrix}r_2 & l_2 & j_1\\ l_1 & r_1 & \frac{1}{2}\end{Bmatrix}, \quad (2.25)$$

where $2l_i+1=L_i, 2r_i+1=R_i, 2j_1+1=V$, and the quantity in brackets is a Wigner 6j symbol. In the analysis that follows, we will take the vector-like masses of the two custodial irreps to be equal $M_1=M_2=M_{\rm ex}$ for simplicity; we have checked that this assumption has a minimal impact on our conclusions. Under this choice, the mass spectrum of the fermionic Loryon is

$$M_V=M_{\rm ex}=\frac{v}{\sqrt{2}}\,y_{\rm ex}\,, \qquad V\in\mathcal{V}_1-\mathcal{V}_2 \text{ or } \mathcal{V}_2-\mathcal{V}_1\,, \quad (2.26a)$$

$$M_{\pm V}=M_{\rm ex}\pm\frac{v}{\sqrt{2}}\,|y_V|=\frac{v}{\sqrt{2}}\,(y_{\rm ex}\pm|y_V|)\,, \qquad V\in\mathcal{V}_1\cap\mathcal{V}_2\,. \quad (2.26b)$$

Note that for each rep in the second line, $V\in\mathcal{V}_1\cap\mathcal{V}_2$, the fermion masses come in pairs. When $|y_V|>y_{\rm ex}$, one of the eigenvalues become negative. For this eigenstate of the Dirac fermion, one could flip the relative sign between its two chiral components to absorb the negative sign, so the physical mass of the particle is still positive (at the expense of introducing additional signs into the interactions).

2.1.2 Criteria for HEFT

Given our finite list of BSM Loryons, this section will delineate the regions of Loryon parameter space that require HEFT as the EFT description that emerges at low energies. In principle, the Loryons can give tree- and loop-level effects. The loop-level effects are

an irreducible consequence of coupling to the Higgs. Although the tree-level effects would give more striking signatures, to highlight the irreducible effects we assume there is an approximate $\mathbb{Z}_2$ symmetry acting on the BSM Loryon fields, which is respected by all their interactions with the Higgs discussed above; see Eqs. (2.1), (2.3) and (2.4) for scalars and Eqs. (2.17) and (2.18) for fermions. Close to the perturbative unitarity bound on the $\mathbb{Z}_2$ symmetric couplings, we expect the loop-level effects to be appreciable within the regime of validity of the EFT. As we will see, indirect constraints from Higgs properties are relevant in the parameter space of interest.

Relaxing the assumption of an approximate $\mathbb{Z}_2$ symmetry acting on the BSM Loryons (due to either explicit or spontaneous breaking) would give rise to a variety of additional signatures that are interesting but not inherent to the definition of Loryons. In the absence of this symmetry, Loryons can couple linearly to Standard Model operators with appreciable strength. This leads to large tree-level effects on Standard Model observables at low energies, as well as resonant or associated production of single Loryons at colliders. Direct and indirect constraints on Loryons are correspondingly stronger in this case. The signatures associated with large spontaneous or explicit breaking of the $\mathbb{Z}_2$ symmetry may lead to additional experimental opportunities for discovering BSM Loryons, which we leave to future work.

In order to compute the leading matching contributions, we utilize functional methods (see [11]) to derive the effective (scalar sector) Lagrangian that results if the UV theory includes a scalar Loryon (including all orders in the Higgs field H),

$$\mathcal{L}_{\text{eff}} \supset \frac{1}{2^{\rho}(4\pi)^2} \sum_{V\in\mathcal{V}} V \left\{ \frac{m_V^4(H)}{2} \left[\ln \frac{\mu^2}{m_V^2(H)} + \frac{3}{2} \right] + \frac{\lambda_V^2}{6m_V^2(H)} \frac{\left[\partial |H|^2\right]^2}{2} + \mathcal{O}\big(\partial^4\big) \right\} , \tag{2.27}$$

for an arbitrary custodial irrep Φ; this result is derived in App. A, see Eq. (A.11). App. A also includes the analogous calculation for fermions, see Eqs. (A.21) and (A.22).

Noting that the (non-derivative) dependence on H in Eq. (2.27) is captured by the effective mass,

$$m_V^2(H) = \frac{1}{2}\lambda_{\rm ex} v^2 + \lambda_V |H|^2 \,, \tag{2.28}$$

we can then obtain a SMEFT description of Eq. (2.27) by expanding about $H = 0$ in powers of $\lambda_V |H|^2 / \left(\frac{1}{2}\lambda_{\rm ex} v^2\right)$. However, the SMEFT description is only useful for predictions of low energy observables if it converges when evaluated about the electroweak breaking vacuum, $|H| = \frac{1}{\sqrt{2}} v$. This requires that[6]

$$\lambda_V < \lambda_{\rm ex} \,, \qquad \forall\, V \in \mathcal{V} \,. \tag{2.29}$$

If this condition is not satisfied, then one is forced to use the HEFT description; see [11]. We will find later that it is useful to introduce the parameter

$$f_V \equiv \frac{\lambda_V}{\lambda_{\rm ex} + \lambda_V} \,, \tag{2.30}$$

which corresponds to the fraction of a scalar Loryon's physical mass-squared that results from its interactions with the Higgs (see Eq. (2.15)). Note that this parameter will generically differ among the states ϕ_V within a given custodial representation. The criterion for necessarily matching onto HEFT then becomes

$$f_{\rm max} \geq \frac{1}{2} \,, \tag{2.31}$$

where we have defined $f_{\rm max} \equiv \max_{V \in \mathcal{V}} f_V$ as a shorthand for the f_V value of the heaviest scalar state.

[6] Eq. (2.27) shows a non-analyticity whenever $m_V^2(H) = 0$, which corresponds to a non-analyticity in the complex plane of $|H|$ at $\mathrm{Im}\,|H| = \pm \frac{\lambda_{\rm ex}}{\lambda_V} \frac{v}{\sqrt{2}}$ that limits the radius of convergence of the SMEFT expansion, see [20, 21].

A similar story holds for fermionic Loryons. In this case, the all-orders-in-H effective Lagrangian is given in Eq. (A.21). Its terms are simple functions of the (signed) Higgs-dependent masses of the states,

$$M_{\pm V}(H) = M_{\rm ex} \pm |y_V||H|\,, \tag{2.32}$$

and some of them become non-analytic when $M_{\pm V}(H) = 0$.[7] Then the SMEFT expansion of the effective Lagrangian converges at our vacuum if

$$|y_V| < y_{\rm ex}\,, \qquad \forall\, V \in \mathcal{V}_1 \cap \mathcal{V}_2\,. \tag{2.33}$$

Therefore, in terms of the fraction of mass that fermionic Loryons get from interacting with the Higgs (see Eq. (2.26)),

$$f_{\pm V} \equiv \frac{\pm\,|y_V|}{y_{\rm ex} \pm |y_V|}\,, \tag{2.34}$$

the criterion for necessarily matching onto HEFT is

$$f_{\rm max} \geq \frac{1}{2}\,, \tag{2.35}$$

where we have defined the shorthand $f_{\rm max} \equiv \max_{V\in\mathcal{V}_1\cap\mathcal{V}_2} f_{+V}$.

2.1.3 Mass Bounds from Unitarity

For particles getting some fixed fraction of their mass from electroweak symmetry breaking, the coupling to the Higgs increases with the mass. Since scattering into Higgses or via Higgs exchange will violate unitarity if this coupling is too large, requiring that

[7] Despite appearances the effective Lagrangian is well behaved when $M_{+V} = M_{-V}$.

the theory be under perturbative control places an upper bound on the mass of the BSM Loryons. To account for these bounds, we impose partial wave unitarity on scattering processes involving Loryons and Higgses. We emphasize that partial wave unitarity does not provide an invariant bound on the Loryon parameter space, and the detailed bound is sensitive to conventions. However, it does provide a useful indication of the region of parameter space in which perturbation theory remains valid. If Loryons exist outside of the region delineated by unitarity, their properties are likely to be poorly described by the treatment presented here. For instance, the formation of bound states is likely to be interesting and merits further study.

Of course, there are other theoretical bounds that may be placed on the couplings of new particles to the Higgs. Chief among these is the vacuum (in)stability of the Higgs: new particles interacting strongly with the Higgs may cause the Higgs self-coupling to run negative at lower scales than in the Standard Model, leading to a prohibitively short lifetime of the metastable vacuum or an outright instability. However, these concerns may be mitigated by additional UV physics (whether in the form of additional particles – not necessarily Loryons – or irrelevant operators contributing to the Higgs potential). As such, in what follows we focus on bounds from perturbative unitarity, but considerations involving Higgs vacuum stability would be an interesting target for further exploration.

We focus on 2-to-2 scattering processes at the tree level for simplicity. The strongest bounds on the Loryon masses come from the scattering of a Loryon pair into a Higgs pair, or a Loryon pair into a Loryon pair, as depicted in Fig. 2.1. For technical simplicity, only contributions from the exchange of scalars and fermions are considered. Diagrams with SM vector boson exchange give subdominant effects.

For a general 2-to-2 scattering process taking an initial state i to a final state f, one can project onto the spin-0 partial wave component by averaging over the scattering

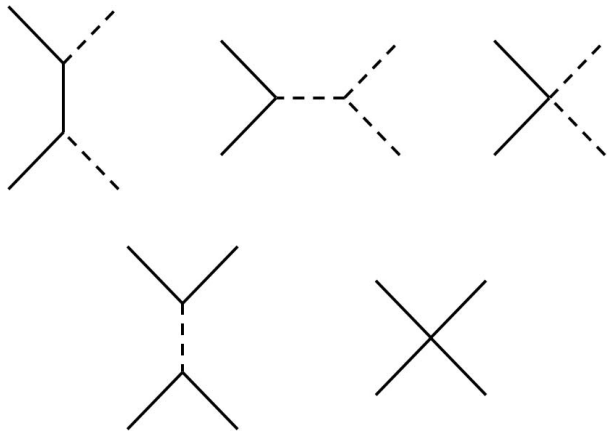

Figure 2.1: Tree-level 2-to-2 scattering processes considered for placing an upper bound on Loryon masses from perturbative unitarity: (upper) Loryon pair scattering to a Higgs pair, and (lower) Loryon pair scattering to a Loryon pair. Dashed lines denote physical Higgs boson h and solid lines are for Loryons. Crossed channels are not explicitly drawn. The last diagram in each row is only available for scalar Loryons assuming renormalizable interactions. For each process, the t-channel exchange diagram dominates the contribution.

angle with normalization appropriate for arbitrary values of s:[8]

$$a_0\left(\sqrt{s}\right) = \sqrt{\frac{4\left|\vec{p}_i\right|\left|\vec{p}_f\right|}{2^{\delta_i+\delta_f}\,s}}\frac{1}{32\pi}\int_{-1}^{1}\mathrm{d}(\cos\theta)\;\mathcal{M}(i\to f)\,, \tag{2.36}$$

where δ_i/δ_f is 1 if the initial/final state particles are identical and 0 otherwise. Unitarity of the S matrix then imposes the bound

$$|\mathrm{Re}(a_0)| \leq \frac{1}{2}\,. \tag{2.37}$$

Of particular note is that the bound applies for all values of the center-of-mass energy $\sqrt{s}$, not just in the high energy limit [23]. For example, in the 2-to-2 scattering of heavy Loryons via t-channel exchange of a Higgs (bottom-left diagram in Fig. 2.1), the

[8]When fermions are involved in the initial or final states, in principle one also needs to project the spinor part onto states with definite helicities using the Wigner d-matrix [22], although when projecting into an overall spin 0 state the formula Eq. (2.36) remains valid for the collision of two spinning particles of equal helicity.

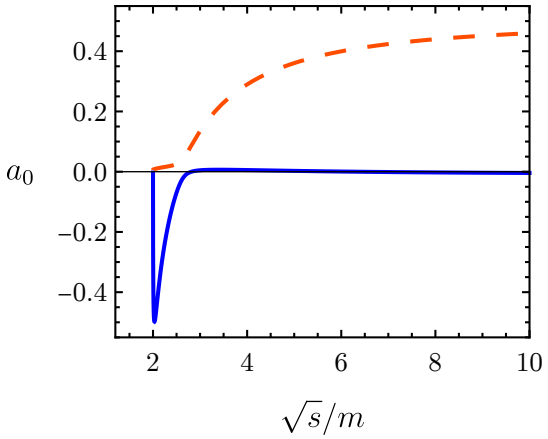

Figure 2.2: An example of the behavior of the zeroth partial wave coefficients $a_0\left(\sqrt{s}\right)$. The plot is for a neutral singlet scalar Loryon S_0 getting all of its mass $m = 525$ GeV from the Higgs. The two curves correspond to the two eigenvalues of the 2 by 2 scattering matrix $\left(S_0S_0, hh\right)^T \to \left(S_0S_0, hh\right)^T$.

maximal value of $|\mathrm{Re}\left(a_0\right)|$ occurs not in the high energy limit but close to the threshold, as illustrated in Fig. 2.2. This channel typically gives the strongest upper bound on the Loryon masses.

For **scalars**, the limit we derive on its mass depends on the quartic self-coupling of the new field. An upper bound on the quartic self-coupling can be obtained from the high energy limit; we then report the weakest bound after marginalizing over the allowed self-couplings. The final result depends on the representation of the Loryon as well as the fraction of mass that it gets from electroweak symmetry breaking. For a singlet Loryon, the upper bound varies smoothly from 530 to 810 GeV as $f_{\max}$ goes from 1 to 1/2. For larger representations, the bounds are stronger by up to $\mathcal{O}(50\,\mathrm{GeV})$, depending on the precise representation chosen and amount of mass splitting. For **fermions**, the upper bound on the heaviest mass varies smoothly from about 470 to 780 GeV as $f_{\max}$ goes from 1 to 1/2 for all possibilities not ruled out by electroweak precision measurements (see Sec. 2.3).

In addition to constraints on elastic scattering, there are unitarity constraints on the

cross-quartic couplings $\lambda_{h\Phi}^{(\prime)}$, or Yukawa squared y_{12}^2, arising from the inelastic process $hh \to$ Loryon Loryon, for which $\sum_{\text{states}} |a_0|^2 \lesssim 1$. They provide a constraint on $\lambda_{h\Phi}^{(\prime)}$ or y_{12}^2 that scales as $N^{-\frac{1}{2}}$ in the number of states N. This is inconsequential for the smaller individual viable custodial irreps plotted below, but is to be borne in mind for larger solutions, particularly when considering their effect on Higgs wavefunction normalization (see Sec. 2.6).

2.2 Higgs Coupling Constraints

Having defined the landscape of Loryons, we now turn to consider the constraints from current experimental data. We begin with Higgs coupling measurements, which are particularly impactful given the non-decoupling nature of Loryons. By assumption, our BSM Loryons have an approximate $\mathbb{Z}_2$ symmetry and therefore would only correct Higgs couplings starting from one-loop order. This makes the following measurements potentially important:

$$h\gamma\gamma \text{ coupling}, \quad hgg \text{ coupling}, \quad h \to \text{invisible or untagged width}. \tag{2.38}$$

Although Loryons modifying the couplings $h\gamma\gamma$ and hgg generically also modify other Higgs couplings, these latter effects are loop-level corrections to tree-level Standard Model couplings and hence not as significant. The constraints from current $hZ\gamma$ coupling measurement is also typically subdominant compared to that from $h\gamma\gamma$, but could potentially play an important role at HL-LHC in future; we briefly discuss this in Sec. 2.6, where we will also comment on the potential impact of Higgs wavefunction and self coupling corrections.

2.2.1 General Formalism

The leading contribution to the $h\gamma\gamma$ (hgg) coupling in the SM occurs via loops of charged (colored) particles that have tree-level couplings to the Higgs. As has long been appreciated, any new charged (colored) particles can run in the loop and modify these couplings [24]. These modifications can be captured by the parameter κ_γ (κ_g), which simply rescales the $h\gamma\gamma$ (hgg) vertex, with $\kappa_\gamma = \kappa_g = 1$ for the SM.

For a scalar Loryon ϕ or a fermionic Loryon ψ discussed in Sec. 2.1, we can read off the tree-level Higgs-Loryon-Loryon coupling from Eqs. (2.13) and (2.24), facilitated by our definitions in Eqs. (2.30) and (2.34):

$$\mathcal{L} \supset -\frac{1}{2^\rho} f_\phi \frac{2m_\phi^2}{v} h \phi^\dagger \phi - f_\psi \frac{m_\psi}{v} h \overline{\psi} \psi \,, \tag{2.39}$$

where f_i is f_V for the ith particle. Generally, particles coupled to the Higgs in this form contribute to κ_γ and κ_g as [25]

$$\kappa_\gamma \propto \sum_i f_i \, Q_i^2 \, A_{s_i}(\tau_i) \,, \tag{2.40a}$$

$$\kappa_g \propto \sum_i f_i \, C_i \, A_{s_i}(\tau_i) \,. \tag{2.40b}$$

The sum runs over all contributing complex scalars, Dirac fermions, or vector bosons. For each contributing particle i, Q_i denotes its electromagnetic charge; C_i is the Dynkin index of its $SU(3)_C$ representation, namely $\mathrm{tr}\left(t_i^A t_i^B\right) = C_i \delta^{AB}$ with t_i^A denoting the $SU(3)_C$ generators; $\tau_i = 4m_i^2/m_h^2$ parameterizes the mass; s_i denotes the spin; and the spin-dependent form factors $A_{s_i}(\tau)$ are given by

$$A_0(\tau) = \tau\big[1 - \tau F(\tau)\big] \,, \tag{2.41a}$$

$$A_{1/2}(\tau) = -2\tau\big[1 + (1-\tau)F(\tau)\big]\,, \tag{2.41b}$$

$$A_1(\tau) = 2 + 3\tau\big[1 + (2-\tau)F(\tau)\big]\,, \tag{2.41c}$$

with

$$F(\tau) = \begin{cases} \arcsin^2\left(1/\sqrt{\tau}\right) & \tau \geq 1 \\ -\frac{1}{4}\left[\log\frac{1+\sqrt{1-\tau}}{1-\sqrt{1-\tau}} - i\pi\right]^2 & \tau < 1 \end{cases}\,. \tag{2.42}$$

When the particles running in the loop are asymptotically heavy, namely $\tau_i \to \infty$, these form factors asymptote to constants,

$$A_0 \to -1/3\,, \qquad A_{1/2} \to -4/3\,, \qquad A_1 \to 7\,. \tag{2.43}$$

In practice, this is a good approximation ($\lesssim 10\%$ error) for particles heavier than the Higgs, which is the case for most BSM Loryons of interest.

2.2.2 $h\gamma\gamma$ Coupling

To compute κ_γ for a particular BSM model, we can simply use (see Eq. (2.40))

$$\kappa_\gamma = 1 + \frac{\sum_{\rm BSM} f_i\, Q_i^2\, A_{s_i}(\tau_i)}{\sum_{\rm SM} f_i\, Q_i^2\, A_{s_i}(\tau_i)}\,. \tag{2.44}$$

In the SM sum, we include the $W^\pm$ bosons, the top, bottom, charm quarks, and the tau lepton. Contributions from other charged SM particles are negligible due to their tiny form factors.

For the experimental constraints on κ_γ, we use the most recent ATLAS and CMS measurements. In particular, we use each collaboration's joint fit to κ_γ, which holds in the absence of deviations to tree-level Higgs couplings and untagged/invisible Higgs decay width. Upon neglecting these small effects, the 2σ allowed region from ATLAS

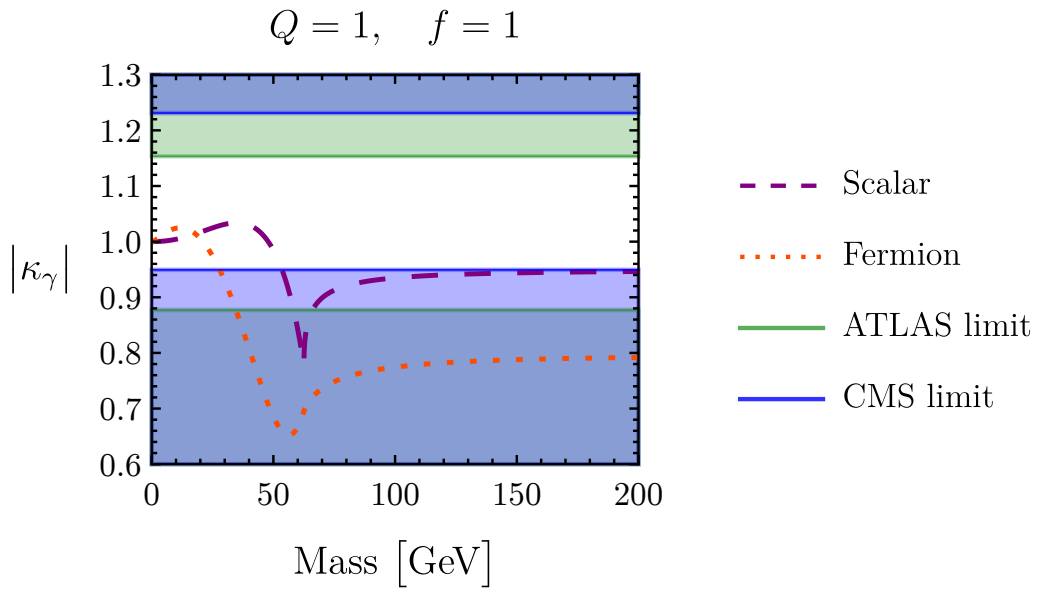

Figure 2.3: The contribution to $|\kappa_\gamma|$ from the addition of a new charge-1 complex scalar or Dirac fermion getting all of its mass from electroweak symmetry breaking as a function of the mass of the new particle. Limits on $|\kappa_\gamma|$ from the ATLAS [26] and CMS [27] collaborations are shaded.

is $|\kappa_\gamma| \in (0.877, 1.15)$ [26], while CMS finds $|\kappa_\gamma| \in (0.949, 1.23)$ [27]. In Fig. 2.3, we show these bounds against contributions from a typical scalar or fermion Loryon. Note in particular that for a BSM Loryon heavier than the Higgs, the relevant asymptote in Eq. (2.43) is already effective. Nevertheless, a larger deviation of $|\kappa_\gamma|$ happens near the threshold mass $m_i = m_h/2$.

Current bounds on $|\kappa_\gamma|$ constrain the sum of the contributions from BSM Loryons,

$$\sum_{\text{BSM}} f_i \, Q_i^2 \, A_{s_i}(\tau_i) \quad \to \quad -\frac{1}{3} \sum_{\text{BSM}} \eta_i \, f_i \, Q_i^2 \,, \tag{2.45}$$

with $\eta_i = 1\,(4)$ for scalars (fermions). One way to satisfy the experimental constraints is of course to ensure that the contribution in Eq. (2.45) sufficiently small. However, there is a second way to satisfy the constraint. Note that the SM contribution to κ_γ is dominated by $W^\pm$ bosons; contributions from BSM scalar and fermionic Loryons (if heavier than

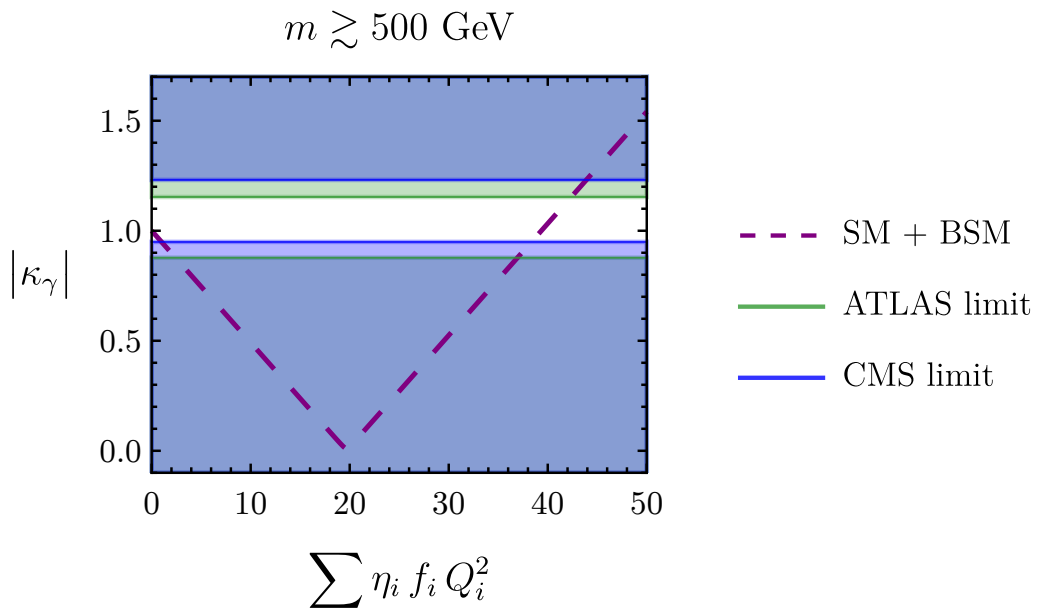

Figure 2.4: The contribution to $|\kappa_\gamma|$ from new particles heavier than ~ 500 GeV as a function of their fraction f_i of mass from EWSB and their electric charge Q_i; $\eta_i = 1\,(4)$ for complex scalars (fermions). Large values of $\sum_i \eta_i f_i Q_i^2$ are sufficient to flip the sign of κ_γ while maintaining the same magnitude. ATLAS and CMS limits are shaded.

half the Higgs mass) would come with an opposite sign compared to this dominant piece in the SM sum. Therefore, there is also a viable window where the magnitude of the second term in Eq. (2.44) becomes big enough to flip the sign of (the real part of) κ_γ, while keeping the magnitude close to the SM-only result. This is illustrated in Fig. 2.4.

To summarize, requiring BSM Loryons to satisfy both the ATLAS and CMS bounds on the $h\gamma\gamma$ coupling measurements, we find the constraints

$$\sum_i \eta_i f_i Q_i^2 < 0.995 \qquad \text{or} \qquad \sum_i \eta_i f_i Q_i^2 \in (38.4, 42.4)\,, \tag{2.46}$$

for asymptotically heavy BSM Loryons, with $\eta_i = 1\,(4)$ for complex scalars (fermions). If the BSM Loryons are not asymptotically heavy, they will contribute more. Therefore, for lighter Loryons, the first limit would become stronger while the second would shift to a window with lower values (see Fig. 2.8).

Field	$[1,1]_1$	$[2,2]_0$	$[3,3]_0$	$[2,3]_{-1/2}$	$[2,1]_{1/2} \oplus [1,2]_{1/2}$	$[1,3]_0 \oplus [2,2]_0$
$\sum \eta_i Q_i^2$	1	1	6	7	8	16

Table 2.3: Values of $\sum \eta_i Q_i^2$ for some possible BSM Loryons with $f_{\max} = 1$. The first four entries are scalars; the last two are fermions.

Scalar Scorecard

	$R=1$	2	3	4	5	6	7	8
$L=1$	$\lvert Y_{max}\rvert = 1, \sim 3$	$\frac{1}{2}, \sim \frac{5}{2}$	$0, \sim 2$	$\sim \frac{3}{2}$	~ 1	$\sim \frac{1}{2}$	~ 0	$\times$
2	$\frac{1}{2}, \sim \frac{7}{2}$	$1, \sim 4$	$\frac{3}{2}, \sim \frac{7}{2}$	$1, \sim 3$	$\frac{1}{2}, \sim \frac{3}{2}$	1	$\frac{1}{2}$	0
3	$0, \sim 3$	$\frac{3}{2}, \sim \frac{7}{2}$	$1, \sim 2$	$\frac{1}{2}, \sim \frac{3}{2}$	$0, \sim 1$	$\frac{1}{2}$	0	$\times$
4	$\sim \frac{7}{2}$	$1, \sim 3$	$\frac{1}{2}, \sim \frac{3}{2}$	~ 1	$\sim \frac{1}{2}$	~ 0	$\times$	$\times$
5	~ 3	$\frac{1}{2}, \sim \frac{3}{2}$	$0, \sim 1$	$\sim \frac{1}{2}$	~ 0	$\times$	$\times$	$\times$
6	$\sim \frac{5}{2}$	1	$\frac{1}{2}$	~ 0	$\times$	$\times$	$\times$	$\times$
7	~ 2	$\frac{1}{2}$	0	$\times$	$\times$	$\times$	$\times$	$\times$
8	$\sim \frac{3}{2}$	0	$\times$	$\times$	$\times$	$\times$	$\times$	$\times$

Table 2.4: The representations of scalar BSM Loryons still viable after considering constraints on κ_γ. A $\sim$ means the representation requires flipping the sign of κ_γ.

Values of $\sum_i \eta_i Q_i^2$ for select Loryons are listed in Table 2.3. The impact of the constraints in Eq. (2.46) on scalar and fermionic Loryons in various custodial irreps is indicated by the "scorecards" of Table 2.4 and Table 2.5, respectively. (In what follows, these scorecards will be updated as successive constraints are taken into account.) If the new Loryons receive all or almost all of their mass from their coupling to the Higgs, the first limit in Eq. (2.46) can be satisfied by adding at most one charge-1 scalar (and possibly some neutral particles). It can also be satisfied by adding a scalar representation with a large mass splitting. Since the largest representation of the unbroken $SU(2)_V$ receives a

Vector-like Fermion Scorecard

	$R=1$	2	3	4	5	6	7	8
$L=1$	$\lvert Y_{max}\rvert = 0, \sim 2$	$\sim \frac{3}{2}$	~ 1	$\times$	$\times$	$\times$	$\times$	$\times$
2	$\sim \frac{3}{2}$	$0, \sim 2$	$\sim \frac{3}{2}$	~ 1	$\times$	$\times$	$\times$	$\times$
3	~ 1	$\sim \frac{3}{2}$	~ 0	$\times$	$\times$	$\times$	$\times$	$\times$
4	$\times$	~ 1	$\times$	$\times$	$\times$	$\times$	$\times$	$\times$
5	$\times$	$\times$	$\times$	$\times$	$\times$	$\times$	$\times$	$\times$
6	$\times$	$\times$	$\times$	$\times$	$\times$	$\times$	$\times$	$\times$
7	$\times$	$\times$	$\times$	$\times$	$\times$	$\times$	$\times$	$\times$
8	$\times$	$\times$	$\times$	$\times$	$\times$	$\times$	$\times$	$\times$

Table 2.5: The representations and corresponding fields for the vector-like fermionic BSM Loryons still viable after considering constraints on κ_γ. A $\sim$ means the representation requires flipping the sign of κ_γ.

mass shift opposite in sign to the others, a large mass splitting will drive the value of f_V towards 0 for the particles in the largest representation, thereby satisfying the limit on κ_γ. Other possibilities, including larger electroweak representations, representations with larger hypercharge, and fermionic representations, make a large enough contribution to Eq. (2.45) that flipping the sign of κ_γ is required. Among other things, this implies that the only way for fermionic Loryons to satisfy constraints on κ_γ is to flip the sign, as indicated in Table 2.5.

Field	$\omega_{\lvert 3Y\rvert}$	$\Pi_{\lvert 6Y\rvert}$	$P_{\lvert 3Y\rvert}$
$\sum \eta_i C_i$	$1/2$	1	2
$\sum \eta_i Q_i^2$	$3Y^2$	$6Y^2 + 3/2$	$12Y^2$

Table 2.6: Values of $\sum \eta_i Q_i^2$ and $\sum \eta_i C_i$ for some possible new SM representations.

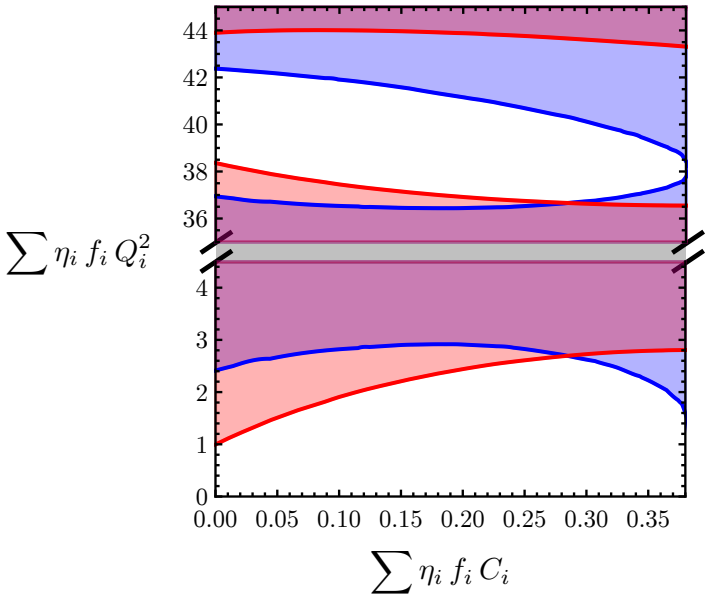

Figure 2.5: The allowed electric charge Q_i as a function of the color charges C_i of new fields due to $\kappa_\gamma - \kappa_g$ constraints. ATLAS constraints [26] are shaded blue, CMS constraints [27] are shaded red.

2.2.3 hgg Coupling

As with κ_γ, we can compute κ_g for a particular BSM model simply using (see Eq. (2.40))

$$\kappa_g = 1 + \frac{\sum_{\text{BSM}} f_i\, C_i\, A_{s_i}(\tau_i)}{\sum_{\text{SM}} f_i\, C_i\, A_{s_i}(\tau_i)}\,. \tag{2.47}$$

In the SM sum, we include the top, bottom, and charm quarks; contributions from other quarks are negligible due to their tiny form factors. For κ_g, BSM scalar and fermionic Loryons (if heavier than half the Higgs mass) contribute with the same sign as the dominant piece (from the top quark) in the SM sum, so there is no flipping sign option

and the sum of the BSM Loryon contributions must not be too large. We constrain these contributions at the 2σ level using the results from ATLAS and CMS expressed in the κ_γ vs κ_g plane [26, 27], again neglecting deviations to tree-level Higgs couplings and new untagged or invisible Higgs decay width. The bounds are translated into the constraints on the $\sum \eta_i f_i Q_i^2$ vs $\sum \eta_i f_i C_i$ plane in Fig. 2.5. We find that these constraints essentially exclude all colored Loryons, except for scalar Loryons of the SM representations $(3,1)_Y$ with $|Y| \leq 1$, as summarized in Table 2.6.

2.2.4 $h \to$ invisible or untagged

Loryons lighter than half the Higgs mass will also make new channels for the Higgs to directly decay at the tree level. For each scalar Loryon ϕ or Dirac fermion Loryon ψ, the partial width is

$$\Gamma_{h\to\phi\phi^{(\dagger)}} = f_\phi^2 \frac{G_F\, m_h\, m_\phi^2}{2^\rho \cdot 8\sqrt{2}\,\pi} \frac{4\, m_\phi^2}{m_h^2} \left(1 - \frac{4\, m_\phi^2}{m_h^2}\right)^{1/2}, \tag{2.48a}$$

$$\Gamma_{h\to\psi\bar{\psi}} = f_\psi^2 \frac{G_F\, m_h\, m_\psi^2}{4\sqrt{2}\,\pi} \left(1 - \frac{4\, m_\psi^2}{m_h^2}\right)^{3/2}. \tag{2.48b}$$

Constraints on new Higgs decay channels depend on the properties and fate of the new particles. If the particle is neutral and detector stable, or if it decays promptly into neutral and detector-stable final states, it would contribute to the Higgs invisible decay width. If it decays promptly into visible final states, it generally contributes to the Higgs "untagged" decay width, which is less constrained than the invisible width (though sufficiently distinctive final states can lead to stronger constraints). There are more exotic possibilities, such as long-lived decays, but these are typically more strongly constrained than invisible or untagged decays. For the purposes of the current discussion, we assume that Loryons which are lighter than half the Higgs mass contribute to the "untagged"

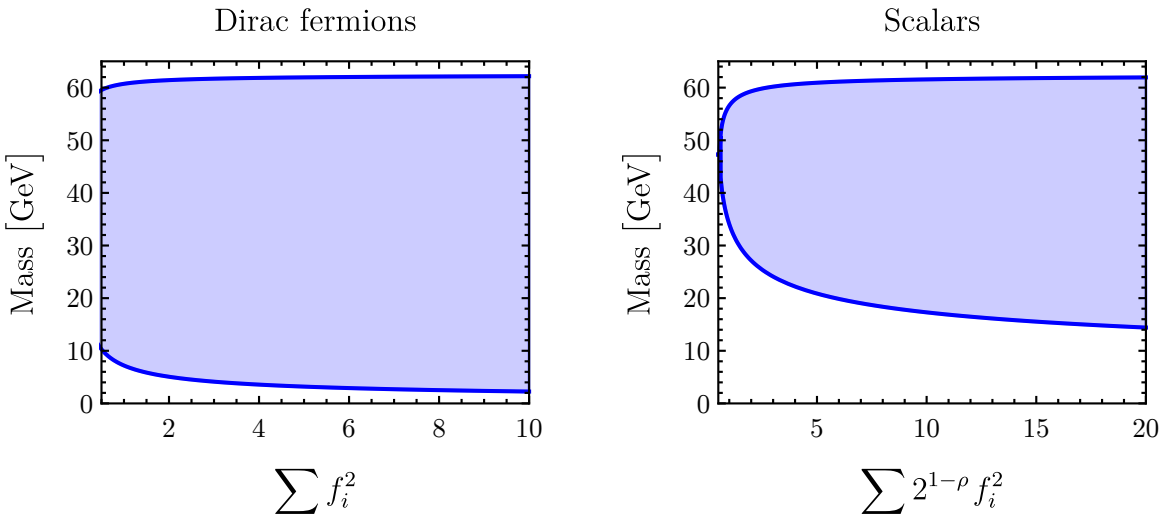

Figure 2.6: Allowed region (unshaded) in the mass vs $\sum f_i^2$ $\left(\sum 2^{1-\rho} f_i^2\right)$ plane for new Dirac fermion (scalar) particles whose mass is less than half the Higgs mass, arising from the upper limit on the Higgs branching ratio to 'untagged'. The plot assumes all new particles have the same mass.

decay width of the Higgs. In this case, the branching ratio to the new decay channels must be less than 0.47 [27], which constrains the size of the BSM Loryon contribution to the Higgs partial widths in Eq. (2.48). For fixed values of f_i^2, the mass of the Loryon has to be either small enough or close enough to the kinematic threshold, such that the partial width is not too big. Allowed regions for scalar and fermionic Loryon are shown in Fig. 2.6.

2.3 Precision Electroweak Constraints

Extending the SM with new particles that carry electroweak quantum numbers could potentially be subject to strong constraints from electroweak precision measurements. In the case of the BSM Loryon models studied here, the oblique framework [28, 29] is a good approximation since they interact with SM primarily through the Higgs and gauge bosons. The leading order (one-loop) corrections therefore modify the electroweak gauge

boson self-energies, which up to $\mathcal{O}(p^4)$ can be parameterized by the seven (extended) electroweak parameters S, T, U, V, W, X, Y [30, 31, 32, 33]. Among these seven parameters, S, T, W, Y arguably capture the most important effects as they are the leading ones in their respective symmetry classes [33]. Since we are considering custodially symmetric BSM Loryon models, the correction to T (and also its higher $\mathcal{O}(p^2)$ analog U) vanishes at one loop order. This leaves us to focus on the parameters S, W, and Y:

$$S = -\frac{4\cos\theta_W \sin\theta_W}{\alpha}\,\Pi'_{3B}(p^2=0)\,, \tag{2.49a}$$

$$W = -\frac{1}{2}\,m_W^2\,\Pi''_{33}(p^2=0)\,, \tag{2.49b}$$

$$Y = -\frac{1}{2}\,m_W^2\,\Pi''_{BB}(p^2=0)\,, \tag{2.49c}$$

where the Πs are the gauge boson self energies, primes denoting differentiation with respect to p^2.

For a scalar Loryon of the custodial irrep $[L,R]_Y$, we find its contributions given by

$$\Delta S = \frac{2}{\pi}\sum_{i,j=1}^{n} T^3_{ij}\,Y_{ji}\,\Pi'_S\left(m_i, m_j\right)\,, \tag{2.50a}$$

$$\Delta W = m_W^2\,\frac{g_2^2}{16\pi^2}\sum_{i,j=1}^{n} T^3_{ij}\,T^3_{ji}\,\Pi''_S\left(m_i, m_j\right)\,, \tag{2.50b}$$

$$\Delta Y = m_W^2\,\frac{g_1^2}{16\pi^2}\sum_{i,j=1}^{n} Y_{ij}\,Y_{ji}\,\Pi''_S\left(m_i, m_j\right)\,, \tag{2.50c}$$

where $n = LR$ denotes the total number of components of the Loryon, and the scalar form factors are

$$\Pi'_S\left(m_i, m_j\right) = \frac{1}{2^{\rho_i}}\int_0^1 \mathrm{d}x\left[x(1-x)\log\frac{\mu^2}{x m_i^2 + (1-x)m_j^2}\right], \tag{2.51a}$$

$$\Pi''_S\left(m_i, m_j\right) = \frac{1}{2^{\rho_i}} \int_0^1 \mathrm{d}x \, \frac{x^2(1-x)^2}{x m_i^2 + (1-x) m_j^2} \,. \tag{2.51b}$$

Note that T^3_{ij} and Y_{ij} are (elements of) the SM generators in the mass basis of the Loryon representation, which are generically not diagonal due to the mass mixings among different gauge eigenstates.

We see that ΔS is only nonzero due to the mass splitting among the Loryon components, namely that $\Pi'_S\left(m_i, m_j\right)$ is not the same for all i, j; terms that are independent of i, j (such as the RG scale μ dependence) will drop upon the sum, as they yield $\mathrm{tr}\left(T^3\, Y\right) = 0$. On the other hand, ΔW and ΔY do not depend on the mass splitting, and can in principle constrain any custodial irrep of Loryons. However, their values are typically more than one order of magnitude smaller than ΔS, due to a combination of the extra mass suppression factor m_W^2/m_i^2, and the smallness of the form factor in Eq. (2.51b). This makes the current constraints from W and Y parameters [34] numerically unimportant for the Loryon mass range of our interest.

Moving on to the fermionic cases, we focus on the S parameter. We find that a pair of fermionic Loryons of the custodial irreps $[L_1, R_1]_Y$ and $[L_2, R_2]_Y$ contribute to S as

$$\Delta S = \frac{4}{\pi} \sum_{i,j=1}^{n} T^3_{ij}\, Y_{ji} \left[\xi_\Sigma\, \Pi'_{F,\,\Sigma}\left(m_i, m_j\right) + \xi_\Delta\, \Pi'_{F,\,\Delta}\left(m_i, m_j\right) \right] , \tag{2.52}$$

with $n = L_1 R_1 + L_2 R_2$ denoting the total number of Dirac fermions and the form factors

$$\Pi'_{F,\,\Sigma}\left(m_i, m_j\right) = \int_0^1 \mathrm{d}x \left[2 \log \frac{\mu^2}{x m_i^2 + (1-x) m_j^2} - 1 \right] x(1-x) \,, \tag{2.53a}$$

$$\Pi'_{F,\,\Delta}\left(m_i, m_j\right) = \int_0^1 \mathrm{d}x \, \frac{m_i m_j}{x m_i^2 + (1-x) m_j^2}\, x(1-x) \,. \tag{2.53b}$$

Rep	$[2,2]_0$	$[3,3]_0$	$[4,4]_0$	$[2,4]_0$	$[2,3]_{-1/2}$
Allowed $r_{\rm split}$	$(-.67, 1.98)$	$(-.25, .28)$	$(-.05, .05)$	$(-.36, .44)$	$(-.46, .58)$

Table 2.7: Examples of the magnitude of allowed mass-splitting Eq. (2.16) if a particular scalar representation is the only new field contributing to S parameter.

Rep	$[2,1],[1,2]_{1/2}$	$[2,2],[1,1]_0$	$[2,3],[1,2]_{1/2}$
Allowed $f_{\rm max}$	$(.66, 1)$	$\emptyset$	$(.51, .58)$
$\sum \eta_i f_i Q_i^2$	$(11, 8)$	$\emptyset$	$(207, 17)$
Rep	$[3,1],[2,2]_0$	$[1,3],[2,2]_0$	$[3,2],[2,3]_{1/2}$
Allowed $f_{\rm max}$	$(.71, 1)$	$(.71, 1)$	$(.68, .81)$
$\sum \eta_i f_i Q_i^2$	$(19, 16)$	$(19, 16)$	$(109, 61)$

Table 2.8: Examples of the allowed $f_{\rm max}$ for new fermionic fields if they are the only new contribution to the S parameter. Also shown is the range of values of $\sum \eta_i f_i Q_i^2$ for the given range of $f_{\rm max}$. The vector-like mass is taken to be the same for both fermions involved in the Yukawa interaction; this gives a weaker bound than allowing two different vector-like masses.

Here our notation in Eq. (2.52) allows for a generic coupling between a Dirac fermion ψ and a gauge boson V,

$$\mathcal{L} \supset g\, \bar{\psi}\, \gamma^\mu \left(\xi_V - \xi_A \gamma^5\right) t^a\, \psi\, V_\mu^a\,, \tag{2.54}$$

and ξ_Σ (ξ_Δ) tracks the contributions from vertex insertions with the same (opposite) chiralities,

$$\xi_\Sigma = \xi_{1,V}\xi_{2,V} + \xi_{1,A}\xi_{2,A}\,, \qquad \xi_\Delta = \xi_{1,V}\xi_{2,V} - \xi_{1,A}\xi_{2,A}\,. \tag{2.55}$$

Applying it to our case of vector-like fermions, we can aggregate the contributions from all the chiral component insertions which all share the same form of the generator; this effectively leads us to plugging in $\xi_\Sigma = \xi_\Delta = 1$.

We take the current 2σ bound on S to be 0.14 [35]. Note that this corresponds to the projection of the combined S, T fit onto the S axis, rather than the 2σ bound on S with

Scalar Scorecard

	$R=1$	2	3	4	5	6	7	8
$L=1$	$\lvert Y_{max}\rvert = 1, \sim 3$	$\frac{1}{2}, \sim \frac{5}{2}$	$0, \sim 2$	$\sim \frac{3}{2}$	~ 1	$\sim \frac{1}{2}$	~ 0	$\times$
2	$\frac{1}{2}, \sim \frac{7}{2}$	$1, \sim 4$	$\frac{1}{2}, \sim \frac{7}{2}$	$0, \sim 3$	$\sim \frac{3}{2}$	~ 1	$\sim \frac{1}{2}$	~ 0
3	$0, \sim 3$	$\frac{1}{2}, \sim \frac{7}{2}$	$0, \sim 2$	$\sim \frac{3}{2}$	~ 1	$\sim \frac{1}{2}$	~ 0	$\times$
4	$\sim \frac{7}{2}$	$0, \sim 3$	$\sim \frac{3}{2}$	~ 1	$\sim \frac{1}{2}$	~ 0	$\times$	$\times$
5	~ 3	$\sim \frac{3}{2}$	~ 1	$\sim \frac{1}{2}$	~ 0	$\times$	$\times$	$\times$
6	$\sim \frac{5}{2}$	~ 1	$\sim \frac{1}{2}$	~ 0	$\times$	$\times$	$\times$	$\times$
7	~ 2	$\sim \frac{1}{2}$	~ 0	$\times$	$\times$	$\times$	$\times$	$\times$
8	$\sim \frac{3}{2}$	~ 0	$\times$	$\times$	$\times$	$\times$	$\times$	$\times$

Table 2.9: The representations of scalar BSM Loryons still viable after considering constraints on S. A $\sim$ means the representation is not viable on its own but can be added together with other BSM representations to flip the sign of κ_γ.

$T = 0$, which would lead to a tighter bound. Although we focus on custodial multiplets to minimize contributions to T, small amounts of soft custodial symmetry breaking in the explicit mass terms allow most of the positive region of the S, T ellipse to be explored. For each choice of representation, we consider the limits placed by requiring that the contribution to S from the Loryons obey this bound.[9]

For **scalars**, the contribution to S is only non-zero if there is a mass splitting among the Loryon states. We therefore report the magnitudes of allowed mass splitting among scalar Loryons in Table 2.7. This is expressed in terms of the parameter r_{split}, a rescaling of $\lambda'_{h\Phi}$ defined in Sec. 2.1.1. Table 2.9 shows the scalar Loryons which remain viable after applying the constraint from the S parameter.

[9]We emphasize that it is possible to go beyond our minimal models to include multiple Loryons that are in various representations. In particular, a representation can yield a negative contribution to S, and so it is possible to exceed the limits in Table 2.7 and Table 2.8 with judicious choice of representations.

Vector-like Fermion Scorecard

	$R=1$	2	3	4	5	6	7	8
$L=1$	$\lvert Y_{max}\rvert=\times$	$\sim\frac{3}{2}$	~ 1	$\times$	$\times$	$\times$	$\times$	$\times$
2	$\sim\frac{3}{2}$	~ 1	$\sim\frac{1}{2}$	$\times$	$\times$	$\times$	$\times$	$\times$
3	~ 1	$\sim\frac{1}{2}$	$\times$	$\times$	$\times$	$\times$	$\times$	$\times$
4	$\times$	$\times$	$\times$	$\times$	$\times$	$\times$	$\times$	$\times$
5	$\times$	$\times$	$\times$	$\times$	$\times$	$\times$	$\times$	$\times$
6	$\times$	$\times$	$\times$	$\times$	$\times$	$\times$	$\times$	$\times$
7	$\times$	$\times$	$\times$	$\times$	$\times$	$\times$	$\times$	$\times$
8	$\times$	$\times$	$\times$	$\times$	$\times$	$\times$	$\times$	$\times$

Table 2.10: The representations and corresponding fields for the vector-like fermion BSM Loryons still viable after considering constraints on S. A $\sim$ means the representation is not viable on its own but can be added together with other BSM representations to flip the sign of κ_γ.

For **fermions**, the situation is more complicated. The Yukawa interaction couples two different representations, so even if there is no vector-like mass and no mass splitting, there can be a significant contribution to S. It is straightforward to interpret the constraints in terms of $f_{\max}$, and this is presented in Table 2.8. There are generally a number of large individual contributions to S which manage to cancel each other. These possibilities can then be ruled out by other constraints. If the lightest mass eigenvalue coupled to the Higgs is less than half the Higgs mass, the scenario is ruled out by Higgs decay constraints. If the lightest mass eigenvalue is greater than half the Higgs mass, the constraint comes from κ_γ. This motivates also presenting the results in terms of $\sum \eta f Q^2$, to make the interplay with constraints on κ_γ clear.[10] Some examples of the range of al-

[10]Note that this is in fact an underestimate of the contribution to κ_γ, since the constraint on $\sum \eta f Q^2$ is for asymptotically heavy particles and lighter particles give a larger contribution than asymptotically

lowed $f_{\max}$ for fermionic Loryons are summarized in Table 2.8, and the scorecard showing those fermionic Loryons which remain viable is presented in Table 2.10.

2.4 Direct Search Constraints

We now turn to consider constraints from direct searches on the Loryon candidates that remain viable when confronted by the indirect constraints studied above. In contrast to indirect bounds, direct bounds are strongly sensitive to Loryon couplings to SM particles other than the Higgs as these interactions typically govern the final state that would be observed at colliders. Our aim here is not to consider all possible direct limits on all possible spectra and couplings but rather to understand the qualitative parameter space allowed by direct searches under generic assumptions.

As noted in Sec. 2.1, we have restricted our attention to Loryon candidates whose hypercharge assignments allow all BSM charged particles to decay into SM final states through either marginal or irrelevant interactions. This is because heavy stable charged particles (HSCPs) are strongly constrained by LHC searches for anomalous ionization energy loss and time of flight, with current bounds above the TeV scale for HSCPs carrying a range of quantum numbers [36, 37, 38]. Although bounds are somewhat weaker on scalars carrying only hypercharge (around 430 GeV per [38]), these limits are still considerably stronger than the corresponding limits on their promptly-decaying counterparts.

For Loryons neutral under $SU(2)_L$, we identify the lowest-dimensional operators that would allow such decays and assume that (1) all allowed decay operators of the lowest nontrivial dimension are present, and (2) Loryon decays are dominated by the combination of these operators giving the weakest bound. We do not require the decay couplings

heavy ones. Properly considering the effect of particles which are not asymptotically heavy on κ_γ does not meaningfully extend the bound past the region excluded by Higgs decays.

to respect custodial symmetry as these couplings may be numerically quite small – consistent with bounds on custodial symmetry violation – while still allowing for prompt decays. In the same spirit, we assume the decay couplings are small enough that they do not provide significant new production modes. In many cases, the leading operators carry SM flavor indices; we assume the flavor structure is such that strong flavor-dependent constraints (from e.g. flavor-changing neutral currents or proton decay) are avoided. In many cases, the bound on a given Loryon candidate depends on the flavor composition of the final state; in quoting a limit we highlight the flavor structure that results in the weakest limit.

For Loryons charged under $SU(2)_L$, there are typically one or more electrically neutral particles in the multiplet that may be the lightest mass eigenstate. In this case, the charged components of the multiplet can decay into the neutral component and SM bosons without assuming any additional couplings. This leads to a missing energy signature whose strength depends sensitively on the mass spectrum of the new particles, with large splittings leading to correspondingly larger (and better-constrained) missing energy signals. In such cases, the bounds on $SU(2)_L$-charged Loryons are typically weakest if no additional interactions are assumed beyond the irreducible couplings to the Higgs.

For scalar Loryons, the bounds from precision electroweak constraints can be avoided by minimizing the mass splitting within a given electroweak multiplet, in which case gauge eigenstates are also approximate mass eigenstates. As such, in determining the state of direct limits on scalar Loryons, it suffices to consider searches for distinct $SU(3)_c \times SU(2)_L \times U(1)_Y$ representations. An approximate direct limit on scalar Loryons in a given custodial representation can then be found by stacking the limits on the $SU(3)_c \times SU(2)_L \times U(1)_Y$ representations that compose the custodial multiplet.

For fermionic Loryons, electroweak symmetry breaking mixes components of different gauge eigenstates, so that gauge eigenstates are no longer approximate mass eigen-

states. Moreover, as a custodial multiplet of fermionic Loryons necessarily contains a field charged under $SU(2)_L$, the strength of direct search limits depends sensitively on the mass splitting between the lightest neutral fermion and heavier fermions, which controls the amount of missing energy in the final state. As such, obtaining the direct limit on fermionic Loryons in a given custodial multiplet requires reinterpreting the relevant searches in the space of couplings for that multiplet. We first present the simpler direct limits on scalar Loryons before treating the more complicated direct limits on fermionic Loryons.

Note that direct search limits on Loryons can be further modified in the presence of couplings between multiple Loryon states. Such couplings can lead to cascade decays into final states different from those we have considered here. The effect of multiple coupled Loryons on direct search constraints depends sensitively on the states involved; cascade decays can either weaken constraints (for example, by softening missing energy signals in the spirit of Stealth Supersymmetry [39]) or strengthen them (by increasing the multiplicity or distinctiveness of the final state). To the extent that these variations are not irreducible signals of BSM Loryons, we leave their study to future work.

2.4.1 Scalar Loryons

The state of direct search limits on the $SU(3)_C \times SU(2)_L \times U(1)_Y$ representations of states that appear as components of the viable custodial multiplets of scalar Loryons is summarized in Table 2.11, subject to the above considerations.

The neutral scalar S need not possess additional couplings that would allow it to decay, leading to a missing energy signature if it remains stable on detector length scales. We assume that it does not couple linearly to invariants constructed purely from the Higgs doublet H as this would lead to mass mixing with correspondingly tighter constraints.

Field	Charge	Decay Couplings	Limit	Ref.
S	$(1,1)_0$	– or $S \times \mathcal{O}_4^{\rm SM}$	–	[40]
S_1	$(1,1)_1$	$S_1^\dagger \bar{L}_i i\sigma_2 L_j^c$	~ 325 GeV	[41]
ω_1	$(3,1)_{-1/3}$	$\omega_1^\dagger \left(\bar{Q} i\sigma_2 Q^c + \bar{d}u^c\right)$	~ 520 GeV	[42]
ω_2	$(3,1)_{+2/3}$	$\omega_2^\dagger \bar{d} d^c$	~ 520 GeV	[42]
Φ_1	$(1,2)_{1/2}$	– (if inert)	~ 70 GeV	[43]
Ξ_0	$(1,3)_0$	Mixing via $\Xi^a H^\dagger \sigma^a H$	~ 230 GeV	[44]
		– (if inert)	~ 275 GeV	[45]
Φ_3	$(1,2)_{3/2}$	$(\Phi_3^\dagger) H \bar{d} u$	~ 80 GeV	[46]
Ξ_1	$(1,3)_1$	$\Xi_1^I [\sigma^I \epsilon]_{\alpha\beta} H_\alpha^\dagger H_\beta^\dagger$	~ 350 GeV	[47]
Θ_1	$(1,4)_{1/2}$	$(\Theta_1^\dagger)_{(abc)} H^a H^b \tilde{H}^c$	$\gtrsim 350$ GeV	[47]
Θ_3	$(1,4)_{3/2}$	$(\Theta_3^\dagger)_{(abc)} H^a H^b H^c$	$\gtrsim 350$ GeV	[47]

Table 2.11: Assumed decay couplings and direct search limits on scalar Loryons organized by SM representation.

This leaves open the possibility that S may decay through dimension-5 operators in which S couples to dimension-4 gauge-invariant SM operators $\mathcal{O}_4^{\rm SM}$, excluding $\mathcal{O}_4^{\rm SM} = |H|^4$. When $m_S < m_h/2$, it may be produced in the decay of on-shell Higgs bosons and is subject to the constraints on the Higgs invisible or BSM width discussed in Sec. 2.2; the strength of these constraints depends on the fraction $f_{\rm max}$ of mass-squared that S acquires from the Higgs. As we account for these bounds in terms of Higgs coupling measurements rather than direct searches, we omit them in Table 2.11. For $m_S \geq m_h/2$, S is produced via off-shell Higgs bosons with a modest rate that remains essentially unconstrained by missing energy searches [40]. The low production rate is such that prompt decays through a variety of SM operators $\mathcal{O}_4^{\rm SM}$ are likewise unconstrained. The HL-LHC with 3/ab is not expected to attain sensitivity to off-shell production for $0.5 \leq f_{\rm max} \leq 1$.

The hypercharged scalar S_1 admits a marginal coupling to two lepton doublets, which is antisymmetric in flavor space due to the antisymmetry of the $SU(2)_L$ contraction. The quoted bound on S_1 in Table 2.11 is obtained in [41] from the reinterpretation of LHC slepton searches, most notably a $\sqrt{s} = 13$ TeV ATLAS analysis with 139/fb of data [48]. The detailed mass reach depends on the relative branching ratios into different lepton flavors; it is maximized at $m \sim 325$ GeV when $\text{BR}(S_1 \to e^+\nu) = 0.5(0), \text{BR}(S_1 \to \mu^+\nu) = 0(0.5)$ and minimized at $m \sim 200$ GeV when $\text{BR}(S_1 \to e^+\nu) = \text{BR}(S_1 \to \mu^+\nu) = 0.25$ using only the same-flavor bins (note that the sum of branching ratios into electrons and muons can never be less than 50%). However, we note that the ATLAS search also includes different-flavor bins, although these are not used in the single-slepton interpretation. These bins have comparable sensitivity to the same-flavor bins, and so we expect the limit from opposite-flavor final states to be comparable to those from same-flavor final states. We thus take the limit to be $m \sim 325$ GeV regardless of the relative branching ratios into electrons and muons. The projected HL-LHC bound with 3/ab is expected to reach $m \sim 400$ GeV under the same assumptions [41].

The colored and hypercharged scalars ω_1 and ω_2 admit marginal couplings allowing them to decay. The ω_1 has the quantum numbers of a leptoquark and can couple to SM fermion bilinears involving one lepton and one quark, as well as SM fermion bilinears consisting solely of quarks. Given the relatively stronger bounds on leptonic decays of colored particles, we assume that the branching ratios into quarks dominate. In contrast, the ω_2 only admits a marginal coupling to pairs of down-type quarks. Assuming that decays into quarks dominate, the quoted bound on ω_1 and ω_2 in Table 2.11 comes from a $\sqrt{s} = 13$ TeV CMS search with 36/fb for pair-produced resonances decaying to pairs of quarks [42], which excludes stops decaying into light-flavor quarks up to $m \sim 520$ GeV. We are currently unaware of projections for the performance of this search at the HL-LHC.

The electroweak doublet scalar Φ_1 extends the Higgs sector to a two Higgs doublet model, with a range of signatures and constraints depending on the parameters of the potential and couplings to fermions. However, a simple irreducible limit may be obtained by treating Φ_1 as inert, forbidding renormalizable couplings to fermions by imposing the discrete symmetry $\Phi_1 \leftrightarrow -\Phi_1$ and assuming the potential is such that Φ_1 does not acquire a vev. Although Φ_1 admits a range of marginal couplings that would allow it to decay, these may be forbidden by the discrete symmetry. The lightest mass eigenstate is typically a neutral scalar, which can be stable on detector length scales. The charged components of Φ_1 are split from the lightest neutral component by both tree-level and one-loop effects; the former effects are bounded by perturbativity constraints, while the latter lead to splittings on the order of ~ 350 MeV. This leads to an experimentally challenging scenario in which the charged-neutral mass splitting is too small to produce distinctive decay products and significant missing energy, but too large to generate a long disappearing track. We take the inferred LEP bound of $m_{H^\pm} > 70$ GeV appearing in [43].

The electroweak triplet, hypercharge-neutral scalar Ξ_0 admits a marginal coupling $\Xi_0^a H^\dagger \sigma^a H$ that allows it to decay via mixing with the Higgs after electroweak symmetry breaking; this mixing can be sufficiently small to allow for prompt decays without running afoul of indirect constraints. In this case, [44] obtained a limit of $m \sim 230$ GeV by the reinterpretation of $\sqrt{s} = 13$ TeV ATLAS [49] and CMS [50] multi-lepton searches with 36/fb, noting that a naive extrapolation to results of the full Run 2 data set were expected to improve the bound to $m \sim 330$ GeV. Alternately, mixing may be forbidden by imposing the discrete symmetry $\Xi_0 \leftrightarrow -\Xi_0$, rendering it inert and the neutral component stable. In this case, the ~ 160 MeV radiative splitting between the charged and neutral components gives rise to a disappearing track signature, leading [45] to obtain a bound of $m \sim 275$ GeV by reinterpreting a $\sqrt{s} = 13$ TeV ATLAS search with 36/fb [51]. An

HL-LHC bound of ~ 520 GeV was projected by [45].

The electroweak doublet, hypercharge-3/2 scalar Φ_3 does not admit marginal couplings that would allow its doubly-charged or singly-charged components to decay. Rather, they may decay via operators coupling Φ_3 to a Higgs boson and two fermions [52]. If the dominant decay coupling involves leptons, strong constraints from same-sign dilepton searches imply $m \gtrsim 700 - 900$ GeV depending on the flavor composition of the leptonic branching ratios [53]. If the dominant decay coupling involves quarks, however, the electroweak production cross section is too small to be meaningfully constrained by the CMS paired dijet resonance search [42]. Instead, the leading bound arises from LEP searches for hadronically decaying singly-charged Higgses, of order $m \sim 80$ GeV [46].

The electroweak triplet, hypercharge-1 scalar Ξ_1 admits marginal couplings to either two same-sign leptons or two Higgs bosons. The former leads to a strong bound of $m \gtrsim 700 - 900$ GeV from same-sign dilepton searches [53], while the latter leads to a somewhat weaker constraint ~ 350 GeV from same-sign WW signals in multi-lepton searches [47]. The situation is similar for the electroweak quartet, hypercharge-1/2 or 3/2 scalars Θ_1 and Θ_3. Both admit renormalizable couplings to three Higgs bosons that lead to same-sign WW production similarly constrained by multi-lepton searches [47]. Note that the higher-dimensional $SU(2)_L$ representations have correspondingly larger cross sections, which we do not account for here; this has a modest effect on the mass limit.

2.4.2 Fermionic Loryons

As noted above, the significant mass mixing among different gauge eigenstates of fermionic Loryons in a given custodial multiplet requires a more detailed treatment of direct search limits. For each of the fermionic Loryon candidates that remains viable

after imposing indirect bounds, mass mixing leads to a split mass spectrum and qualitatively similar collider signatures: heavy mass eigenstates are pair produced via Drell-Yan before decaying into light mass eigenstates via the emission of W, Z, and Higgs bosons. The light mass eigenstates typically include both charged and neutral fermions that are degenerate at tree-level in the limit of exact custodial symmetry, but one-loop corrections induce small splittings that allow the light charged fermions to decay into their neutral counterparts plus soft SM particles. If the splittings are sufficiently small, the light charged fermions give rise to a distinctive disappearing track signature. If the splittings are somewhat larger, above about 400 MeV, the disappearing tracks are too short to be picked up in existing searches. For fermionic Loryons in larger custodial representations, the spectrum includes additional mass eigenstates intermediate between the light and heavy states. These can lead to two-step cascade decays with higher multiplicities of SM vector bosons in the final state.

To determine limits on fermionic Loryons coming from the decay of heavy mass eigenstates into lighter ones via W, Z, and h, we reinterpret a series of ATLAS and CMS electroweakino searches at $\sqrt{s} = 13$ TeV, namely the CMS search for two oppositely charged same-flavor leptons and missing transverse momentum [54] and the ATLAS search for three leptons from on-shell W, Z bosons plus missing transverse momentum [55], both of which are sensitive to pair production events in which one heavy eigenstate decays via a W boson and the other via a Z boson; the ATLAS [56] and CMS [57] searches for final states with one lepton, missing transverse momentum, and a Higgs decaying to $b\bar{b}$, are sensitive to pair production events in which one heavy eigenstate decays via a W boson and the other via a Higgs boson; and the ATLAS search for two leptons and missing transverse momentum [48] is sensitive to pair production events in which both heavy eigenstates decay via a W boson. For each of these searches, the collaborations present excluded cross sections for an exclusive channel as a function of the heavy and

light fermion masses, allowing for straightforward reinterpretation. Although both collaborations also pursue searches sensitive to pair production events with hh, ZZ, or hZ plus missing transverse momentum, these limits are presented as a function of the heavy mass assuming a (small) fixed value of the light mass, so we are unable to reinterpret these constraints in the full parameter space of interest. The reach of these searches is comparable to the corresponding limits of the searches we reinterpret. For larger custodial representations with additional mass eigenstates intermediate between the light and heavy states, we have estimated the sensitivity of ATLAS and CMS multi-lepton searches [58, 59] to the resulting multi-boson final states; we find that they do not significantly improve the limits set by searches for single-step decays into di-boson final states.

In addition, we must consider possible limits on the light mass eigenstates coming from disappearing track searches, which are controlled by the splitting between the lightest charged and neutral fermions. If the splitting is sufficiently small, the light charged fermions become long-lived, and the resulting disappearing track signature may provide an even stronger constraint on the parameter space. For the custodial multiplets under consideration, the splitting between the charged and neutral fermions depends on possible soft breaking of custodial symmetry at tree level, as well as two different types of one-loop corrections. At tree level, it is possible to softly break custodial symmetry by introducing different vector-like mass terms for the Standard Model representations within a given custodial multiplet. For example, in the $[2,1]_{1/2} \oplus [1,2]_{1/2}$ model, differences in the vector-like masses of the E_0 and E_1 fields comprising the $[1,2]_{1/2}$ custodial irrep will split the masses of the lightest charged and neutral fermions. In principle, a small soft breaking of custodial symmetry can always be introduced to generate a sufficiently large charged-neutral mass splitting to avoid constraints from disappearing track searches without significantly worsening precision electroweak constraints.

However, it is perhaps more compelling to assume exact custodial symmetry at tree

level and consider the two types of irreducible splitting due to radiative corrections. The first of these is the familiar finite radiative correction due to the Coulomb energy stored in the charged fields [60, 61]. The second is the logarithmically divergent radiative correction due to the breaking of custodial symmetry by hypercharge. The latter effect can be straightforwardly computed from *e.g.* the renormalization group evolution of the Loryons' vector-like masses and Yukawa couplings proportional to the hypercharge gauge coupling. For the $[2,1]_{1/2} \oplus [1,2]_{1/2}$ and $[1,3]_0 \oplus [2,2]_0$ models, the resulting one loop splitting between the lightest charged and neutral mass eigenvalues $m_1^\pm, m_1^0$ at leading logarithmic order is given by

$$m_1^\pm - m_1^0 \simeq \frac{3g'^2}{16\pi^2} m_1^0 \log\frac{\Lambda}{\mu}\,, \tag{2.56}$$

where Λ is a UV scale at which custodial symmetry is presumed to be exact and μ is the renormalization scale. The logarithmic enhancement of this effect causes it to dominate over the finite correction and for $\Lambda \gtrsim$ TeV yields a mass splitting large enough to evade current limits from disappearing track searches [62]. As such, the direct search limits on fermionic Loryons remain dominated by the decays of heavy mass eigenstates into light ones, even before including possible tree-level soft breaking of custodial symmetry.

In order to determine the bound on fermionic Loryons in a given custodial multiplet from these searches, we compute the leading-order production cross sections and branching ratios for the heavy mass eigenstates in a given multiplet using `FeynRules` [63], `FeynArts` [64], and `FormCalc` [65, 66] and compare the relevant production cross sections times branching ratios to the excluded cross section in each search. In doing so, we include decays into both charged and neutral fermions among the light mass eigenstates as the charged mass eigenstates subsequently decay into the neutral mass eigenstates plus additional soft particles that should not significantly impact the acceptance of the

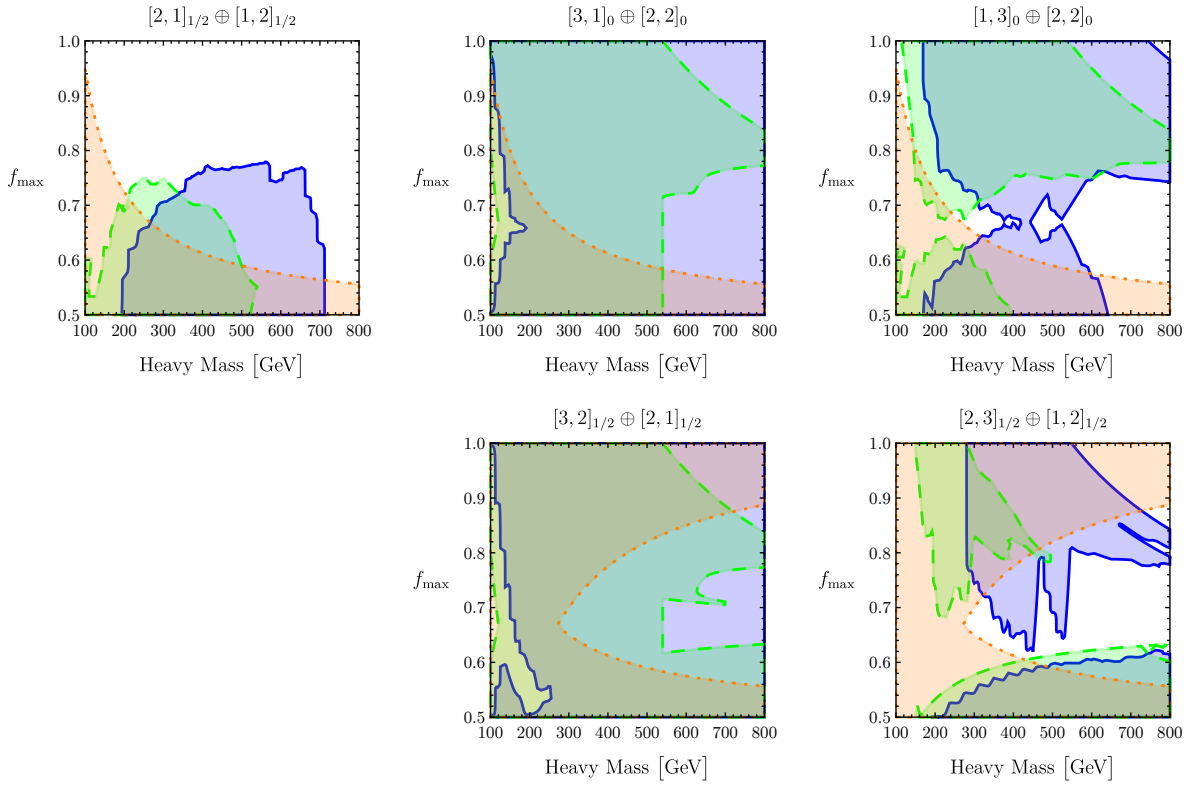

Figure 2.7: Exclusions on fermionic Loryons from LHC searches for missing energy plus WZ (blue, solid) or WW (green, dashed) bosons, along with the the LEP II bound (orange, dotted) on charged fermions, as a function of the mass of the heaviest fermions and the fraction $f_{\max}$ of their mass which is Higgs-dependent. Only combinations of custodial representations that remained viable after imposing the constraints in previous sections are shown.

searches in question. We further include the combined LEP bound on charged fermions [67], taking the limit to be $m^{\pm} \gtrsim 90$ GeV in light of the possible variations in the charged-neutral mass splitting [68]. The results are summarized in Fig. 2.7.

The parametric behavior of the limits in Fig. 2.7 can be most clearly understood for the $[2,1]_{1/2} \oplus [1,2]_{1/2}$ model shown in the first panel. The LHC searches are most sensitive when the splitting between heavy and light mass eigenstates is large, for this leads to the largest amount of missing energy. In the parameter space of Fig. 2.7, this corresponds to smaller values of $f_{\max}$, for which mass splittings are induced by competition between EWSB-dependent and -independent contributions. At lower values of the heavy mass,

the available phase space for producing electroweak bosons begins to close off, while at higher values of the heavy mass, the production cross section falls off. The shape of the LEP exclusion in this parameter space is set by the mass of the light mass eigenstates, which include a charged Dirac fermion; at lower values of $f_{\max}$ the large mass splitting drives the light mass eigenstates below the LEP bound, and less splitting is required to reach the LEP bound as the heavy mass decreases. The shape of the limits for larger custodial representations in the remaining panels of Fig. 2.7 is governed by the same logic but no longer takes a simple form in the plane of $f_{\max}$ and the heavy mass. This is because the higher-dimensional custodial representations lead to more than two clusters of mass eigenstates, so direct search limits are most sensitive to the splitting between intermediate and light mass eigenstates. The precise values of these splittings and the electromagnetic charges of the light eigenstates varies from multiplet to multiplet, leading to the observed pattern of exclusion regions.

2.5 Viable Loryons

Putting everything together, we may now address the animating question of this work: does current data allow for Loryons beyond the Standard Model? Surprisingly, a number of Loryon candidates remain viable in light of direct and indirect limits, although the situation is far more optimistic for scalar Loryons relative to their fermionic counterparts.

The current status of **scalar** Loryons is summarized in Fig. 2.8 and Fig. 2.9. The parameter space has particularly large regions of viability for the custodial representations $[1,1]_0, [2,2]_0, [1,3]_0$, and $[3,1]_0$ since the current direct search bounds on the SM singlet S_0, the charged singlet S_1, the bi-doublet Φ_1, and the hypercharge-neutral triplet Ξ_0 vary from essentially nonexistent to ~ 325 GeV, while the indirect bounds from Higgs coupling measurements are modest. Among the scalar Loryons, constraints from κ_γ

Vector-like Fermion Scorecard

	$R=1$	2	3	4	5	6	7	8
$L=1$	$\lvert Y_{\max}\rvert=\times$	$\sim\frac{1}{2}$	~ 0	$\times$	$\times$	$\times$	$\times$	$\times$
2	$\sim\frac{1}{2}$	~ 0	$\times$	$\times$	$\times$	$\times$	$\times$	$\times$
3	$\times$	$\times$	$\times$	$\times$	$\times$	$\times$	$\times$	$\times$
4	$\times$	$\times$	$\times$	$\times$	$\times$	$\times$	$\times$	$\times$
5	$\times$	$\times$	$\times$	$\times$	$\times$	$\times$	$\times$	$\times$
6	$\times$	$\times$	$\times$	$\times$	$\times$	$\times$	$\times$	$\times$
7	$\times$	$\times$	$\times$	$\times$	$\times$	$\times$	$\times$	$\times$
8	$\times$	$\times$	$\times$	$\times$	$\times$	$\times$	$\times$	$\times$

Table 2.12: The representations for the vector-like fermionic BSM Loryons still viable after considering direct search constraints. A $\sim$ means the representation is not viable on its own but can be added together with other BSM representations to flip the sign of κ_γ.

permit a charge-1 scalar Loryon without flipping the sign of κ_γ, but they narrowly exclude charged Loryons acquiring *all* of their mass from the Higgs. The custodial symmetry representations $[1,1]_0$, $[2,2]_0$, $[3,1]_0$, and $[1,3]_0$ each include a single charge-1 particle. For the $[1,1]_Y$ representation, constraints on κ_g leave open the possibility for the Loryon to be a color triplet. In addition, scalars in larger custodial representations can remain viable if sufficient mass splitting is introduced so that only a single charge-1 state has a significant coupling to the Higgs; this can be done for the representations $[3,3]_0$, $[2,4]_0$, and $[4,2]_0$ (see Fig. 2.9). Another avenue by which larger custodial representations can survive the bounds is to give them larger hypercharges; this yields enough charged particles to flip the sign of κ_γ. Direct searches place lower bounds on the masses ranging from $\sim$ one hundred to several hundred GeV, while perturbative unitarity places upper bounds on

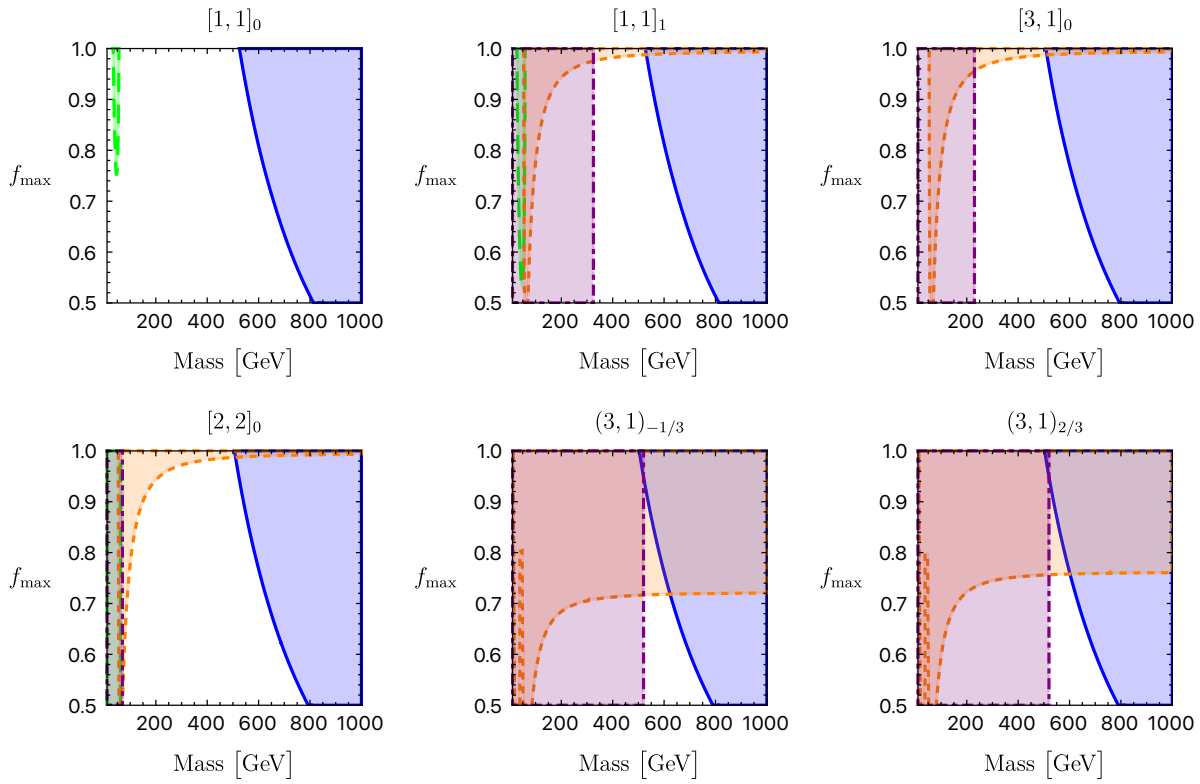

Figure 2.8: Regions of parameter space for scalar Loryons which are ruled out by one of the constraints described earlier. The orange, dotted region is ruled out by constraints on κ_γ or κ_g; the blue, solid region is ruled out by unitarity bounds; the green, dashed region is ruled out by constraints on Higgs decay; and the purple, dot-dashed region is ruled out by direct search bounds. All plots assume no mass splitting between the components of the Loryon multiplet, which is a non-trivial assumption for $[2,2]_0$. Note that the bottom middle and right plots are indicated by their SM gauge quantum numbers.

their mass to be at most ~ 800 GeV.

The current status of **fermionic** Loryons is summarized in Fig. 2.10. In contrast with the scalar case, the viable parameter space is much more tightly constrained. As noted above, fermionic Loryons are only viable if the model results in flipping the sign of κ_γ. While any individual custodial multiplet is insufficient to achieve this, flipping the sign of κ_γ can occur if there are multiple copies of a given multiplet. However, these additional copies increase the contribution to the S-parameter such that the constraints of κ_γ and S cannot be simultaneously satisfied by multiple copies of a given multiplet. We conclude

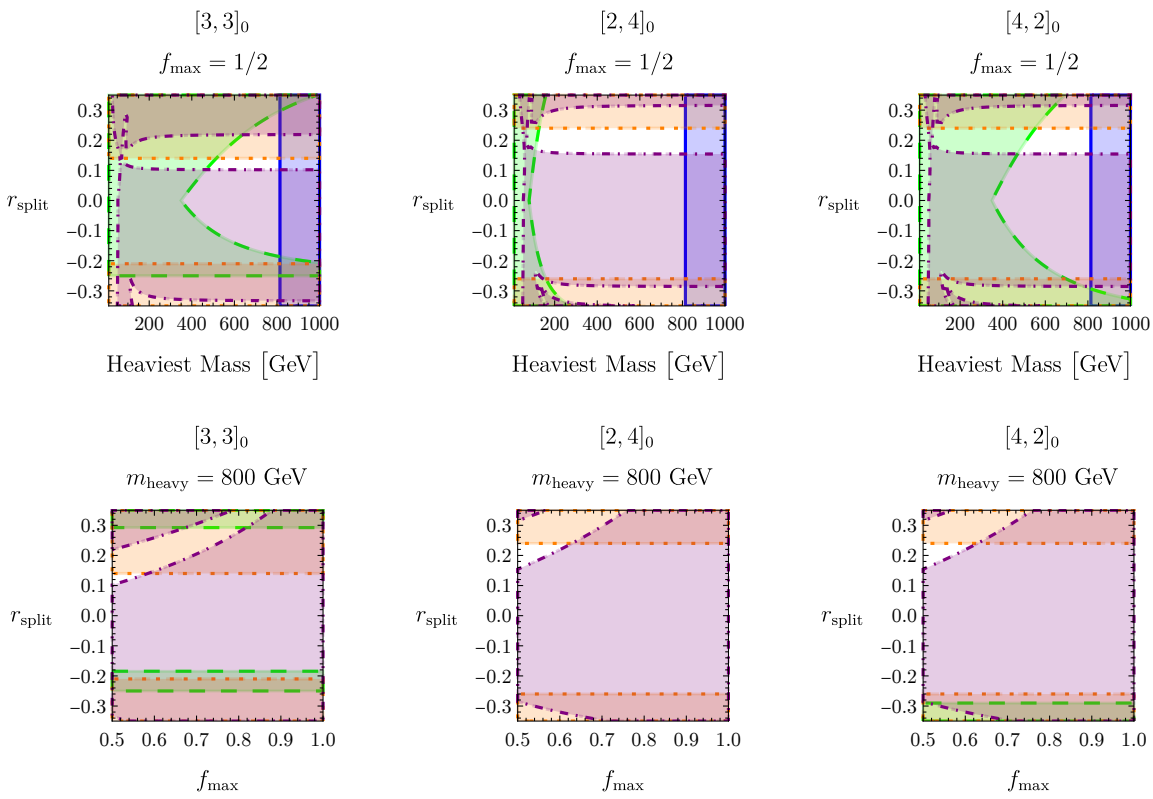

Figure 2.9: Regions of parameter space for scalar Loryons which are ruled out by one of the constraints described earlier. The orange, dotted region is ruled out by the electroweak precision parameter S; the purple, dot-dashed region is ruled out by constraints on κ_γ; the blue, solid region is ruled out by unitarity bounds; the green, dashed region is ruled out by direct search bounds. The first row has fixed $f_{\max} = .5$; the second row has fixed the heaviest mass eigenvalue at 800 GeV.

that *fermionic Loryons, in isolation, are excluded by current data.* In principle, it is possible to satisfy the constraints from κ_γ and S by adding a set of additional states to flip the sign of κ_γ without running afoul of precision electroweak measurements.

Assuming the κ_γ constraints are satisfied in this way (and assuming these other states do not impact the Loryon phenomenology), there are two combinations of custodial representations which still have viable regions of parameter space: $[2,1]_{1/2} \oplus [1,2]_{1/2}$ and $[1,3]_0 \oplus [2,2]_0$. For fermionic Loryons transforming in the $[2,1]_{1/2} \oplus [1,2]_{1/2}$ representation, direct search bounds and precision electroweak constraints both exclude regions where

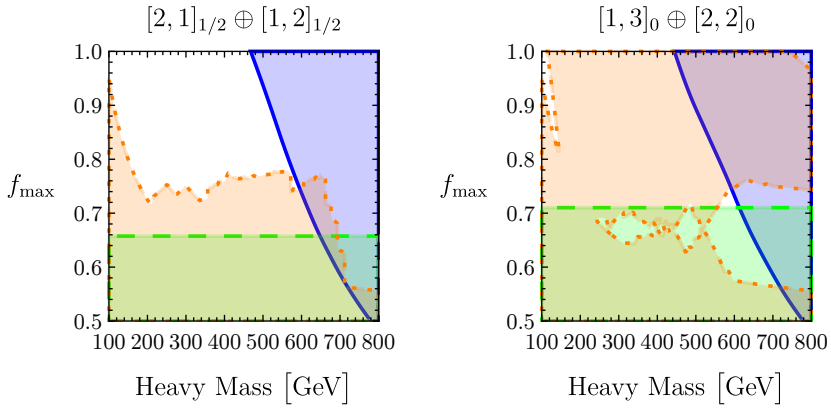

Figure 2.10: Regions of parameter space for fermionic Loryons which are ruled out by one of the constraints described earlier. The blue, solid region is ruled out by unitarity bounds; the green, dashed region is ruled out by precision electroweak measurements; the orange, dotted region is ruled out by direct search constraints. Note that we do not include constraints from Higgs couplings, which nominally rule out all fermionic Loryon candidates in combination with precision electroweak measurements; constraints from κ_γ may only be satisfied by including some additional number of scalar Loryons or non-Loryons coupling to the Higgs.

the Higgs-independent contributions to fermion masses are comparable in size to the Higgs-dependent contributions. In this limit, there is large splitting among the mass eigenstates, which both increases the contribution to the S-parameter and increases the sensitivity of direct searches that require large missing energy. LEP limits place a lower bound on the overall mass scale, while perturbative unitarity places an upper bound. In the remaining viable region for the $[2,1]_{1/2} \oplus [1,2]_{1/2}$ model, the heavy mass eigenstate is between $\sim 100 - 600$ GeV, and the Higgs-independent contributions to fermion masses are no more than about one-third the size of the Higgs-dependent contributions.

Constraints are tighter still for the $[1,3]_0 \oplus [2,2]_0$ model; it is likely that the viable parameter space could be entirely closed by a proper statistical combination of all limits, an exercise beyond the scope of this work. As with the $[2,1]_{1/2} \oplus [1,2]_{1/2}$ model, precision electroweak measurements exclude regions where the Higgs-independent contributions to fermion masses are comparable in size to the Higgs-dependent contributions. How-

ever, direct searches exclude disjoint regions where the Higgs-independent contributions to fermion masses are either comparable in size to, or much smaller than, the Higgs-dependent contributions, on account of how these contributions translate into the spectrum of mass eigenstates. In conjunction with LEP and perturbative unitarity bounds, this essentially closes the parameter space for the $[1,3]_0 \oplus [2,2]_0$, with the exception of a very small window, see Fig. 2.10.

2.6 Future Prospects

Given the viable parameter space for scalar and fermionic Loryons in light of current data, it is natural to wonder what the prospects might be for discovering or excluding Loryons at the HL-LHC. In particular, we anticipate that the HL-LHC will significantly improve the precision with which Higgs couplings are determined. This improved sensitivity will either lead to increased coverage of the Loryon parameter space or point the way towards a discovery.

For the most part, we use the HL-LHC Higgs coupling projections in [69]. We begin with the channels that already provide nontrivial constraints with current data. Using the projected improvement for κ_γ and κ_g in [69], we find that color triplet scalar Loryons could be entirely ruled out. None of the color singlet cases would be ruled out by the improvement in κ_γ alone since the constraint is not expected to tighten enough to eliminate a single charge 1 scalar; the increased precision narrows the open parameter space that survives by flipping the sign of κ_γ.

The HL-LHC is also projected to make a fairly precise determination of $\kappa_{Z\gamma}$. While the overall magnitude of the resulting constraint is expected to be much weaker than the ones derived using κ_γ, the interplay of $\kappa_{Z\gamma}$ and κ_γ is quite powerful. In particular, the expected constraint on $\kappa_{Z\gamma}$ would probe scenarios that currently remain viable by flipping the sign

Rep	$[1,1]_1$	$[3,1]_0$	$[1,3]_0$	$[2,2]_0$	$[3,3]_0$	$[4,2]_0$	$[2,4]_0$	$[2,3]_{-1/2}$
$\frac{\sum \eta_i C_i^{Z\gamma}}{\sum \eta_i Q_i^2}$	$-.12$	.38	$-.12$	.13	.13	.30	$-.032$	$-.008$

Table 2.13: The contribution of viable scalar Loryons to $\kappa_{Z\gamma}$ as a ratio to the contribution to κ_γ. To maintain $\kappa_{Z\gamma}$ within 20 percent of the SM value while flipping the sign of κ_γ requires $|\sum \eta_i C_i^{Z\gamma} / \sum \eta_i Q_i^2| < .074$.

Rep	$[2,1]_{1/2} \oplus [1,2]_{1/2}$	$[1,3]_0 \oplus [2,2]_0$
$\frac{\sum \eta_i C_i^{Z\gamma}}{\sum \eta_i Q_i^2}$	$-.019$	$-.019$

Table 2.14: The contribution of viable fermionic Loryons to $\kappa_{Z\gamma}$ as a ratio to the contribution to κ_γ. To maintain $\kappa_{Z\gamma}$ within 20 percent of the SM value while flipping the sign of κ_γ requires $|\sum \eta_i C_i^{Z\gamma} / \sum \eta_i Q_i^2| < .074$.

of κ_γ since the relevant parameter space generally also yields a significant contribution to $\kappa_{Z\gamma}$. The contribution of viable Loryons to $\kappa_{Z\gamma}$ relative to their contribution to κ_γ is shown in Tables 2.13 and 2.14. Weak singlet scalars and the viable fermions contribute to $\kappa_{Z\gamma}$ with opposite sign relative to the SM, while the other viable new scalar Loryons contribute to $\kappa_{Z\gamma}$ with the same sign as the SM. The contribution to $\kappa_{Z\gamma}$ is too small to flip the sign of $\kappa_{Z\gamma}$ and κ_γ simultaneously. In more complicated models, a combination of some new singlets and fermions and/or some new non-singlet scalars could conspire to have their contributions to $\kappa_{Z\gamma}$ cancel while flipping the sign of κ_γ.

Higgs cross section measurements at the LHC are sensitive to the wavefunction renormalization of the physical Higgs scalar h, which is expected to become relevant in the HL-LHC era. For Loryons carrying SM quantum numbers, this constraint is typically weaker than the bounds from κ_γ and $\kappa_{Z\gamma}$. However, for the SM singlet S_0, this will eventually provide a non-trivial constraint on the parameter space that is complementary to the existing bounds from exotic Higgs decays or partial wave unitarity. To determine the

projected HL-LHC sensitivity to this effect, we use the single-operator bound on

$$\mathcal{O}_H \equiv \frac{C_H}{\Lambda^2}\frac{1}{2}\left(\partial^\mu |H|^2\right)^2 . \tag{2.57}$$

The HEPFit collaboration projects a 95% CL bound of $\Lambda/\sqrt{|C_H|} = 1.4$ TeV [69]. Two comments are in order. First, although the bound is quoted on the Wilson coefficient of a SMEFT operator (which is never the appropriate EFT description for the low-energy effects of Loryons), the fit simply reflects a bound on a common shift to single-Higgs production processes. As such, it may be equivalently interpreted as a limit on the parameter κ_h defined via

$$\mathcal{L} \supset \kappa_h \times \frac{1}{2}(\partial h)^2 , \tag{2.58}$$

which uniformly shifts single-Higgs production rates when h is canonically normalized. With this interpretation, the projected 95% CL HL-LHC limit on $\Lambda/\sqrt{|C_H|}$ translates to

$$\kappa_h \in [0.97, 1.03] . \tag{2.59}$$

Second, although integrating out any heavy state typically generates multiple EFT operators and lead to bounds weaker than those expected from single-operator projections, in the case of the SM singlet S_0 the only low-energy effects at the LHC are the common shift in production rates noted above and a shift in the di-Higgs rate from radiative corrections to the Higgs potential. As the anticipated bounds on κ_h are much stronger than those expected from di-Higgs measurement, the projected single-operator bound on $\mathcal{O}_H$ provides a reasonable approximation of the expected sensitivity of a global fit to the specific low-energy effects of S_0.

Unfortunately, the expected HL-LHC precision lies parallel to, and is somewhat weaker than, the bound from perturbative unitarity, so the HL-LHC is unlikely to significantly improve constraints on an individual singlet scalar Loryon in this channel within the regime of perturbative validity. That being said, if there are some number N of singlet scalar Loryons, the HL-LHC bound on κ_h scales with N, while the leading contribution to the perturbative unitarity bound is unaffected. Subleading contributions to the perturbative unitarity bound scale with N; further study is required to understand if HL-LHC sensitivity may play an interesting role.

A more promising observable at the HL-LHC is the Higgs self-coupling. Although the anticipated sensitivity of the HL-LHC to deviations in the Higgs self-coupling is significantly less than its sensitivity to wavefunction renormalization effects, the Loryon contribution to the Higgs cubic coupling is enhanced relative to wavefunction renormalization when the Higgs-Loryon coupling is large. Near the perturbative unitarity bound, the correction becomes a $\mathcal{O}(1)$ effect. The leading effect of Loryons on di-Higgs production in the large-coupling limit comes from the direct shift in the coefficient of h^3, while subleading effects at large coupling include the above-mentioned shift due to wavefunction renormalization as well as new momentum-dependent contact interactions between h and longitudinal vectors. For simplicity, we consider only the leading effect. As shown in Fig. 2.11, the 95% CL constraint $0.1 < \kappa_\lambda < 2.3$ [69] on modifications to the Higgs self-interaction – as projected for the HL-LHC – would provide sensitivity to regions of parameter space otherwise allowed by the perturbative unitarity bound. As the unitarity bound is fixed, more precise measurements of the Higgs self-interaction (such as that expected from the ILC) will have a significant effect on the viable parameter space for new Loryons.

There is also scope for improvement in direct searches for Loryon resonances. Of the scalars with large amounts of viable parameter space remaining in Fig. 2.8, $[1,1]_0$

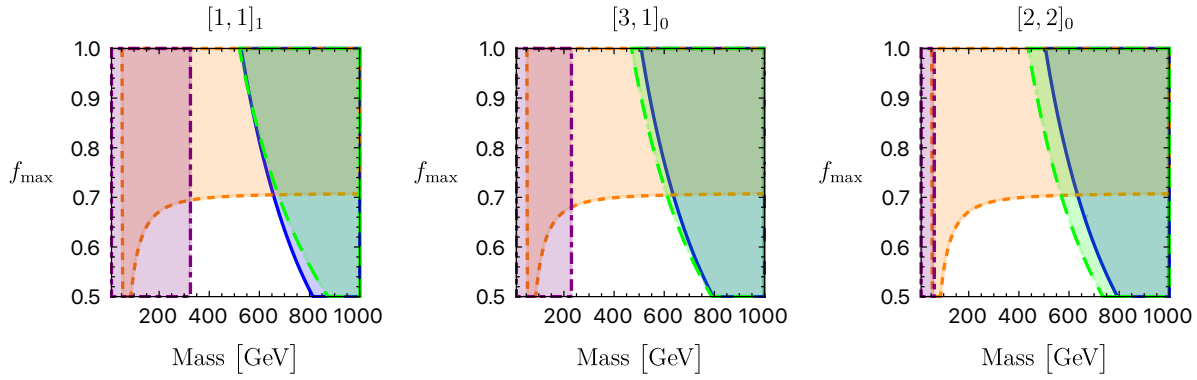

Figure 2.11: Expected sensitivity of the HL-LHC to Loryons based on the Higgs coupling projections in [69]. The orange, dotted region is projected to be ruled out by improved constraints on κ_γ or κ_g; the green, dashed region can be ruled out by the HL-LHC measurement of the Higgs cubic; the blue, solid region is ruled out by unitarity bounds; and the purple, dot-dashed region is ruled out by current direct search bounds.

and $[2,2]_0$ are assumed inert and are difficult to see directly. However, the neutral triplet $[3,1]_0$, if inert, has a projected HL-LHC bound from displaced vertices that rules out most of the viable parameter space – see Sec. 2.4 and [45]. If, on the other hand, the neutral triplet has a small mixing with the Higgs, there are many potential dedicated searches for the pair production of (charged or neutral) heavy Higgses, decaying to *e.g.* WW, WZ, tb, that could fill in the gap [44]. For the $[1,1]_1$, a dedicated interpretation of the opposite-flavor bins in the existing ATLAS dilepton analysis [48] and future analyses would be valuable. For the fermion models, there would be immediate gains from an analysis of neutral diboson signals (hh, hZ, ZZ) in the plane of heavy and light fermion masses, analogous to those provided for charged diboson final states that were reinterpreted in Sec. 2.4.2.

2.7 Conclusions

Our goal in this chapter was to classify non-decoupling new particles ("Loryons") that are still experimentally viable. By non-decoupling, we mean that the Loryons acquire at least half of their mass from the Higgs vacuum expectation value; this implies that the low energy effective theory obtained by integrating out the Loryons must be described using HEFT. Taking a mild set of phenomenologically reasonable assumptions, including imposing approximate custodial symmetry, approximate $\mathbb{Z}_2$ symmetry, and prompt decays of electromagnetically charged particles, the list of possible new states is finite. We determined the allowed parameter space by imposing partial wave unitarity, along with a set of indirect and direct experimental constraints. The available parameter space for scalar Loryons remains large, while the fermionic cases are essentially ruled out.

Loryons provide a set of concrete targets for future searches. One can either search for the Loryons directly, or indirectly by interpreting constraints on the HEFT parameter space. In both cases, the HL-LHC stands to significantly improve on existing bounds. Such improvement is strongly motivated as the persistence of Loryons demonstrates that HEFT remains a viable framework for the interpretation of current Higgs data. The exclusion of Loryons would represent significant progress towards verifying that electroweak symmetry can be linearly realized by the known particles. On the other hand, evidence for a Loryon – above and beyond the thrill of discovery – would imply that electroweak symmetry is not linearly realized by Standard Model particles on their own.

The viability of many Loryon models adds further motivation to the study of the correlated effects of individual SMEFT operators over different final states at the HL-LHC. For example, [70] details pairs of processes (with different Higgs multiplicities) that could yield comparable HL-LHC sensitivity to the same SMEFT operator. Notably, these pairs include $\kappa_\gamma/\kappa_{Z\gamma}$ with vector boson scattering, and Higgs trilinear measurements with

rates in $W^{\pm}W^{\pm}jjh$. As future measurements of κ_γ, $\kappa_{Z\gamma}$, and the Higgs self coupling can give a signal in the presence of Loryons (see Sec. 2.6), it is likely that these accompanying measurements would exhibit decorrelated deviations that would tension a combined fit to dimension 6 operators in the SMEFT. Along similar lines, [21] shows how single and di-Higgs measurements can be measureably decorrelated from the SMEFT expectation in the presence of a scalar multiplet that gets an extra electroweak symmetry breaking vev — another class of UV models whose low energy effects require a HEFT description.

There are many future directions to explore. In principle, now that the viable Loryon parameter space is known, it is possible to design new LHC searches to target these interesting regions either directly or indirectly. We discussed many potential new searches/reinterpretations in Sec. 2.6, but there is considerable room for further development. The complete Loryon parameter space is unlikely to be fully probed at the LHC, and so a dedicated study determining the reach of future colliders is warranted. It would also be interesting to relax some of the assumptions shaping our definition of the Loryon parameter space, which would lead to new signatures. For example, one of the phenomenological requirements made here was that the Loryon decays are all prompt; relaxing this assumption leads to signals in a variety of long-lived particle searches that would open up new pathways to discovery. We have also assumed that Loryon contributions to flavor- or CP-violating observables are minimized; exploring a wider flavor structure and/or allowing for CP violating couplings would yield many interesting complementary probes of these non-decoupling new particles. Finally, we have assumed a $\mathbb{Z}_2$ symmetry acting on the Loryons to highlight their irreducible loop-level signatures, but relaxing this assumption would lead to additional experimental opportunities (and constraints) from tree-level signatures.

There are also implications for cosmology. Many of the multiplets include an electrically neutral lightest state, which is an obvious candidate for dark matter. Some of

the Loryons have been studied as dark matter, *e.g.* the singlet extension of the Standard Model [71, 72, 73], singlet-doublet dark matter [74], or the minimal dark matter program [61], but others have not been as widely explored. In general, the relic density of Loryon dark matter candidates is expected to be a rich subject since there are a number of non-trivial allowed couplings between Loryons and the electroweak/Higgs bosons. Imposing a relic density requirement could be used to further motivate regions of viable Loryon parameter space. The Loryons are also expected to have an impact on the stability of the Higgs potential, and in fact, one might need to add some additional new physics to (meta-)stabilize the Higgs potential to make these models viable. Finally, in Chap. 3 we study the impact of Loryons on the electroweak phase transition. With this exception, we leave the exploration of these connections to cosmology and their impact on the viable Loryon parameter space for future work.

It is remarkable that new particles obtaining most of their mass from electroweak symmetry breaking could still be lurking under our noses. This work serves to highlight the fact. Our hope is that this provides a new set of concrete targets to both motivate new searches at current experiments and augment the case for future colliders.

Chapter 3

A Strongly First-Order Electroweak Phase Transition from Loryons

This chapter is based on work published as [3].

The electroweak phase transition (EWPT), the point in the universe's history when the Higgs boson acquires a vev and the $SU(2)_L \times U(1)_Y$ electroweak symmetry is broken to the $U(1)_{\text{em}}$ symmetry of electromagnetism, is of great physical interest. It is possible that the matter-antimatter asymmetry observed today is created during the EWPT, a phenomenon termed electroweak baryogenesis (EWBG) [75, 76, 77, 78]. Doing so requires that the three Sakharov conditions [79] be satisfied at the EWPT. It is also possible for the EWPT to source a stochastic background of gravitational waves (GW), which could be detected by a near-future GW observatory such as LISA [80, 81], BBO [82], or DECIGO [83]. Both of these possibilities require the EWPT to be first-order and sufficiently strong. This is not the case in the Standard Model, as the Higgs mass is too small to give a first-order EWPT [84]. However, by extending the Standard Model with additional particles which couple to the Higgs, the Higgs potential can be modified to

give a strongly first-order phase transition, potentially enabling both EWBG[1] and the creation of a stochastic GW background. In addition to the possibility of an observable GW background, such extensions are generally also potentially observable at future colliders through modification of Higgs properties [85, 86]. Much work has explored these possibilities; see, e.g., [44, 87, 88, 89, 90, 91, 92, 93, 94, 95, 96, 97, 98, 99, 100, 101, 102, 103, 104, 105, 106, 107, 108, 109, 110].

In Chap. 2, we examined the phenomenological viability of BSM Loryons, particles which receive most of their mass from the vev of the Higgs boson. Such particles are a notable class because the effective field theory obtained by integrating out Loryons must be described using HEFT, not SMEFT [11, 12, 13, 14]. We found a number of examples of Loryons which are consistent with current constraints. By definition, Loryons have a sizable coupling to the Higgs and thus make a significant contribution to the Higgs effective potential. In this chapter, we leverage the Loryon parametrization and the experimental constraints from Chap. 2 to determine where in the experimentally viable parameter space the EWPT is strongly first-order. We both examine the Loryon parameter space to investigate how prevalent it is to have a strongly first-order EWPT and extend our analysis beyond Loryons to see how relevant the category of Loryons is in picking out extensions which furnish a strongly first-order EWPT.

Apart from the focus on Loryons, this work also improves on previous analyses. We consider a complete enumeration of viable scalars and vector-like fermions, subject to some assumptions, as opposed to picking out a subset of benchmark models. We have carefully considered direct search bounds on the variety of possible Loryons as well as used the most up-to-date collider constraints and projections, thus providing a more

[1]Sufficient CP-violation is one of the Sakharov conditions which must be satisfied for EWBG, and a fully viable theory of EWBG requires additional CP-violation; this can be added independently through an additional extension of the SM, and in this work we consider only making the EWPT strongly first-order.

comprehensive and detailed analysis of the constraints. In addition to these, we also impose partial wave unitarity bounds to give an additional constraint. While previous studies (e.g. [93]) have included some consideration of unitarity bounds, our treatment is more thorough and leads to a significantly stronger constraint. Exceeding this constraint does not mean a model is absolutely ruled out, but it does mean perturbation theory cannot be relied on to give accurate answers. Finally, much previous work has analyzed the phase transition by focusing on the dynamics at the critical temperature; as discussed in [100, 106], it is better and makes a significant difference to calculate at the nucleation temperature, and we do so here.

For scalar Loryons, a neutral singlet, charged singlet, hypercharge 0 electroweak triplet, hypercharge 1/2 electroweak doublet, and charge 2/3 and -1/3 color triplet are experimentally viable for broad swathes of their parameter space. A few additional scalar Loryons, such as a hypercharge 1 electroweak triplet and hypercharge 1/2 electroweak quadruplet, have small regions of viability. Additional possibilities, including fermionic Loryons and scalar Loryons in larger representations or with larger charges, are experimentally ruled out when added on their own but viable when added in combination with other BSM particles. There are a large number of possibilities which generally have delicate cancellations to evade the experimental constaints; see the previous chapter for more detailed discussion. Due to the number of possibilities, we do not perform a complete analysis of the parameter space for these cases, but do discuss the general features and compute with particular models to check that these hold.

The rest of this chapter is organized as follows: In Sec. 3.1, we describe our process for determining whether a particular model possesses a strongly first-order EWPT and sources a stochastic GW background. In Sec. 3.2, we then show for specific models where in their parameter space they predict a strongly first-order EWPT and detectable GW background. Finally, we present our conclusions in Sec. 3.3.

3.1 Calculating the EWPT Characteristics

The characteristics of the EWPT can be calculated from the effective potential for the Higgs boson. Doing so with a perturbative calculation in finite-temperature field theory has problems such as gauge-dependence, infrared divergences, and others; see, e.g., [111, 112, 113, 114, 115, 116]. A non-perturbative calculation using e.g. lattice computations is necessary for a fully accurate result; here, we do not deal with these issues, using standard perturbative techiniques to estimate the properties of the EWPT (see, e.g., [78, 105, 106, 108]). We expect, given the approximations inherent in doing a perturbative calculation, that the borders of the region we determine to have an appropriate EWPT will be fuzzy; for any particular model, a more precise calculation resolving the issues described above could be carried out to give a more definitive answer. However, our intention is only to characterize the broad regions of parameter space and show the degree to which they overlap with the viable parameter space from the previous study, and for this the perturbative calculation presented here is sufficient.

This section is split into three subsections. In Sec. 3.1.1, we describe the procedure we use to compute the effective potential for the Higgs boson. In Sec. 3.1.2, we discuss how we use this effective potential to determine whether there is a strongly first-order EWPT. In Sec. 3.1.3, we discuss our criteria for whether an EWPT will source a detectable stochastic background of gravitational waves.

3.1.1 The Effective Potential

Our construction of the effective potential follows standard methods; see, e.g., [117]. At zero temperature and to one-loop order, the effective potential can be written

$$V_{\text{eff},T=0}(h,\phi) = V_0(h,\phi) + \sum_i n_i V_{\text{CW,b}}(m_i^2(h,\phi)) + \sum_i n_i V_{\text{CW,f}}(m_i^2(h,\phi))\,. \tag{3.1}$$

Here h is the Standard Model Higgs; ϕ are the BSM Loryons; V_0 is the tree-level potential; $V_{\mathrm{CW,b/f}}$ is the one-loop Coleman-Weinberg correction for bosons/fermions; n_i is the number of degrees of freedom of the particle; and the sum runs over all particles but in practice receives significant contributions only from those with significant coupling to h, ϕ. The one-loop corrections take the form

$$V_{\mathrm{CW,b/f}}(m_i^2(h,\phi)) = \pm\frac{1}{64\pi^2} m_i^2(h,\phi)\left(m_i^2(h,\phi)\log\left(\frac{m_i^2(h,\phi)}{m_i^2(v_h,v_\phi)}\right) + 2m_i^2(v_h,v_\phi)\right)\,, \quad (3.2)$$

where the $\pm$ is for bosons/fermions and (v_h, v_ϕ) are the tree-level vacuum expectation values of h, ϕ; this form has fixed counterterms such that the tree-level relations between the Lagrangian parameters and the Higgs mass and vev are preserved. At finite temperature, there are two corrections. The first is the addition of a one-loop thermal potential to the Coleman-Weinberg term,

$$\Delta V_{\mathrm{eff},T>0}(h,\phi,T) = \sum_i n_i V_{\mathrm{T,b}}(m_i^2(h,\phi),T) + \sum_i n_i V_{\mathrm{T,f}}(m_i^2(h,\phi),T)\,, \quad (3.3)$$

where

$$V_{\mathrm{T,b/f}}(m_i^2(h,\phi),T) = \frac{T^4}{2\pi^2} J_{\mathrm{b/f}}\left(\frac{m_i^2(h,\phi)}{T^2}\right)\,, \quad (3.4)$$

$$J_{\mathrm{b/f}}(y^2) = \pm\int_0^\infty \mathrm{d}x\, x^2 \log\left(1 \mp \exp\left(-\sqrt{x^2+y^2}\right)\right). \quad (3.5)$$

The second correction is due to the resummation of hard thermal loops, which are nominally of higher-loop order but give a significant numerical contribution due to the presence of the additional dimensionless ratio T/m, where m is a mass scale [118, 119]. This can

be handled by making the substitution

$$m_i^2(h,\phi) \to m_i^2(h,\phi) + \Pi_i(T)\,, \tag{3.6}$$

where Π_i is found by differentiating $V_{\rm T}$; typically only the non-zero contribution of leading-order in T is kept, for which

$$J_{\rm b,lo}\left(\frac{m^2}{T^2}\right) = 2J_{\rm f,lo}\left(\frac{m^2}{T^2}\right) \approx \frac{\pi^2}{12}\frac{m^2}{T^2}\,, \tag{3.7}$$

and thus all the Π_i are directly proportional to T^2.

The calculation described above is not the state of the art even for a perturbative calculation; it can be improved through methods such as dimensional reduction [120], higher loop order [110, 121], and renormalization group improvement [86, 122]. As our intention is only to characterize broad regions of parameter space, we do not improve our calculation in any of these ways. For a particular model of interest, a more precise calculation using these methods would be desirable to obtain a more robust answer.

Due to the assumptions of $\mathbb{Z}_2$ symmetry and positive quadratic terms for the new Loryons, we assume that only the Higgs field acquires a non-zero vacuum expectation value (and have checked models throughout the parameter space to confirm that this assumption holds). This means that we can drop all ϕ dependence in the above formulae so that the effective potential is a function of just h, T.

3.1.2 Conditions for a Strongly First-Order EWPT

Given an effective potential, we now need to determine whether it gives a strongly first-order transition. As noted earlier, this is a necessary (but not sufficient) condition for electroweak baryogenesis. A first-order transition can occur between two local minima,

the symmetry-preserving minimum at $h = 0$ and the symmetry-breaking one at $h > 0$. At the critical temperature T_c, these two minima are degenerate,

$$V_{\text{eff}}(0, T_c) = V_{\text{eff}}(h_c, T_c)\,, \tag{3.8}$$

where $h_c > 0$ minimizes $V_{\text{eff}}(h, T_c)$. Below this temperature, the symmetry-breaking minimum becomes the global minimum, and bubbles of the symmetry-breaking minimum can nucleate by tunneling through the barrier between the two minima. The nucleation temperature T_n is defined as the temperature at which the probability of a bubble nucleating within one Hubble volume per Hubble time is $\mathcal{O}(1)$; this corresponds to $S_3/T \approx 140$, where S_3 is the three-dimensional Euclidean action of the critical bubble [117, 123, 124]. For the EWPT to be strongly first-order and potentially suitable for electroweak baryogenesis, the Higgs vev in the broken phase must be large enough to suppress sphalerons. We make the standard approximation of using v_n/T_n to measure the strength of the phase transition, with $v_n/T_n \gtrsim 1$ the condition for strong enough to be suitable for electroweak baryogenesis [117]. We then make a rough estimate of the precision of our computation by varying the thresholds for S_3/T and v_n/T_n. For S_3/T we vary by a factor of 1.4, computing with a threshold of $S_3/T = 100, 200$; for v_n/T_n we vary by a factor of 1.6, computing with $v_n/T_n > .6, 1.6$.

In the Standard Model, the EWPT is a crossover, not a first-order transition [84]; the minimum moves smoothly away from $h = 0$ rather than having two degenerate local minima and tunneling between them. Adding new particles coupled to the Higgs can lower the symmetry-breaking minimum relative to the symmetry-preserving minimum and enhance the barrier between the two minima, leading to a first-order transition. Requiring a strongly first-order EWPT thus requires some minimum contribution from BSM physics; in Sec. 3.2, we will see this play out as requiring sufficiently large mass and

$f_{\max}$. There is also a maximum workable contribution; adding too many new scalars too strongly coupled to the Higgs can stabilize the Higgs effective potential at the symmetry-preserving minimum in violation of the observed zero-temperature symmetry breaking. We impose as a condition $T_n > 10$ GeV; the location of the upper bound in the parameter space is only weakly sensitive to the precise condition imposed as long as it is below ~ 50 GeV.

3.1.3 Gravitational Wave Background

We are also interested in when the EWPT sources a GW background which could be detected by a near-future GW observatory such as LISA, BBO, or DECIGO. GW are primarily sourced from the EWPT through collision of bubble walls, sound waves, and turbulence during and after collisions of bubbles of broken phase [80]. It is possible to calculate spectra for the GW and compare these to sensitivity curves; see, e.g., [80, 81, 125, 126, 127, 128, 129]. An approximate answer can be obtained based on only two properties of the phase transition: the ratio of the vacuum energy density released in the transition to the radiation energy density,

$$\alpha = \left(\Delta V_{\text{eff}} - \frac{T_n}{4} \Delta \frac{\mathrm{d}V_{\text{eff}}}{\mathrm{d}T} \right) \Big/ \frac{g_* \pi^2 T_n^4}{30} \ , \tag{3.9}$$

and the inverse duration of the phase transition over the Hubble parameter [80, 81],

$$\beta / H_* = \left. \frac{\mathrm{d}S_3}{\mathrm{d}T} \right|_{T_n} - \frac{S_3}{T_n} \, . \tag{3.10}$$

Physically, both a larger energy release in transitioning out of the metastable minimum (large α) and a longer duration (small β) source a stronger GW signal. Both large α and small β tend to apply for stronger transitions; thus, the regions of the parameter space

with the strongest transitions are expected to produce a detectable GW background. Based on [81, 128], we use

$$\log(\beta/H_*) \lesssim 1.2 \log \alpha + 8.8 \tag{3.11}$$

as the condition for the phase transition to source a GW background detectable by LISA. The cutoff for where in the model parameter space we expect a detectable GW background is only weakly dependent on the condition chosen; adjusting the required value of β/H_* by an order of magnitude only shifts the bound on the Loryon mass by $\mathcal{O}(3)$ GeV. For BBO and DECIGO, we estimate from [126] that the constant 8.8 should be increased to around 9.2. Again we emphasize that this is an approximate estimate, but the end result as displayed in the Loryon parameter space is only weakly dependent on the condition chosen. For a more precise estimate for a particular model, a more detailed calculation would be needed; however, as stated before, we are interested only in characterizing broad regions of parameter space, for which this estimate is sufficient.

3.2 Results

Results for a selection of viable Loryons are shown in Fig. 3.1. We see that the region of parameter space in which there is a strongly first-order EWPT overlaps heavily with the region of parameter space consistent with current experimental and theoretical constraints. There is a much smaller region for which the EWPT sources a GW background detectable by near-future GW observatories; however, this also lies within the experimentally viable parameter space for all models except the neutral singlet Loryon.

For purposes of comparison, the plots show the parameter space through smaller values of $f_{\max}$, going below the cutoff for Loryons of $f_{\max} = 1/2$. The unitarity bound

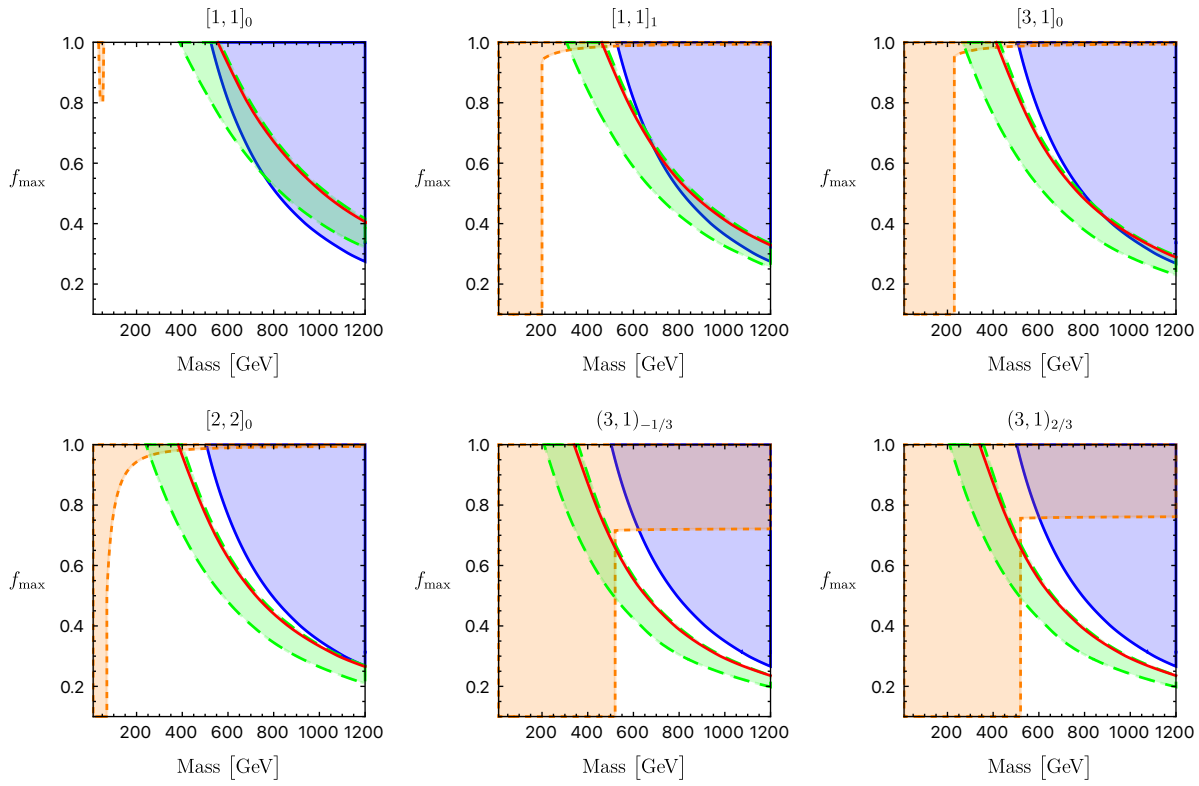

Figure 3.1: The allowed parameter space for which there is a strongly first-order electroweak phase transition. The mass quoted is the physical mass of the Loryon. $f_{\max}$ is the fraction of its mass-squared the particle gets from its coupling to the Higgs; $f_{\max} > 1/2$ is the condition for a Loryon. The orange region (dotted boundary) is ruled out by experimental constraints; the blue region (solid boundary) is ruled out by perturbative unitarity. The green region (dashed boundary) is where a strongly first-order phase transition is predicted. The solid red line through this region is the lower bound for production of a stochastic gravitational wave background detectable by LISA, which is only marginally below the upper bound for an appropriate phase transition.

increases sharply outside the Loryons regime, as does the band with a viable phase transition. It is thus not required to add Loryons in order to achieve a strongly first-order EWPT; however, the viable region overlaps with a larger portion of the experimentally viable parameter space for Loryons as compared to non-Loryons, with (typically) ∼30-50% of the experimentally viable region producing a suitable phase transition for Loryons and ∼10% for non-Loryons. These estimates vary significantly with $f_{\max}$ and with the representation chosen; we refer the reader to Fig. 3.1 for more detailed information. The larger viable region for Loryons is not an artifact of the chosen parametrization of $(m, f_{\max})$; if viewed in terms of the cross-quartic between the Higgs and the new field rather than the mass, smaller values of $f_{\max}$ require a cross-quartic larger by a factor of $\mathcal{O}(3)$, while the range of cross-quartics giving a viable EWPT remains approximately the same size.

The plots are shown for our standard values of $S_3/T = 140$, $v_n/T_n > 1$. Varying the value of S_3/T shifts the bounds by $\mathcal{O}(3)$ GeV, a negligible effect. Varying the value of v_n/T_n has a stronger effect; a factor of 1.6 variation shifts the lower bound of the viable region by $\mathcal{O}(50)$ GeV. Increasing the Loryon self-coupling increases both the upper and lower bound by $\mathcal{O}(30)$ GeV. The curve for a detectable GW background is drawn using our estimate for LISA; for BBO or DECIGO, the curve would shift to the left by $\mathcal{O}(5)$ GeV.

As shown in Fig. 3.1, larger representations have the region for a strongly first-order phase transition shifted to lower masses. This is due to the greater number of degrees of freedom in the larger representations. The viable region depends principally on the number of degrees of freedom added; the exact electroweak representation has only a small effect on the region for which there is a viable phase transition. One can thus read the first four panels of 3.1 as showing the approximate viable region for adding 1, 2, 3, and 4 real scalar degrees of freedom; adding 5, 6, etc. would continue to shift the viable

region to lower masses. The principal experimental constraint, due to Higgs decay to two photons, is that there may be at most one charged particle, so additional Loryons beyond the representations given would need to be neutral singlets. Of course, there are a larger number of parameters when adding Loryons in multiple representations, as the different representations can have different masses and values of $f_{\max}$; interpreting the plots as showing the viable region for an appropriate number of new fields in different representations is projecting the allowed region into a slice wherein all new particles have the same mass and coupling to the Higgs.

In Chap. 2, we also discussed the possibility of fermionic Loryons and scalar Loryons in larger representations being viable by adding enough charged BSM particles; this flips the sign of the Higgs coupling to two photons but matches the magnitude of the SM [130]. There are a number of possibilities for doing so and we have not exhaustively characterized where in their parameter spaces one predicts a strongly first-order EWPT; however, a few general comments are in order. Adding too many scalar degrees of freedom renders the symmetric minimum too stable. How many is too many depends on the mass and fraction of that mass from the Higgs; as an example, only up to 6 electroweak quadruplet scalars getting half their mass-squared from the Higgs with mass 400 GeV can be added in isolation, while 8 would be required to flip the $h\gamma\gamma$ coupling. It is thus not possible to add only scalars while flipping the $h\gamma\gamma$ coupling. The one-loop correction to the effective potential from fermions is of opposite sign to that from scalars, and so it is possible to add a mix of scalar and fermionic Loryons and get the desired behavior for the EWPT. While the parameter space is too extensive to perform a broad scan, we have checked particular examples in detail to confirm that we can in principle get a strongly first-order phase transition. For a model with an appropriate mix of scalars and fermions, there is a non-trivial mass range at a mass of several hundred GeV for which we predict a strongly first-order electroweak phase transition.

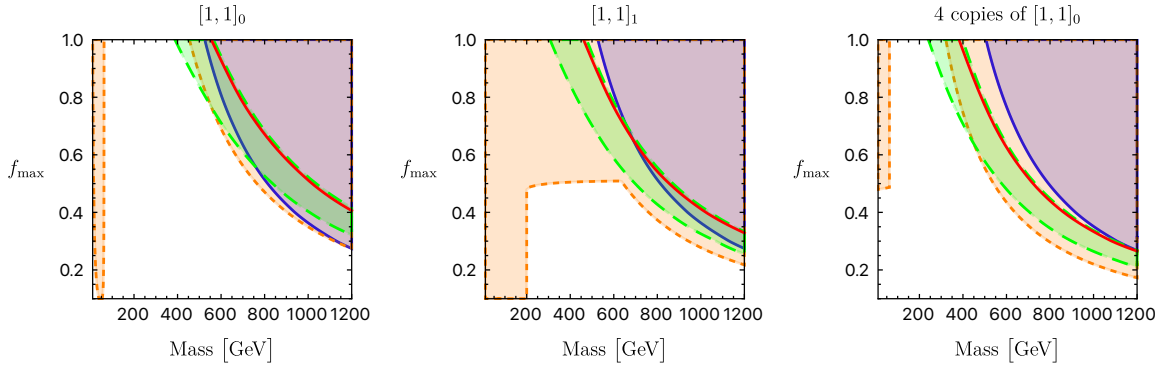

Figure 3.2: The allowed parameter space based on the projections for near-future colliders. We use the one-sigma projections for the FCC-ee at 240 GeV from [131], doubled to give an estimate of the two-sigma bound; other colliders, such as ILC and CLIC, have comparable projections [131]. Labels are as Fig. 3.1. The two principal constraints are $h\gamma\gamma$, which comes down from the top in the middle panel, for which the projected two-sigma constraint is 2.6%; and the Higgs cubic self-coupling, which comes in from the left in the figure, for which the projected two-sigma constraint is 38%.

In Fig. 3.2, we show the viable parameter space with projected two-sigma constraints from the FCC-ee; other near-future colliders, such as ILC and CLIC, have similar projections [131]. The measurement of the $h\gamma\gamma$ interaction is projected to be precise enough to rule out charged and colored Loryons, leaving some number of neutral singlets as the only viable possibility. The Higgs cubic self-coupling then places a stringent constraint; we predict that achieving a strongly first-order EWPT while evading the constraint from the Higgs cubic would require singlets getting at least $\sim .7$ of their mass-squared from the Higgs and occupying a narrow mass range. However, recall that our calculations of the viable region are approximate, with an estimated error of $\mathcal{O}(50)$ GeV. This is enough for the boundary of the viable region to move substantially relative to the projected Higgs cubic constraint, and so a more precise calculation of the phase transition would be required for definitive conclusions. Nevertheless, it is likely that a model of Loryons giving a strongly first-order EWPT would furnish a detectable signal at a near-future collider

such as the FCC-ee. Additionally, a model which produces a stochastic GW background would be expected to be observable at a near-future collider.

3.3 Conclusions

In this chapter we have examined particles getting most of their mass from their coupling to the Higgs field ("Loryons"), subject to some modest assumptions, and their potential effect on the electroweak phase transition. As Loryons by definition have a significant coupling to the Higgs, it is reasonable to expect that they have a significant effect on the Higgs effective potential and can enable a strongly first-order EWPT. For BSM Loryons which are viable when added by themselves, we performed scans over the parameter space and calculated the properties of the EWPT. We find that the region of parameter space in which the Loryons are experimentally viable overlaps heavily with the parameter space for which a strongly first-order phase transition is predicted.

Loryons cut off at $f_{\max} = 1/2$, as this is the point at which a BSM particle requires HEFT for an effective field theory description. The viable band has generally not yet run into the unitarity bound by $f_{\max} = 1/2$, and so it is not required to add Loryons to achieve a strongly first-order EWPT. However, beyond the Loryon regime the viable band turns sharply to higher masses, so the portion of the experimentally allowed parameter space which gives a strongly first-order phase transition is significantly larger for Loryons as compared to non-Loryons. This is not an artifact of the chosen parametrization of $(m, f_{\max})$; if viewed in terms of the cross-quartic between the Higgs and the new field rather than the mass, smaller values of $f_{\max}$ require a cross-quartic larger by factor of $\mathcal{O}(3)$, while the range of cross-quartics giving a viable EWPT remains approximately the same size.

There are Loryons which are not viable on their own but which can satisfy the ex-

perimental constraints when added with enough appropriate other Loryons. For these cases, not as much of the parameter space gives an appropriate EWPT since adding too many new scalar Loryons stabilizes the effective potential at the origin. However, when both scalar and fermionic Loryons are added there are still broad ranges of the parameter space which would predict a strongly first-order EWPT.

The parameter space for which the EWPT produces a stochastic gravitational wave background detectable by near-future observatories is much smaller. However, it once again overlaps with the experimentally viable parameter space. Of particular note, however, is that it does not overlap with the viable parameter space for the neutral singlet; we conclude that the bound from imposing partial wave unitarity on the S-matrix is sufficient to rule out a detectable stochastic GW background from a (one-step) first-order EWPT driven by a neutral singlet. The $\mathbb{Z}_2$-symmetric neutral singlet is popularly referred to as a "nightmare scenario" due to its paucity of collider signals, and this would mean that a viable model obeying our assumptions could not be detected by near-future GW observatories. However, a few points of caution are in order. First, as stated before, we have made only an approximate calculation of the phase transition and its characteristics; nevertheless, our result is consistent with more detailed calculations in the literature such as [81, 99]. Second, we have only considered the possibility of a one-step phase transition, with no vev for the singlet; the partial wave unitarity bound does not rule out the region of parameter space with a two-step transition and a detectable GW background. Third, only a model with a single neutral singlet is ruled out in this way; the partial wave unitarity is only slightly affected by adding more singlets, while the region of parameter space with a detectable GW background shifts down.

Due to their coupling to the Higgs, new Loryons would have a significant effect on Higgs properties and could be detected via this avenue at future colliders. Improveed measurement of $h\gamma\gamma$ could detect or rule out charged Loryons. Measurements of the

Higgs cubic self-coupling are projected to overlap heavily with the region predicted to have a strongly first-order phase transition, with a measurement of order tens of percent probing much of this region and potentially leading to a discovery. For a precision such as that projected for the FCC-ee, ILC, or CLIC, a more detailed calculation of the phase transition would be required to give precise results, but we expect only Loryons getting at least $\sim .7$ of their mass-squared from the Higgs in a narrow mass range could provide a strongly first-order EWPT while evading detection via modifications to the Higgs cubic. In particular, this means that the viable region for non-Loryons could be entirely ruled out.

We imposed a $\mathbb{Z}_2$ symmetry on the new Loryons and required that they have positive mass-squared terms. It is possible to relax these assumptions; doing so would be particularly notable for EWBG as it would allow the possibility of a two-step transition where one of the new fields acquires a vev. Relaxing these assumptions leads to tree-level signatures and thus additional experimental constraints on the new Loryons, but it would be interesting to examine this broader parameter space for the existence of a viable EWPT.

The calculations herein have only characterized broad regions of parameter space. For models of particular interest, one could make a more precise calculation of the effective potential, the phase transition, and its properties. In addition, we have only examined the question of whether the phase transition is strongly first-order. While this is a necessary condition for electroweak baryogenesis, it is not the only one. Future work could develop a model with additional CP-violating ingredients added to one or more BSM Loryons to give a full theory of electroweak baryogenesis. Similarly, more precise calculations could be done for specific models of interest to confirm their possible detectability via gravitational wave backgrounds.

BSM particles which receive most of their mass from couplings to the Higgs boson remain experimentally viable. Thanks to this coupling, they not only have novel,

detectable collider phenomenology but also have a strong effect on the physics of the electroweak phase transition, may contribute to baryogenesis, and could potentially be detected through gravitational wave observation.

Chapter 4

Effective Field Theory of the Two Higgs Doublet Model

This chapter is based on work with Timothy Cohen, Nathaniel Craig, Xiaochuan Lu, and Dave Sutherland, published as [2].

They say good things come in pairs. This is certainly true in the search for new particles, where a second Higgs doublet has long been a quintessential candidate for BSM physics. The resulting two Higgs doublet model (2HDM) has been a subject of active study since its introduction in the 1970's (the original goal was to provide a model with spontaneous CP violation that could explain the CKM phase) [132, 133]. Two Higgs doublet models arise in many motivated extensions of the Standard Model and provide perhaps the simplest realization of a spin-0 sector that matches the richness of the observed spin-1/2 and spin-1 sectors. Subsequent exploration of the many facets of 2HDMs has given rise to a vast literature; see *e.g.* [134] for a classic review.

The model predicts the addition of four new physical degrees of freedom to the Standard Model. The existence of these BSM states may be inferred from both their direct

production and their indirect imprints on the couplings of the already observed Higgs boson. Over time, dedicated searches for these experimental signatures have been used to constrain the allowed parameter space. This has engendered the generic expectation that the extra Higgs bosons in the 2HDM are likely to be at least several hundreds of GeV (barring a number of known loopholes in certain regions of parameter space). If the new states in the 2HDM are heavy compared to the electroweak scale, an effective field theory description becomes a useful way to characterize the resulting deviations from the Standard Model at low energies.

Subtleties arise when matching a 2HDM onto an EFT with only one light Higgs boson. Integrating out the BSM Higgs bosons generically leads to an EFT for the observed Higgs boson h in which electroweak symmetry is nonlinearly realized, often referred to as the Higgs EFT (HEFT). Alternately, integrating out an $SU(2)_L$ doublet of approximate mass eigenstates *can* lead to an EFT for a Higgs doublet H in which electroweak symmetry is linearly realized, often referred to as the Standard Model EFT (SMEFT). In this case, the misalignment between the gauge and mass eigenstates is encoded by irrelevant operators in the EFT. Whenever SMEFT is admissible, it is often the preferred framework due to its compact parameterization and more transparent power-counting in the decoupling limit.

In a general 2HDM, there is a global $U(2)$ flavor symmetry acting on the two Higgs doublets. Hence, there are infinitely many different basis choices one can specify in the UV description from which an infinite number of EFTs can be derived by integrating out one doublet. These EFTs are only formally equivalent when the full tower of effective operators are included; different choices lead to different EFT Wilson coefficients and potentially different linearly realized symmetries.

Given the freedom to choose a UV basis, what constitutes a good choice? Among many possible criteria, two stand out. First, the relative advantages of SMEFT over

HEFT makes it preferable to choose a basis in which the low-energy theory is SMEFT, provided such a basis exists. Second, a good basis should allow the resulting EFT to accurately reproduce the effects of the full theory with as few operators as possible (*e.g.* at low orders in the EFT expansion).

In previous literature [135, 136, 137, 138, 139, 140], satisfying the first criterion has favored a particular basis for constructing 2HDM EFTs. Integrating out a doublet that acquires a vacuum expectation value implies that the low-energy theory does not in general contain an electroweak symmetric point and thus requires HEFT instead of SMEFT. This fate can be avoided by using the *Higgs basis* [141], for which the light doublet contains all of the vacuum expectation value that breaks electroweak symmetry.[1] Furthermore, the Higgs basis and the mass eigenstate basis become approximately aligned in the decoupling limit [142, 143] of CP-conserving 2HDMs, making the Higgs basis sensible for constructing the 2HDM SMEFT in this limit. However, exclusive use of the Higgs basis to meet our first criterion often makes it hard to meet the second criterion. The Higgs basis typically results in a poorly-convergent EFT expansion away from the decoupling limit even when SMEFT is formally appropriate for describing the low-energy theory. A more convergent EFT expansion can be obtained away from the decoupling limit by integrating out heavy mass eigenstates, but this generically yields HEFT. This tension has been a long-standing obstruction to the general EFT treatment of 2HDM.

For better insight, it helps to recognize that the two criteria involve different points in field space. The origin in field space (where electroweak symmetry is restored) is essential for determining whether SMEFT can describe the low-energy theory, while our physical vacuum determines the composition of the mass eigenstates. It is therefore useful to rethink the basis choice in terms of a trajectory in field space that connects the origin,

[1] As emphasized in [137], this definition of the Higgs basis leaves a $U(1)_{\rm PQ}$ subgroup of the original $U(2)$ flavor symmetry intact, leading to a $U(1)$ family of Higgs bases.

where electroweak symmetry is linearly realized, to the physical vacuum. This motivates interpreting the field space of the theory in a geometric language where the EFT defines a submanifold of the UV description, as detailed in [11]. The submanifold picture presents a new perspective on matching calculations: instead of integrating out approximate mass eigenstates or fields without vevs, one instead attempts to find a basis in the full theory that yields a simple parameterization of the EFT submanifold.

In this chapter, we follow this strategy and identify a new basis for the 2HDM that simplifies integrating out the BSM states and matching to SMEFT (when possible) while also vastly improving convergence away from the decoupling limit. The key observation is that when there is a charge-preserving global minimum, there exists a basis choice for which (the zero-derivative part of) the classical solution of the heavy Higgs doublet is a *linear* function of the light Higgs doublet; this defines what we call the "straight-line" (SL) basis.[2] This basis — which can be defined in *any* 2HDM with a charge-conserving global minimum — unsurprisingly simplifies the matching calculation.

Whether the EFT that results from matching in the SL basis can be SMEFT-like (linearly realizing electroweak symmetry) or must be HEFT-like depends on the parameters of the 2HDM itself; the SL basis is useful in either case. Since the vev of the heavy Higgs doublet vanishes at the same point as the vev of the light Higgs doublet (preserving an electroweak symmetric point in the EFT even though the heavy doublet acquires a vev elsewhere on the EFT submanifold), the SL basis satisfies our first criterion by enabling matching onto a SMEFT-like EFT whenever the parameters of the 2HDM admit it. This is not guaranteed in the Higgs basis, for which matching may lead to a HEFT-like EFT even if the 2HDM admits a SMEFT-like description.

As we will see, matching in the SL basis also satisfies our second criterion by resum-

[2]While SL nominally denotes "straight-line," four of the five authors would prefer to think of it as standing for "SutherLand", after its discoverer. The fifth author is too modest to contemplate naming a basis after himself. We leave it to the reader to decide.

ming the zero-derivative Higgs field dependence to all orders in the Wilson coefficients of the EFT, similar to the so-called "vev-improved matching" prescription introduced in [136]. When the 2HDM allows it, the resultant EFT is SMEFT-like in the sense that it linearly realizes electroweak symmetry, but it has a power-counting expansion determined by counting derivatives and SM fermion fields.[3] The resummation of Higgs field dependence leads to improved convergence away from the decoupling limit. In the decoupling limit, one can of course expand the field dependence contained in these Wilson coefficients, thereby obtaining a conventional SMEFT expansion (which is understood to involve both linearly-realized electroweak symmetry and a power-counting expansion in operator dimensions). We concretely demonstrate the advantages of the SL basis by comparing the predictions for three pseudo-observables — the Higgs coupling to gauge bosons, the Higgs self-coupling, and the Higgs coupling to fermions — between the full theory and EFTs obtained from matching in the Higgs basis and the SL basis, finding that the SL basis generically outperforms the Higgs basis by a significant margin away from the decoupling limit.

The rest of this chapter is organized as follows. In Section 4.1 we begin by reviewing the general 2HDM parameterization and conditions for charge conservation. We then define the SL basis and the transformation relating it to the Higgs basis and explore the circumstances under which each basis admits a SMEFT expansion. We carry out tree-level matching in the SL basis using functional methods in Section 4.2. Matching in the SL basis involves an expansion in powers of derivatives and fermions, which we carry out up to six derivatives and/or fermions, and all orders in the light Higgs doublet. Matching to all orders in the light Higgs doublet — a feat enabled by the simplicity

[3]This combination of symmetries and power-counting is reminiscent of geoSMEFT [144], although our matching procedure incorporates higher-derivative structures that lie outside the scope of geoSMEFT (and Riemannian field-space geometry in general), and we do not organize the field dependence of Wilson coefficients geometrically.

of the SL basis — effectively resums zero-derivative terms in the SMEFT expansion associated with the physical masses of the heavy Higgs bosons. In Section 4.3 we compare numerical predictions for key Higgs pseudo-observables between the full theory, the EFT obtained from matching in the Higgs basis, and the EFT obtained from matching in the SL basis, demonstrating the improved precision of the SL basis. We illustrate aspects of the mapping between EFTs obtained from the Higgs basis and the SL basis in Appendices B and C.

4.1 More Higgses, More Bases

The goal of this section is to introduce the general 2HDM and to provide a discussion of its vacuum structure. Many intricacies of the 2HDM stem from the ability to change basis by mixing the two doublets with each other. This freedom allows us to define the straight-line (SL) basis, for which (the zero-derivative part of) the classical solution of the "heavy" Higgs doublet will be proportional to the "light" doublet. We will then provide a map between the SL basis and the Higgs basis, which will facilitate a comparison between the convergence properties of the EFTs that result when integrating out the BSM states for these two basis choices.

4.1.1 Defining the 2HDM

The 2HDM is defined as the most general renormalizable Lagrangian built out of the Standard Model fermions and gauge bosons along with two $SU(2)_L$ doublet complex scalar fields with $U(1)_Y$ hypercharge 1/2. We denote them by Φ_a^α, together with their conjugate $\Phi^\dagger_{a\alpha}$. There are two types of indices on the Higgs fields: a flavor index $a = 1, 2$ differentiates between the two doublets and the upper gauge index α transforms in the fundamental representation of $SU(2)_L$.

The Lagrangian comprises a set of kinetic terms (including the minimal coupling to gauge bosons through the covariant derivative D_μ), the scalar potential, and Yukawa couplings,

$$\mathcal{L} = \mathcal{L}_2 + \mathcal{L}_0 + \mathcal{L}_J \,, \tag{4.1a}$$

$$\mathcal{L}_2 = \big(D_\mu \Phi_a^\dagger\big)\big(D^\mu \Phi_a\big) \,, \tag{4.1b}$$

$$-\mathcal{L}_0 = \mathcal{Y}_{ab}\big(\Phi_a^\dagger \Phi_b\big) + \frac{1}{2}\mathcal{Z}_{abcd}\big(\Phi_a^\dagger \Phi_b\big)\big(\Phi_c^\dagger \Phi_d\big) \,, \tag{4.1c}$$

$$\begin{aligned} -\mathcal{L}_J &= \mathbf{y}^D_{ija}\,\overline{Q}_i d_j \Phi_a + \mathbf{y}^{U\dagger}_{ija}\,\overline{u}_i(\varepsilon Q_j)\Phi_a + \mathbf{y}^E_{ija}\,\overline{L}_i e_j \Phi_a + \text{h.c.} \\ &\equiv J_a^\dagger \Phi_a + \text{h.c.} \,, \end{aligned} \tag{4.1d}$$

where we have suppressed $SU(2)_L$ gauge indices and omitted terms that are independent of the Φ fields for brevity. The Q, d, u, L, and e represent the three families of Standard Model fermions. We have expressed the scalar potential in terms of the mass-dimension-2 couplings $\mathcal{Y}_{ab}$ and dimensionless couplings $\mathcal{Z}_{abcd}$ introduced in [145] (see also [146, 147]), which satisfy

$$\mathcal{Y}_{ab} = \mathcal{Y}^*_{ba} \,, \qquad \mathcal{Z}_{abcd} = \mathcal{Z}_{cdab} = \mathcal{Z}^*_{badc} \,. \tag{4.2}$$

These can be related to the standard 2HDM notation,

$$(\mathcal{Y}_{11}, \mathcal{Y}_{12}, \mathcal{Y}_{22}) = \big(m_1^2, -m_{12}^2, m_2^2\big) \,, \tag{4.3a}$$

$$(\mathcal{Z}_{1111}, \mathcal{Z}_{1112}, \mathcal{Z}_{1122}, \mathcal{Z}_{1221}, \mathcal{Z}_{1212}, \mathcal{Z}_{1222}, \mathcal{Z}_{2222}) = (\lambda_1, \lambda_6, \lambda_3, \lambda_4, \lambda_5, \lambda_7, \lambda_2) \,. \tag{4.3b}$$

The Yukawa matrices $\mathbf{y}$ are *a priori* arbitrary complex matrices, and together with the SM fermions they are subsumed into the $SU(2)_L$ doublet scalar currents J_a^α, which couple to the Higgs fields.

The kinetic term $\mathcal{L}_2$ is invariant under a $U(2)$ flavor symmetry,

$$\Phi_a \to U_{ab}^{\text{flavor}} \Phi_b \,, \qquad \text{with} \qquad U^{\text{flavor}} \in U(2) \,. \tag{4.4}$$

Under this transformation, the couplings $\mathcal{Y}_{ab}$, $\mathcal{Z}_{abcd}$, and $\mathbf{y}_a$ rotate accordingly. One consequence of this freedom is that, starting from the 14 real parameters in the scalar potential (of which 4 are phases), only 11 (of which 2 phases) are physical.[4]

Within the 11-dimensional physical parameter space of the scalar potential, one can identify phenomenologically viable subspaces. Requiring *explicit CP conservation* amounts to turning off the 2 physical phases, which is equivalent to demanding that there exists a basis, accessed by flavor rotations, where all $\mathcal{Y}_{ab}$ and $\mathcal{Z}_{abcd}$ parameters are real [148]. If we further require *explicit custodial symmetry conservation* in the scalar potential, then this is equivalent to further requiring $\mathcal{Z}_{1221} = \mathcal{Z}_{1212}$ in the basis with real valued $\mathcal{Y}_{ab}$ and $\mathcal{Z}_{abcd}$ [149] (see also [150]). In spite of their explicit conservation, CP and custodial symmetry may yet be spontaneously broken by the vacuum configuration of the two Higgses.

Electric charge can be spontaneously broken by the vacuum configuration of the 2HDM with or without explicit CP conservation. It is understood that a vacuum configuration conserves charge if and only if a unitary gauge rotation can be found to simultaneously set the upper components of both Higgs vevs to zero [151, 152],

$$\Phi_1\big|_{\text{vev}} = \frac{1}{\sqrt{2}} \begin{pmatrix} 0 \\ v_1 \end{pmatrix} , \qquad \Phi_2\big|_{\text{vev}} = \frac{1}{\sqrt{2}} \begin{pmatrix} 0 \\ v_2 \end{pmatrix} . \tag{4.5}$$

[4]Note that the central $U(1)$ subgroup of the $U(2)$, which just rephases both doublets equally, leaves the parameters invariant.

We introduce a complex number (assuming w.l.o.g. that v_1 is real)

$$\kappa \equiv \frac{v_2}{v_1} \in \mathbb{C}\,, \tag{4.6}$$

where $|\kappa| = \tan\beta$. This allows us to recast the above criterion in a general gauge basis as the requirement that the two Higgs vevs are multiples of each other (*i.e.* aligned in the gauge space),

$$\Phi_2^\alpha\big|_{\rm vev} = \kappa\,\Phi_1^\alpha\big|_{\rm vev}\,. \tag{4.7}$$

On phenomenological grounds, we work with the 2HDM parameter space for which this criterion is satisfied. Note that if this criterion is satisfied in one flavor basis, it is satisfied in any flavor basis, but the ratio κ is different in different bases.

4.1.2 The Straight-line Basis

We assume that we are working in a region of parameter space where the BSM Higgs states are sufficiently heavy for it to be useful to integrate them out. There then exists a direction in flavor space such that the second Higgs doublet Φ_2 is "heavy," meaning that its components are sufficiently well aligned with the larger eigendirections of the mass matrix at the global minimum. Our goal is then to integrate out Φ_2 in order to obtain an EFT describing the low energy behavior of the "light" doublet Φ_1. Here, we employ the functional approach for matching onto the EFT by integrating out the heavy states in the path integral in the semiclassical approximation (see [153, 154] for recent reviews of functional matching and implementation). At tree level this amounts to finding a classical solution, $\Phi_{2,\mathbf{c}}[\Phi_1]$, to the equations of motion for the heavy doublet,

$$D^2\Phi_2 + \mathcal{Y}_{2b}\Phi_b + \mathcal{Z}_{2bcd}\Phi_b\big(\Phi_c^\dagger\Phi_d\big) + J_2 = 0\,, \tag{4.8}$$

and substituting the classical solution back into the 2HDM action to yield the tree-level EFT. This generates the EFT operators and their Wilson coefficients together and facilitates working to all orders in the field Φ_1.

Eq. (4.8) is solved by working order-by-order in powers of derivatives and fermions. First, we require that the zero-derivative-and-fermion part of the classical solution,

$$\Phi_{2,\mathbf{c}}[\Phi_1] = \Phi^{(0)}_{2,\mathbf{c}}(\Phi_1) + O\big(\partial^2, J\big)\,, \tag{4.9}$$

solves the zero-derivative-and-fermion part of Φ_2's equation of motion, namely,

$$-\frac{\partial \mathcal{L}_0}{\partial \Phi_2^\dagger}\bigg|_{\Phi_2=\Phi^{(0)}_{2,\mathbf{c}}(\Phi_1)} = \mathcal{Y}_{2b}\Phi_b\big|_{\Phi_2=\Phi^{(0)}_{2,\mathbf{c}}(\Phi_1)} + \mathcal{Z}_{2bcd}\Phi_b\big(\Phi_c^\dagger\Phi_d\big)\big|_{\Phi_2=\Phi^{(0)}_{2,\mathbf{c}}(\Phi_1)} = 0\,. \tag{4.10}$$

This is a cubic equation in Φ_2; in a generic 2HDM basis it yields an EFT submanifold curve $\Phi^{(0)}_{2,\mathbf{c}}(\Phi_1)$ that is a complicated function. Now we will show that one can find a special 2HDM basis in which the solution curve $\Phi^{(0)}_{2,\mathbf{c}}(\Phi_1)$ is simply a straight line as long as the 2HDM has a global minimum that preserves electric charge. We refer to this basis as the SL basis.

We begin by noting that Eq. (4.10) must be satisfied at the point corresponding to the global minimum because by definition this is a point that minimizes the potential,

$$\mathcal{Y}_{2b}\Phi_b\big|_{\rm vev} + \mathcal{Z}_{2bcd}\Phi_b\big(\Phi_c^\dagger\Phi_d\big)\big|_{\rm vev} = 0\,. \tag{4.11}$$

Let us focus on the first term. The key observation is that it is the lower component of the "vector"

$$\mathcal{Y}_{ab}\Phi_b\big|_{\rm vev}\,, \tag{4.12}$$

which transforms in the fundamental representation of the flavor rotation group in

Eq. (4.4). Therefore, one can always find a flavor basis such that its lower component vanishes,

$$Y_{2b}\Phi_b\big|_{\text{vev}} = 0 \qquad \text{(SL basis condition)}\,. \tag{4.13}$$

This defines our SL basis. We adopt a convention of Roman letters Y_{ab}, Z_{abcd}, v_a, and k to denote quantities $\mathcal{Y}_{ab}$, $\mathcal{Z}_{abcd}$, $\mathcal{v}_a$, and $\mathcal{k}$ evaluated in the SL basis. In the SL basis, the two terms in Eq. (4.11) both vanish independently,

$$Y_{2b}\Phi_b\big|_{\text{vev}} = Z_{2bcd}\Phi_b\big(\Phi_c^\dagger\Phi_d\big)\big|_{\text{vev}} = 0\,. \tag{4.14}$$

Note that if a homogeneous function of Φ_a vanishes at a certain charge-conserving point (where their values are multiples of each other), then it vanishes on the whole (charge-conserving) straight line that connects that point with the origin. Since the two terms in Eq. (4.10) are both homogeneous functions of Φ_a, Eq. (4.14) implies that they both also vanish on the straight line,

$$Y_{2b}\Phi_b\big|_{\Phi_2=k\,\Phi_1} = Z_{2bcd}\Phi_b\big(\Phi_c^\dagger\Phi_d\big)\big|_{\Phi_2=k\,\Phi_1} = 0\,. \tag{4.15}$$

Therefore, in the SL basis the EOM Eq. (4.10) has the straight line solution

$$\Phi^{(0)}_{2,\mathbf{c}}(\Phi_1) = k\,\Phi_1\,, \qquad \text{with} \qquad k \equiv \frac{v_2}{v_1} \in \mathbb{C} \qquad \text{in the SL basis.} \tag{4.16}$$

Although in the SL basis Eq. (4.16) is always a solution to the EOM in Eq. (4.10), this straight-line EFT submanifold can only correspond to a well-behaved SMEFT when $Y_{22} > 0$ in the SL basis; see Sec. 4.1.4.

4.1.3 Mapping Between the Straight-line and Higgs Bases

Let us write the doublets in the SL basis as Φ_a $(a = 1, 2)$, and the doublets in the Higgs basis as $\Phi_{\dot{a}}$ $(\dot{a} = \dot{1}, \dot{2})$, adopting a convention of *dotting* Higgs-basis indices on the fields and the corresponding parameters $Y_{\dot{a}\dot{b}}$ and $Z_{\dot{a}\dot{b}\dot{c}\dot{d}}$.[5] We seek the unitary matrix $U_{\dot{a}b}$ that relates the two sets of doublets,

$$\Phi_{\dot{a}} = U_{\dot{a}b}\Phi_b\,. \tag{4.17}$$

The vevs in the two bases are similarly related,

$$v_{\dot{a}} = U_{\dot{a}b}v_b\,. \tag{4.18}$$

As the vevs in the respective bases are defined as

$$v_{\dot{a}} = \begin{pmatrix} v \\ 0 \end{pmatrix}, \qquad v_a = \begin{pmatrix} v_1 \\ v_2 \end{pmatrix} = \frac{v}{\sqrt{1+|k|^2}}\begin{pmatrix} 1 \\ k \end{pmatrix}, \tag{4.19}$$

where $v^2 = v_1^2 + |v_2|^2$, it follows that

$$U_{\dot{a}b} = \frac{1}{\sqrt{1+|k|^2}}\begin{pmatrix} 1 & k^* \\ -k & 1 \end{pmatrix}. \tag{4.20}$$

Rearranging the definition of the SL basis in Eq. (4.13) allows us to define k in terms of quadratic pieces of the SL basis potential,

$$k = \frac{v_2}{v_1} = -\frac{Y_{21}}{Y_{22}}\,. \tag{4.21}$$

[5]Note that $\mathcal{K} = 0$ in the Higgs basis, and k always refers to ratio of vevs in the SL basis, see Eq. (4.16).

As U relates the quadratic parameters in the SL and Higgs bases via

$$Y_{\dot{a}\dot{b}} = U_{\dot{a}c}\, Y_{cd}\, U^{\dagger}_{d\dot{b}}\,, \tag{4.22}$$

k can also be written in terms of Higgs basis quantities,

$$-k = \frac{Y_{\dot{2}\mathrm{i}}}{Y_{\mathrm{i}\mathrm{i}}} = \frac{Z_{\dot{2}\mathrm{i}\mathrm{i}\mathrm{i}}}{Z_{\mathrm{i}\mathrm{i}\mathrm{i}\mathrm{i}}}\,. \tag{4.23}$$

The last equality comes from the vev conditions in the Higgs basis, which relate

$$-v^2 = \frac{2Y_{\mathrm{i}\mathrm{i}}}{Z_{\mathrm{i}\mathrm{i}\mathrm{i}\mathrm{i}}} = \frac{2Y_{\dot{2}\mathrm{i}}}{Z_{\dot{2}\mathrm{i}\mathrm{i}\mathrm{i}}}\,. \tag{4.24}$$

The map between other SL and Higgs basis quantities that appear in the EFT matching is provided in App. B.

We note that both the SL and the Higgs basis are actually a $U(1)$ family of bases. This corresponds to the freedom to rephase the second Higgs doublet, without affecting the respective bases' vev conditions of Eq. (4.13) and $v_{\dot{2}} = 0$. The above procedure details a one-to-one map between equivalent SL and Higgs bases. This means that real scalar potential parameters unaffected by this rephasing — in the SL basis as in the Higgs basis — are physical.[6]

4.1.4 Prospects for Matching onto SMEFT

As we emphasized in the introduction, SMEFT is the EFT extension of the Standard Model that is expressed about the origin in field space where $|\Phi_1| = 0$ such that electroweak symmetry can be linearly realized. For SMEFT to be well defined, the EFT must be built from analytic functions of Φ_1, which admit a convergent expansion of local

[6] We thank H. Haber for pointing this out.

operators at this point. If it is not, then the UV theory must be matched onto HEFT [11]. This invites the question: is it possible to determine which regions of the 2HDM parameter space can be matched onto SMEFT? Crucially, the answer depends on the (basis-dependent) value of $\mathcal{Y}_{22}$.

Fig. 4.1 visualizes the charge conserving solutions $\Phi^{(0)}_{2,\mathbf{c}}(\Phi_1)$ of Φ_2's zero-derivative EOM, Eq. (4.10), by plotting

$$\frac{\mathrm{Re}\left(\Phi_1^\dagger \Phi^{(0)}_{2,\mathbf{c}}\right)\sqrt{2}}{|\Phi_1|\, v} \quad \text{versus} \quad \frac{|\Phi_1|\sqrt{2}}{v}\,. \tag{4.25}$$

In these coordinates, the global minimum lies at $(\cos\beta, \sin\beta)$, and in the SL basis, one of the solutions is a straight line of gradient $\mathrm{Re}\, k$. Fig. 4.1 shows two different custodially symmetric UV parameter points in both their respective Higgs and SL bases; custodial symmetry guarantees that $\mathrm{Im}\left(\Phi_1^\dagger \Phi^{(0)}_{2,\mathbf{c}}\right) = 0$ and $\mathrm{Im}\, k = 0$. Black contours show the 2HDM potential in the space of Φ_1 and $\Phi^{(0)}_{2,\mathbf{c}}$. The global minimum is shown by a black dot. The potential contours and global minimum are rotated between the Higgs and SL bases.

The multiple solutions for $\Phi^{(0)}_{2,\mathbf{c}}$ are the paths that extremize the potential in the vertical direction. The solutions shown in blue are stable — the mass matrix of the Φ_2 modes about blue solutions is positive definite; those shown in orange are not. Notably, the solutions $\Phi^{(0)}_{2,\mathbf{c}}$ in the Higgs and SL basis EFTs are not simple rotations of each other. Even when starting from the same UV parameter point, the resulting Higgs and SL basis EFTs are generally different (truncated to zero derivative order) and are not both guaranteed to admit a SMEFT expansion.

Following the treatment of [11], consider the behavior of the EFTs in the $|\Phi_1| \to 0$ limit. $\mathcal{Y}_{22} < 0$ is a sufficient criterion for a given basis' EFT not to match onto SMEFT. In the SL basis, $Y_{22} < 0$ leads to tachyonic Φ_2 modes in the $|\Phi_1| \to 0$ limit. This EFT

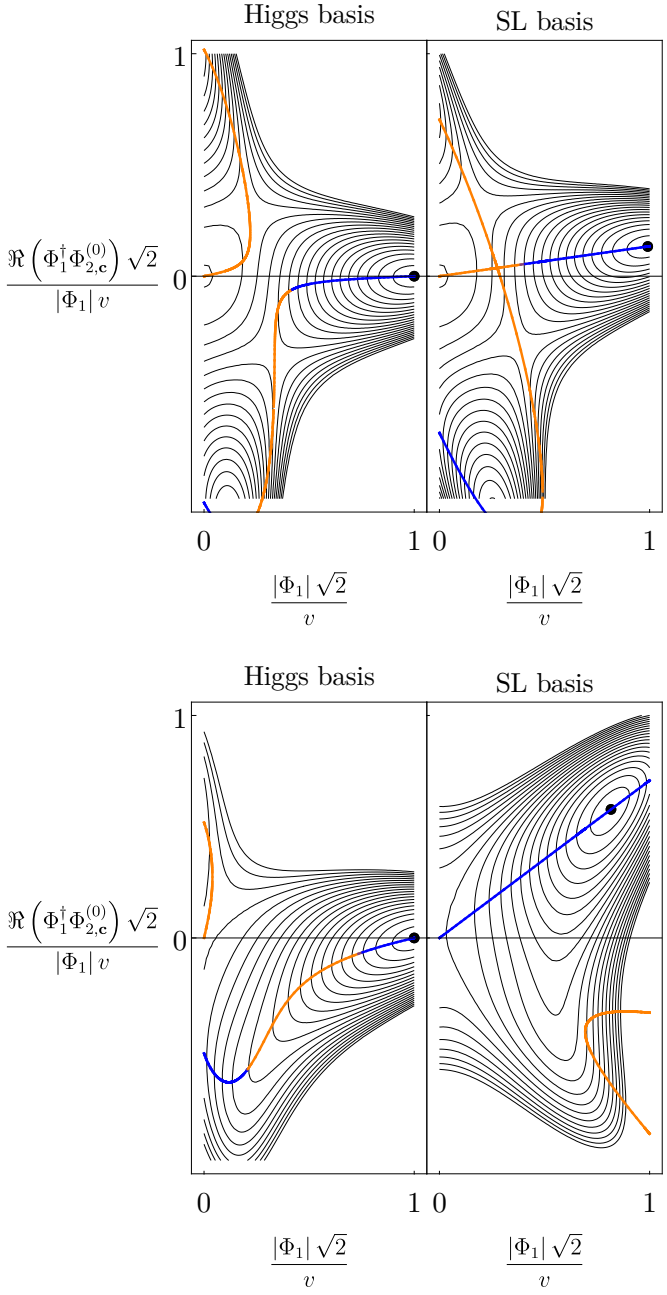

Figure 4.1: The Higgs and SL basis behavior for two example custodially symmetric 2HDM models. Black contours show the potential, and a black dot shows the global minimum, which has coordinates $(\cos\beta, \sin\beta)$ on these axes. The zero-derivative solutions of Φ_2's EOM, $\Phi_{2,\mathbf{c}}^{(0)}$, are shown in blue if the Φ_2 mass matrix is positive definite and in orange otherwise. Top: an example where $Y_{22} < 0$ and $Y_{\dot{2}\dot{2}} < 0$, and neither basis matches onto SMEFT. Bottom: $Y_{22} > 0$ in the SL basis, whereas $Y_{\dot{2}\dot{2}} < 0$ in the Higgs basis.

does not have a region of small p^2 where the effects of Φ_2 are purely virtual. The sickness is most apparent when matching at loop level: when $|\Phi_1| \to 0$ the Lagrangian would have an anti-Hermitian component corresponding to a rate for tunneling out of the false vacuum $\Phi^{(0)}_{2,\mathbf{c}}$.

In the Higgs basis, $Y_{\dot{2}\dot{2}} < 0$ generally leads to $\Phi^{(0)}_{2,\mathbf{c}}$ approaching a non-zero constant as $|\Phi_1| \to 0$. This does not yield a SMEFT, as can be verified by substituting $\Phi^{(0)}_{2,\mathbf{c}}$ back into the kinetic term Eq. (4.1b). As $|\Phi_1| \to 0$, the W mass remains non-zero, which cannot be reproduced using SMEFT operators.

Of course, whether $\mathcal{Y}_{22} < 0$ can be a *basis dependent* statement. If both eigenvalues of the matrix $\mathcal{Y}_{ab}$ are negative, then $\mathcal{Y}_{22} < 0$ in all bases, and it is therefore guaranteed that both $Y_{\dot{2}\dot{2}} < 0$ (in the Higgs basis) and $Y_{22} < 0$ (in the SL basis). This is the case for the potential in the top half of Fig. 4.1. However, if only one eigenvalue of $\mathcal{Y}_{ab}$ is negative, the sign of $\mathcal{Y}_{22}$ varies. In this case, Eq. (B.1a) guarantees that in the SL basis,

$$Y_{22} = \frac{1}{1+|k|^2}\frac{\det \mathcal{Y}}{Y_{\dot{1}\dot{1}}} > 0\,, \tag{4.26}$$

because $Y_{\dot{1}\dot{1}} < 0$ in the Higgs basis.

When $Y_{22} > 0$, the SL basis EFT formally admits a SMEFT expansion, in the sense that our expressions can be expanded in terms of local operators with powers of the positive Y_{22} in the denominator, and powers of $|\Phi_1|^2$ in the numerator. However, this does not necessarily result in a useful SMEFT, because such an expansion may not converge at the global minimum. In other words, the effects of dimension 8 operators in observables may not be smaller than dimension 6 operators, and so on. Note also that such an expansion is in any case impossible if $Y_{22} = 0$.

Even if only one eigenvalue of $\mathcal{Y}_{ab}$ is negative, and therefore $Y_{22} > 0$ in the SL basis, it is still possible that $Y_{\dot{2}\dot{2}} < 0$ in the Higgs basis, as shown in the bottom example of

Fig. 4.1. Thus, working in the SL basis improves the chances of matching onto SMEFT as $Y_{22} > 0$ whenever possible. As we will see in Sec. 4.3, working in the SL basis also improves the convergence of the resulting EFT expansion.

4.2 Matching in the SL Basis

We will now use the classical solution to the equation of motion of the second Higgs doublet to integrate out Φ_2 at tree level. In Sec. 4.1.2, we saw how the SL basis vastly simplifies the zero-derivative-and-fermion solution of the equation of motion. Here, this zero-derivative-and-fermion part is used to iteratively construct the higher order terms in the classical solution, which are in turn vastly simpler in the SL basis. In the end, we will include terms in the EFT up to six- derivative-and/or-fermion order and to all orders in the light field Φ_1.

4.2.1 Organizing the EFT Expansion

Since we need to derive terms involving as many as six derivatives and/or fermions in the EFT, we begin by setting up the expansion of the UV action on the classical equations of motion for the heavy doublet. We write the UV action derived using the Lagrangian in Eq. (4.1) as

$$S_{\rm UV}[\Phi_2] = S_0[\Phi_2] + \epsilon\big(S_2[\Phi_2] + S_J[\Phi_2]\big) = S_0[\Phi_2] + \epsilon S_\epsilon[\Phi_2]\,, \tag{4.27}$$

where $S_\epsilon[\Phi_2]$ is implicitly defined here, $S_0[\Phi_2]$ contains the zero-derivative scalar terms, $S_2[\Phi_2]$ contains the two-derivative scalar terms, $S_J[\Phi_2]$ contains the Yukawa interactions, and ϵ is an order parameter which we use to track the sum of the number of fermions

and derivatives,

$$2\epsilon = \#\text{ of derivatives} + \#\text{ of fermions}\,. \tag{4.28}$$

Ultimately, we will set $\epsilon = 1$. Note that we are only writing the explicit functional dependence on Φ_2 here for brevity, but of course $S_{\rm UV}$ also depends on the light Standard Model fields.

We will denote the Higgs doublet we are integrating out at tree level as

$$\mathcal{H}_x = \begin{pmatrix} \Phi_2^\alpha(x) \\ \\ \Phi^\dagger_{2\alpha}(x) \end{pmatrix}, \tag{4.29}$$

where the x label simultaneously stands for 1) the spacetime coordinate, 2) the $SU(2)_L$ index, and 3) the Higgs doublet versus its conjugate, as we need to vary with respect to all of them. We want to find $\mathcal{H}_{\mathbf{c},x}$, the classical solution to the equation of motion for $\mathcal{H}_x$, order-by-order in ϵ,

$$\mathcal{H}_{\mathbf{c},x} = \sum_{n=0}^{\infty} \epsilon^n\, \mathcal{H}^{(n)}_{\mathbf{c},x}\,. \tag{4.30}$$

This allows us to derive the EFT action as a semiclassical expansion,

$$S^{\rm tree}_{\rm EFT} = S_{\rm UV}[\mathcal{H}_{\mathbf{c},x}]\,. \tag{4.31}$$

Substituting the expansion defined in Eq. (4.30) into Eq. (4.27), we find

$$\begin{aligned} S^{\rm tree}_{\rm EFT} = {}& \epsilon^0 \overline{S_0} \\ & + \epsilon^1 \left[\overline{S_\epsilon} + (\overline{\delta S_0})_x\, \mathcal{H}^{(1)}_{\mathbf{c},x} \right] \\ & + \epsilon^2 \left[\frac{1}{2}\, (\overline{\delta^2 S_0})_{xy}\, \mathcal{H}^{(1)}_{\mathbf{c},x}\, \mathcal{H}^{(1)}_{\mathbf{c},y} + (\overline{\delta S_\epsilon})_x\, \mathcal{H}^{(1)}_{\mathbf{c},x} + (\overline{\delta S_0})_x\, \mathcal{H}^{(2)}_{\mathbf{c},x} \right] \end{aligned}$$

$$+\epsilon^3\bigg[\frac{1}{2}\,(\overline{\delta^2 S_\epsilon})_{xy}\,\mathcal{H}^{(1)}_{\mathbf{c},x}\,\mathcal{H}^{(1)}_{\mathbf{c},y}+\frac{1}{6}\,(\overline{\delta^3 S_0})_{xyz}\,\mathcal{H}^{(1)}_{\mathbf{c},x}\,\mathcal{H}^{(1)}_{\mathbf{c},y}\,\mathcal{H}^{(1)}_{\mathbf{c},z}$$
$$+(\overline{\delta^2 S_0})_{xy}\,\mathcal{H}^{(1)}_{\mathbf{c},x}\,\mathcal{H}^{(2)}_{\mathbf{c},y}+(\overline{\delta S_\epsilon})_x\,\mathcal{H}^{(2)}_{\mathbf{c},x}+(\overline{\delta S_0})_x\,\mathcal{H}^{(3)}_{\mathbf{c},x}\bigg]$$
$$+O\big(\epsilon^4\big)\,. \tag{4.32}$$

We use a bar to denote quantities evaluated on the zeroth-order classical solution $\mathcal{H}^{(0)}_{\mathbf{c},x}$, and we have defined the shorthand

$$(\delta S)_x\equiv\frac{\delta S}{\delta\mathcal{H}_x}\,,\qquad(\delta^2 S)_{xy}\equiv\frac{\delta^2 S}{\delta\mathcal{H}_x\delta\mathcal{H}_y}\,,\qquad(\delta^3 S)_{xyz}\equiv\frac{\delta^3 S}{\delta\mathcal{H}_x\delta\mathcal{H}_y\delta\mathcal{H}_z}\,. \tag{4.33}$$

Note that a repeated index implies an integral over the associated spacetime coordinate as well as a sum over the components of the Higgs doublet and their conjugates.

To find $\mathcal{H}_{\mathbf{c},x}$, we expand the equation of motion in powers of ϵ,

$$0=\frac{\delta S_{\rm UV}}{\delta\mathcal{H}_x}\bigg|_{\mathcal{H}_x=\mathcal{H}_{\mathbf{c},x}}$$
$$=\epsilon^0\,(\overline{\delta S_0})_x+\epsilon^1\Big[(\overline{\delta S_\epsilon})_x+(\overline{\delta^2 S_0})_{xy}\,\mathcal{H}^{(1)}_{\mathbf{c},y}\Big]$$
$$+\epsilon^2\bigg[(\overline{\delta^2 S_\epsilon})_{xy}\,\mathcal{H}^{(1)}_{\mathbf{c},y}+(\overline{\delta^2 S_0})_{xy}\,\mathcal{H}^{(2)}_{\mathbf{c},y}+\frac{1}{2}\,(\overline{\delta^3 S_0})_{xyz}\,\mathcal{H}^{(1)}_{\mathbf{c},y}\,\mathcal{H}^{(1)}_{\mathbf{c},z}\bigg]+O\big(\epsilon^3\big)\,. \tag{4.34}$$

Each order in ϵ must independently be zero. This gives

$$(\overline{\delta S_0})_x=0\,, \tag{4.35a}$$

$$(\overline{\delta S_\epsilon})_x+(\overline{\delta^2 S_0})_{xy}\,\mathcal{H}^{(1)}_{\mathbf{c},y}=0\,, \tag{4.35b}$$

$$(\overline{\delta^2 S_\epsilon})_{xy}\,\mathcal{H}^{(1)}_{\mathbf{c},y}+(\overline{\delta^2 S_0})_{xy}\,\mathcal{H}^{(2)}_{\mathbf{c},y}+\frac{1}{2}(\overline{\delta^3 S_0})_{xyz}\,\mathcal{H}^{(1)}_{\mathbf{c},y}\,\mathcal{H}^{(1)}_{\mathbf{c},z}=0\,, \tag{4.35c}$$

which can be solved to give $\mathcal{H}_{\mathbf{c},x}$ order-by-order in ϵ. Note that Eqs. (4.35) imply an

immediate simplification of Eq. (4.32),

$$S_{\rm EFT}^{\rm tree} = \epsilon^0\,\overline{S_0} + \epsilon^1\,\overline{S_\epsilon} + \epsilon^2\bigg[-\frac{1}{2}\,(\overline{\delta^2 S_0})_{xy}\,\mathcal{H}^{(1)}_{\mathbf{c},x}\,\mathcal{H}^{(1)}_{\mathbf{c},y}\bigg] + \epsilon^3\bigg[\frac{1}{2}\,(\overline{\delta^2 S_\epsilon})_{xy}\,\mathcal{H}^{(1)}_{\mathbf{c},x}\,\mathcal{H}^{(1)}_{\mathbf{c},y} + \frac{1}{6}\,(\overline{\delta^3 S_0})_{xyz}\,\mathcal{H}^{(1)}_{\mathbf{c},x}\,\mathcal{H}^{(1)}_{\mathbf{c},y}\,\mathcal{H}^{(1)}_{\mathbf{c},z}\bigg]. \tag{4.36}$$

We thus only need to compute $\mathcal{H}^{(1)}_{\mathbf{c},x}$, which amounts to solving Eq. (4.35b). This requires inverting the mass matrix $(\overline{\delta^2 S_0})_{xy}$, as described in the next section.

4.2.2 Inverting the Mass Matrix

The general expansion derived in the preceding subsection is valid in a general flavor basis. As mentioned above, deriving the EFT to the desired order requires solving Eq. (4.35b). We therefore must invert the mass matrix. To do so, we now specialize to the SL basis as defined in Eq. (4.16), for which

$$(\overline{\delta^2 S_0})_{xy} = -\delta^{(4)}(x-y) \begin{pmatrix} Z_1\Phi^\dagger_{1\alpha}\Phi^\dagger_{1\beta} & (Y_{22}+Z_2|\Phi_1|^2)\delta^\beta_\alpha + Z_3\Phi^\dagger_{1\alpha}\Phi^\beta_1 \\ (Y_{22}+Z_2|\Phi_1|^2)\delta^\alpha_\beta + Z_3\Phi^\dagger_{1\beta}\Phi^\alpha_1 & Z_1^*\Phi^\alpha_1\Phi^\beta_1 \end{pmatrix}, \tag{4.37}$$

where

$$Z_1 = Z_{1212} + 2k^*Z_{1222} + (k^*)^2 Z_{2222} = \begin{pmatrix} 1 & k^* \end{pmatrix} \begin{pmatrix} Z_{1212} & Z_{1222} \\ Z_{1222} & Z_{2222} \end{pmatrix} \begin{pmatrix} 1 \\ k^* \end{pmatrix}, \tag{4.38a}$$

$$Z_2 = Z_{1122} + 2\,\mathrm{Re}\big[kZ_{1222}\big] + |k|^2 Z_{2222} = \begin{pmatrix} 1 & k^* \end{pmatrix} \begin{pmatrix} Z_{1122} & Z_{1222} \\ Z_{2122} & Z_{2222} \end{pmatrix} \begin{pmatrix} 1 \\ k \end{pmatrix}, \tag{4.38b}$$

$$Z_3 = Z_{1221} + 2\,\mathrm{Re}\big[kZ_{1222}\big] + |k|^2 Z_{2222} = \begin{pmatrix} 1 & k^* \end{pmatrix} \begin{pmatrix} Z_{1221} & Z_{1222} \\ Z_{2122} & Z_{2222} \end{pmatrix} \begin{pmatrix} 1 \\ k \end{pmatrix} . \tag{4.38c}$$

Note that Z_2 and Z_3 are real valued. Note also that, if $Y_{22} < 0$, the eigenvalues of the mass matrix are negative in the $|\Phi_1| \to 0$ limit, as mentioned in Sec. 4.1.4.

Consistency with the $SU(2)_L$ structure implies an ansatz for the inverse,

$$(\overline{\delta^2 S_0})^{-1}_{yz} = -\delta^{(4)}(y-z) \begin{pmatrix} A\,\Phi_1^\beta \Phi_1^\gamma & B\,\delta^\beta_\gamma + C\,\Phi^\dagger_{1\gamma}\Phi_1^\beta \\ B\,\delta^\gamma_\beta + C\,\Phi^\dagger_{1\beta}\Phi_1^\gamma & A^*\,\Phi^\dagger_{1\beta}\Phi^\dagger_{1\gamma} \end{pmatrix} , \tag{4.39}$$

with $B = B^*$ and $C = C^*$. The solution is given by

$$A = -\frac{Z_1^*}{\big[Y_{22} + (Z_2+Z_3)|\Phi_1|^2\big]^2 - |Z_1|^2|\Phi_1|^4} , \tag{4.40a}$$

$$B = \frac{1}{Y_{22} + Z_2|\Phi_1|^2} , \tag{4.40b}$$

$$C = -\frac{1}{Y_{22} + Z_2|\Phi_1|^2} \frac{Z_3\big[Y_{22} + (Z_2+Z_3)|\Phi_1|^2\big] - |Z_1|^2|\Phi_1|^2}{\big[Y_{22} + (Z_2+Z_3)|\Phi_1|^2\big]^2 - |Z_1|^2|\Phi_1|^4} , \tag{4.40c}$$

as can be checked by explicit matrix multiplication. With the result in Eq. (4.39), we obtain an $O(\epsilon)$ solution to the EOM,

$$\Phi^{(1)}_{2,\mathbf{c}} = -\Big[A\left(\Phi_1^\dagger R\right)^* + C\left(\Phi_1^\dagger R\right)\Big]\Phi_1 - BR\,, \quad \text{with} \quad R \equiv kD^2\Phi_1 + J_2\,. \tag{4.41}$$

These results simplify in the custodial limit, for which, without loss of generality, all potential parameters and therefore k are real, and $Z_{1221} = Z_{1212}$ [149] (implying $Z_1 = Z_3$).

The coefficients of the inverse mass matrix defined in Eqs. (4.40) therefore simplify to

$$A = C = -\frac{Z_1}{(Y_{22} + Z_2|\Phi_1|^2)\,[Y_{22} + (Z_2 + 2Z_1)|\Phi_1|^2]}\,, \tag{4.42a}$$

$$B = \frac{1}{Y_{22} + Z_2|\Phi_1|^2}\,, \tag{4.42b}$$

when the UV 2HDM respects custodial symmetry.

4.2.3 The EFT Result

We now have everything we need to determine an EFT action for the light doublet Φ_1. Combining Eq. (4.36) with Eqs. (4.16) and (4.41), we have

$$\begin{aligned}
\mathcal{L}_{\rm EFT} = &-\left(1 + |k|^2\right) m_{\rm eff}^2 \,|\Phi_1|^2 - \frac{1}{2}\left(1 + |k|^2\right)^2 \lambda_{\rm eff}\,|\Phi_1|^4 \\
&+ \left(1 + |k|^2\right)|D_\mu \Phi_1|^2 - \left[\left(J_1^\dagger + k J_2^\dagger\right)\Phi_1 + \text{h.c.}\right] \\
&+ B\,|R|^2 + C\left|\Phi_1^\dagger R\right|^2 + \frac{1}{2}\left[A^*\left(\Phi_1^\dagger R\right)^2 + \text{h.c.}\right] + \left|D_\mu \Phi_{2,\mathbf{c}}^{(1)}\right|^2 \\
&- \left[Z_4\left(\Phi_1^\dagger \Phi_{2,\mathbf{c}}^{(1)}\right)\left|\Phi_{2,\mathbf{c}}^{(1)}\right|^2 + \text{h.c.}\right]\,,
\end{aligned} \tag{4.43}$$

where A, B, C are given in Eqs. (4.40); $\Phi_{2,\mathbf{c}}^{(1)}$ and R are given in Eq. (4.41). We have also introduced the notation $m_{\rm eff}^2$ and $\lambda_{\rm eff}$,

$$\left(1 + |k|^2\right) m_{\rm eff}^2 = Y_{ab} \begin{pmatrix} 1 \\ k^* \end{pmatrix}_a \begin{pmatrix} 1 \\ k \end{pmatrix}_b\,, \tag{4.44a}$$

$$\left(1 + |k|^2\right)^2 \lambda_{\rm eff} = Z_{abcd} \begin{pmatrix} 1 \\ k^* \end{pmatrix}_a \begin{pmatrix} 1 \\ k \end{pmatrix}_b \begin{pmatrix} 1 \\ k^* \end{pmatrix}_c \begin{pmatrix} 1 \\ k \end{pmatrix}_d\,, \tag{4.44b}$$

as well as Z_4, which populates the elements of $(\overline{\delta^3 S_0})_{xyz}$,

$$Z_4 = Z_{1222} + k^* Z_{2222} = \begin{pmatrix} 1 & k^* \end{pmatrix} \begin{pmatrix} Z_{1222} \\ Z_{2222} \end{pmatrix} . \tag{4.45}$$

4.2.4 EFT Predictions for Benchmark Pseudo-observables

We will use the matching result Eq. (4.43) to compute three pseudo-observables: the shift in the hW^+W^- coupling relative to the Standard Model κ_V, the shift in the Higgs self-coupling h^3 relative to the Standard Model κ_λ, and the shift in the $h\bar{f}f$ coupling relative to the Standard Model κ_f. We will compute all of these to the leading order in ϵ at which a correction to the Standard Model value appears. In the SL basis, these corrections are suppressed by powers of $\frac{m_h^2}{M_{\rm SL}^2}$, where $M_{\rm SL}^2$ is a characteristic heavy mass scale defined in Eq. (4.55).

We can drop the last line of Eq. (4.43) — which originates from the second $O\big(\epsilon^3\big)$ term in Eq. (4.36) — because it does not contribute to our pseudo-observables at the truncation order imposed in this section. Note also that the kinetic term for Φ_1 is not canonically normalized. Rewriting with the normalized field,

$$H \equiv \big(1 + |k|^2\big)^{1/2} \Phi_1 \,, \tag{4.46}$$

we get

$$\begin{aligned} \mathcal{L}_{\rm EFT} \supset\; & |D_\mu H|^2 - m_{\rm eff}^2 |H|^2 - \frac{1}{2}\lambda_{\rm eff} |H|^4 - \big(1 + |k|^2\big)^{-1} \Big[\big(\hat{J}_1^\dagger + k\, \hat{J}_2^\dagger\big) H + \text{h.c.}\Big] \\ & + \hat{B}\big|\hat{R}\big|^2 + \hat{C}\big|H^\dagger \hat{R}\big|^2 + \frac{1}{2}\Big[\hat{A}^* \big(H^\dagger \hat{R}\big)^2 + \text{h.c.}\Big] + \big(1 + |k|^2\big) \Big|D_\mu \hat{\Phi}_{2,\mathbf{c}}^{(1)}\Big|^2 \,, \end{aligned} \tag{4.47}$$

with a variety of rescaled quantities,

$$\hat{Y}_{22} \equiv \left(1+|k|^2\right) Y_{22}\,, \tag{4.48a}$$

$$\hat{J}_i \equiv \left(1+|k|^2\right)^{1/2} J_i\,, \tag{4.48b}$$

$$\hat{A} \equiv \left(1+|k|^2\right)^{-2} A = -\frac{Z_1^*}{\left[\hat{Y}_{22}+(Z_2+Z_3)|H|^2\right]^2 - |Z_1|^2|H|^4}\,, \tag{4.48c}$$

$$\hat{B} \equiv \left(1+|k|^2\right)^{-1} B = \frac{1}{\hat{Y}_{22}+Z_2|H|^2}\,, \tag{4.48d}$$

$$\hat{C} \equiv \left(1+|k|^2\right)^{-2} C = -\frac{1}{\hat{Y}_{22}+Z_2|H|^2}\frac{Z_3\left[\hat{Y}_{22}+(Z_2+Z_3)|H|^2\right]-|Z_1|^2|H|^2}{\left[\hat{Y}_{22}+(Z_2+Z_3)|H|^2\right]^2-|Z_1|^2|H|^4}\,, \tag{4.48e}$$

$$\hat{R} \equiv \left(1+|k|^2\right)^{1/2} R = kD^2H + \hat{J}_2\,, \tag{4.48f}$$

$$\hat{\Phi}^{(1)}_{2,\mathbf{c}} \equiv \left(1+|k|^2\right)^{-1/2}\Phi^{(1)}_{2,\mathbf{c}} = -\left[\hat{A}\left(H^\dagger\hat{R}\right)^* + \hat{C}\left(H^\dagger\hat{R}\right)\right]H - \hat{B}\hat{R}\,. \tag{4.48g}$$

We see that when restricted to two-derivative/fermion order, *i.e.*, the first line of Eq. (4.47), the matching result is the Standard Model. This is peculiar to the SL basis, where $\Phi^{(0)}_{2,\mathbf{c}} = k\Phi_1$. Working in a different basis would involve substituting a more complicated function $\Phi^{(0)}_{2,\mathbf{c}}(\Phi_1)$ into the ϵ^1 piece of Eq. (4.36), resulting in higher dimension operators at two-derivative/fermion order. Instead, in the SL basis, corrections to the pseudo-observables come from terms at the four- and six-derivative/fermion orders presented in the second line of Eq. (4.47). To compute these corrections, we will take Eq. (4.47) and expand around the physical vacuum where H has a non-zero vev. We will only keep terms that are relevant for κ_V (to six-derivative/fermion order), κ_f (to potentially six-derivative/fermion order), and κ_λ (to four-derivative/fermion order). We also need the propagator residue factors for all the external legs of these amplitudes. It is clear that the four- and six-derivative/fermion terms in Eq. (4.47) do not yield nontrivial corrections

to the propagator residues of the gauge bosons or the fermions, but they do modify the Higgs propagator residue factor Z_h.

In summary, when we expand Eq. (4.47), we would like to keep all the terms of the forms

$$h^2\,\partial^n\,, \qquad h^3\,\partial^n\,, \qquad W_\mu^+ W_\nu^- h\,\partial^n\,, \qquad \hat{j}_i\,h\,\partial^n\,, \tag{4.49}$$

where ∂^n denotes an arbitrary power of derivatives (up to our truncation order) and $\hat{j}_i$ are the neutral components of $\hat{J}_i$,

$$\hat{J}_i \supset \begin{pmatrix} 0 \\ \hat{j}_i \end{pmatrix}. \tag{4.50}$$

Note that all the four- and six-derivative/fermion terms in Eq. (4.47) are quadratic in $\hat{R}$. For finding the terms listed in Eq. (4.49), it is therefore sufficient to keep only part of $\hat{R}$,

$$\hat{R} = kD^2H + \hat{J}_2 \supset \begin{pmatrix} 0 \\ \frac{k}{\sqrt{2}}\left[(\partial^2 h) - \frac{1}{2}\,g_2^2 v\,W_\mu^+ W^{-\mu}\right] + \hat{j}_2 \end{pmatrix}, \tag{4.51}$$

and make the replacement

$$H \to \frac{1}{\sqrt{2}} \begin{pmatrix} 0 \\ v+h \end{pmatrix}, \tag{4.52}$$

for all the other factors of H fields in the four- and six-derivative/fermion terms in Eq. (4.47) (including the implicit ones in $\hat{A}, \hat{B}, \hat{C}$). Performing these substitutions, we obtain

$$\begin{aligned}\mathcal{L}_{\rm EFT} \supset\; & \frac{1}{2}(\partial h)^2 - \frac{1}{2}m^2h^2 - \frac{m^2}{2v}\,h^3 + \frac{1}{2}\,g_2^2 v\,W_\mu^+ W^{-\mu} h - \frac{1}{\sqrt{2}}\frac{v+h}{1+|k|^2}\left(\hat{j}_1 + k^*\hat{j}_2 + \text{h.c.}\right) \\ & + b_4\,\frac{1}{2}\,(\partial^2 h)\Big[(\partial^2 h) - g_2^2 v\,W_\mu^+ W^{-\mu}\Big] + \left[\frac{f_4}{\sqrt{2}k^*}\,\hat{j}_2^*\,(\partial^2 h) + \text{h.c.}\right] + \frac{c_4}{2}\,h\,\big(\partial^2 h\big)^2\end{aligned}$$

$$+ b_6 \frac{1}{2} (\partial_\mu \partial^2 h) \Big[(\partial^\mu \partial^2 h) - g_2^2 v \, \partial^\mu (W_\nu^+ W^{-\nu}) \Big] - \left[\frac{f_6}{\sqrt{2} k^*} \hat{j}_2^* \, (\partial^4 h) + \text{h.c.} \right] , \quad (4.53)$$

where the coefficients are

$$m^2 = \lambda_{\text{eff}} \, v^2 = -2 m_{\text{eff}}^2 , \quad (4.54a)$$

$$b_4 = \frac{1}{M_{\text{SL}}^4} \left\{ |k|^2 \left[\hat{Y}_{22} + (Z_2 + Z_3) \frac{v^2}{2} \right] - \text{Re} \left(k^2 Z_1 \frac{v^2}{2} \right) \right\} , \quad (4.54b)$$

$$\text{Re} \, f_4 = b_4 , \quad (4.54c)$$

$$\text{Im} \, f_4 = \frac{1}{M_{\text{SL}}^4} \, \text{Im} \left(k^2 Z_1 \frac{v^2}{2} \right) , \quad (4.54d)$$

$$c_4 = \frac{\partial}{\partial v} b_4 , \quad (4.54e)$$

$$b_6 = \frac{1}{M_{\text{SL}}^8} \left(1 + |k|^2 \right) \left| k \left[\hat{Y}_{22} + (Z_2 + Z_3) \frac{v^2}{2} \right] - k^* Z_1^* \frac{v^2}{2} \right|^2 , \quad (4.54f)$$

$$\text{Re} \, f_6 = b_6 , \quad (4.54g)$$

$$\text{Im} \, f_6 = \frac{1}{M_{\text{SL}}^8} \left(1 + |k|^2 \right) \left[\hat{Y}_{22} + (Z_2 + Z_3) \frac{v^2}{2} \right] \text{Im} \left(k^2 Z_1 v^2 \right) . \quad (4.54h)$$

Note the appearance of the mass scale

$$M_{\text{SL}}^4 = \left[\hat{Y}_{22} + (Z_2 + Z_3) \frac{v^2}{2} \right]^2 - |Z_1|^2 \, \frac{v^4}{4} , \quad (4.55)$$

which is closely related to the determinant of the mass matrix for the heavy Higgs doublet. (The only difference is the factor of $(1 + |k|^2)$ in $\hat{Y}_{22}$, which comes from canonically normalizing Φ_1 to H using Eq. (4.46).) M_{SL} includes both the explicit mass parameter Y_{22} and the vev-dependent contributions to the mass through the quartic couplings.

From Eq. (4.53), the terms that are quadratic in h with no other fields determine

that the dispersion relation for h is

$$-m^2 + p^2 + b_4 p^4 + b_6 p^6 + O\big(p^8\big) = 0\,, \tag{4.56}$$

which implies that the pole mass m_h^2 can be determined by solving

$$m^2 = m_h^2 + b_4 m_h^4 + b_6 m_h^6 + O\big(p^8\big)\,, \tag{4.57}$$

and that the residue is

$$\begin{aligned} Z_h^{-1} &= \frac{\partial}{\partial p^2}\left(-m^2 + p^2 + b_4 p^4 + b_6 p^6 + O\big(p^8\big)\right)\Big|_{p^2=m_h^2} \\ &= 1 + 2b_4 m_h^2 + 3b_6 m_h^4 + O\big(p^6\big)\,. \end{aligned} \tag{4.58}$$

Note that by including higher order momentum terms in the dispersion relation, we are effectively resumming a class of EFT corrections into the propagator. This is one of the systematic improvements that is facilitated by working in the SL basis. Using Eq. (4.53), we have

$$\kappa_V = Z_h^{1/2}(1 + b_4 m_h^2 + b_6 m_h^4) + O\big(m_h^6\big) = 1 - \frac{1}{2} m_h^4 \left(b_6 - b_4^2\right) + O\big(m_h^6\big)\,, \tag{4.59}$$

and

$$\kappa_\lambda = 1 - 2m_h^2 \frac{\partial}{\partial v^2}\left(v^2 b_4\right) + O\big(m_h^4\big)\,. \tag{4.60}$$

In particular, we note that the quantity appearing in κ_V is non-negative,

$$b_6 - b_4^2 = \frac{1}{M_{\rm SL}^8}\left\{\left|k\left[\hat{Y}_{22} + (Z_2 + Z_3)\frac{v^2}{2}\right] - \frac{v^2}{2} k^* Z_1^*\right|^2 + \left[\frac{v^2}{2}\,\mathrm{Im}(k^2 Z_1)\right]^2\right\} \geq 0\,, \tag{4.61}$$

which guarantees that the correction $\kappa_V - 1 \leq 0$ has the correct sign. Observe also that the correction in Eq. (4.59) is formally $\mathrm{O}(\epsilon^4)$: b_4^2 is the square of an $\mathrm{O}(\epsilon^2)$ piece, whereas the b_6 term is an $\mathrm{O}(\epsilon^3)$ piece multiplied by the 1 in $Z_h^{\frac{1}{2}}$, which is the uncorrected residue coming from the $\mathrm{O}(\epsilon^1)$ kinetic term.

Determining κ_f is complicated by the fact that there are different possibilities for the fermion couplings to the two doublets. It is most transparent to write the couplings to fermions in the Higgs basis, for which the neutral components of the currents are

$$J_{\mathrm{i}} = \begin{pmatrix} 0 \\ \\ j_{\mathrm{i}} \end{pmatrix}, \qquad J_{\dot{2}} = \begin{pmatrix} 0 \\ \\ j_{\dot{2}} \end{pmatrix}. \tag{4.62}$$

Using the mappings given in App. B, the SL basis currents are then

$$J_a = \frac{1}{\sqrt{1+|k|^2}} \begin{pmatrix} 1 & -k^* \\ k & 1 \end{pmatrix}_{a\dot{b}} J_{\dot{b}}\,. \tag{4.63}$$

This implies

$$\hat{j}_1 = j_{\mathrm{i}} - k^* j_{\dot{2}}\,, \tag{4.64a}$$

$$\hat{j}_2 = k j_{\mathrm{i}} + j_{\dot{2}}\,. \tag{4.64b}$$

The part of Eq. (4.53) containing fermions can be expressed in terms of Higgs basis currents as

$$\mathcal{L}_{\text{eff}} \supset -\frac{1}{\sqrt{2}} j_{\mathrm{i}} \left(v + h - f_4^* \partial^2 h + f_6^* \partial^4 h\right) - \frac{1}{\sqrt{2}} \frac{j_{\dot{2}}}{k} \left(-f_4^* \partial^2 h + f_6^* \partial^4 h\right) + \text{h.c.}\,. \tag{4.65}$$

We see that matching the fermion masses determines j_{i} and places no constraint on

$j_{\dot{2}}$; this is why it is useful to write the Lagrangian in terms of these quantities. The amplitude for a Higgs to decay to a particular chirality of fermions is then proportional to the matrix element of the unconjugated currents,

$$\begin{aligned}\mathcal{A}_{h\to\bar{f}_L f_R} &= -\frac{\langle j_{\dot{1}}\rangle}{\sqrt{2}}\, Z_h^{1/2}\left(1+f_4^* m_h^2+f_6^* m_h^4\right) - \frac{\langle j_{\dot{2}}\rangle}{k\sqrt{2}}\, Z_h^{1/2}\left(f_4^* m_h^2+f_6^* m_h^4\right) + O\big(m_h^6\big) \\ &= -\frac{\langle j_{\dot{1}}\rangle}{\sqrt{2}}\left[1-\frac{1}{2}\left(b_6-b_4^2\right)m_h^4\right] + i\frac{\langle j_{\dot{1}}\rangle}{\sqrt{2}}\Big[m_h^2\,\mathrm{Im}\, f_4 + m_h^4\big(\mathrm{Im}\, f_6 - b_4\,\mathrm{Im}\, f_4\big)\Big] \\ &\quad - \frac{\langle j_{\dot{2}}\rangle}{k\sqrt{2}}\left[b_4 m_h^2+\left(b_6-b_4^2\right)m_h^4\right] + i\frac{\langle j_{\dot{2}}\rangle}{k\sqrt{2}}\Big[m_h^2\,\mathrm{Im}\, f_4 + m_h^4\big(\mathrm{Im}\, f_6 - b_4\,\mathrm{Im}\, f_4\big)\Big] \\ &\quad + O\big(m_h^6\big)\,, \end{aligned} \tag{4.66}$$

where we are using a shorthand $\langle j\rangle = \big\langle \bar{f}_L f_R|j|0\big\rangle$.

To calculate κ_f, we then need to specify $j_{\dot{2}}$. There are a wide variety of possibilities with rich phenomenological implications, including conventional choices satisfying the Glashow-Weinberg condition [155]. In this work, we consider two specific choices. For both, we require the UV 2HDM potential to be CP-preserving; this means $\mathrm{Im}\, f_4 = \mathrm{Im}\, f_6 = 0$. For our first example, we set $j_{\dot{2}} = 0$, such that the fermion currents only couple to the linear combination of Higgses that gets a vev. In this case,

$$\kappa_f = 1 - \frac{1}{2}\left(b_6 - b_4^2\right)m_h^4 = \kappa_V\,. \tag{4.67}$$

In other words, to this order in the EFT expansion there is simply a universal rescaling of all Higgs couplings for this scenario. This is the unique choice for which κ_f does not receive a contribution at leading order. For our second example, we set $j_{\dot{2}} = j_{\dot{1}}$, in which case,

$$\kappa_f = 1 + \frac{b_4}{k}\, m_h^2\,, \tag{4.68}$$

where we have truncated to the leading order correction. Note that both of the possibilities we consider automatically ensure that there are no FCNC's at tree level.

4.3 Numerical Comparison

We will now provide the results of a scan in the 2HDM parameter space in order to compare the efficacy of the SL basis EFT with the Higgs basis EFT. We will provide results for the three pseudo-observables derived in the previous section: the shift in the hW^+W^- coupling κ_V, the shift in the h^3 coupling κ_λ, and the shift in the $h\bar{f}f$ coupling κ_f. For κ_f, we consider specifically the case when the Yukawa couplings of both doublets are the same in the Higgs basis; see Eq. (4.68). We will present the results in terms of the fractional error of the EFT prediction as compared to the UV prediction,

$$\delta\kappa_{i,\mathrm{EFT}} \equiv \frac{\kappa_{i,\mathrm{EFT}} - \kappa_{i,\mathrm{UV}}}{\kappa_{i,\mathrm{UV}} - 1}\,, \tag{4.69}$$

where $\kappa_{i,\mathrm{UV}}$ use the couplings computed in the full 2HDM; both the UV and the Higgs basis EFT results are taken from [137].

To make this comparison, we reduce the general 2HDM down to a four-parameter space of models. We first impose custodial symmetry and work in the resulting Higgs basis for which all parameters are real and $Z_{\mathrm{i\dot{2}i\dot{2}}} = Z_{\mathrm{i\dot{2}\dot{2}i}}$. We then scan over the 4 parameters

$$Y_{\mathrm{i\dot{2}}}\,, \quad Y_{\dot{2}\dot{2}}\,, \quad Z_{\mathrm{iiii}}\,, \quad Z_{\mathrm{ii\dot{2}\dot{2}}}\,. \tag{4.70}$$

Of the remaining parameters, Y_{ii} and $Z_{\mathrm{iii\dot{2}}}$ are fixed by the Higgs basis vev conditions Eq. (4.24); the others we fix to satisfy

$$Z_{\mathrm{i\dot{2}\dot{2}\dot{2}}} = Z_{\mathrm{i\dot{2}i\dot{2}}} = 0\,; \qquad Z_{\dot{2}\dot{2}\dot{2}\dot{2}} = Z_{\mathrm{iiii}}\,, \tag{4.71}$$

for simplicity. Note that it is important that $Y_{\mathrm{i}\dot{2}} \neq 0$ for the Higgs and SL bases to be distinct.

The four free parameters, Eq. (4.70), are scanned in units of $v = 246\,\mathrm{GeV}$ via a Markov Chain Monte Carlo (MCMC) method, which samples from the Gaussian likelihood of approximate current experimental constraints on m_h and $\kappa_V \equiv \sin(\beta - \alpha)$. Here α is the familiar Higgs mixing angle and $\sin(\beta - \alpha) \to 1$ is known as the *alignment limit*. Explicitly, we take

$$\frac{m_h^2}{v^2} = 0.2587 \pm 0.0007\,, \tag{4.72a}$$

$$\kappa_V = 1.0 \pm 0.1\,. \tag{4.72b}$$

The κ_V constraint assumes a Standard Model central value, and a 10% error based on the order-of-magnitude of ATLAS and CMS Run 2 1σ errors on κ_W and κ_Z, in the absence of invisible or untagged decays [156, 157]. Note that $\kappa_V \leq 1$ in the 2HDM. The MCMC is seeded on a grid of inert 2HDMs, where

$$Y_{\mathrm{i}\dot{2}} = 0\,, \tag{4.73a}$$

$$Y_{\dot{2}\dot{2}} = m_H^2(1 - f)\,, \tag{4.73b}$$

$$Z_{\mathrm{iii}\dot{\mathrm{i}}} = 0.2587\,, \tag{4.73c}$$

$$Z_{\mathrm{ii}\dot{2}\dot{2}} = 2f\frac{m_H^2}{v^2}\,, \tag{4.73d}$$

where m_H^2 is the heavy Higgs mass at the global minimum and f is the fraction of it which comes through the cross quartic interaction $\frac{1}{2}Z_{\mathrm{ii}\dot{2}\dot{2}}v^2$. We sample m_H^2 and f from

the discrete sets

$$\frac{m_H^2}{\text{GeV}} = \{400, 500, 600, 700, 800\} \ , \tag{4.74a}$$

$$f = \{0.1, 0.2, 0.3, 0.4, 0.5, 0.6, 0.7, 0.8, 0.9\} \ . \tag{4.74b}$$

We discard all models whose quartic couplings either make the potential unbounded or violate the perturbative unitarity constraints of [158]. This leaves ~ 7000 2HDM model points in the following analysis.

The performance of the SL basis EFT can be understood primarily by looking at two parameters: the alignment of the 2HDM and the mass scale from the mass matrix of the heavy doublet, M_{SL}, defined in Eq. (4.55). Recall from Sec. 4.2.1 that the SL basis EFT is an expansion in powers of derivatives (and fermions). We thus expect the n^{th} order corrections to our pseudo-observables to scale as

$$\left(D^2\right)^n \sim m_h^{2n} \sim v^{2n} \, . \tag{4.75}$$

By dimensional analysis, the n^{th} order corrections must also scale as some mass scale to the power of $-2n$. From Eqs. (4.35), these powers of mass dimension come from the inverse of the mass matrix for the heavy doublet; the n^{th} order corrections to our pseudo-observables thus scale as M_{SL}^{-2n}. The corrections therefore scale as

$$\text{SL basis power counting} \sim \left(\frac{v}{M_{\text{SL}}}\right)^{2n} \ , \tag{4.76}$$

and we expect that the SL EFT expansion will provide a good approximation when M_{SL} is large.

We plot our pseudo-observables in the $\cos(\alpha - \beta)$ versus M_{SL} plane in Figs. 4.2 to 4.4,

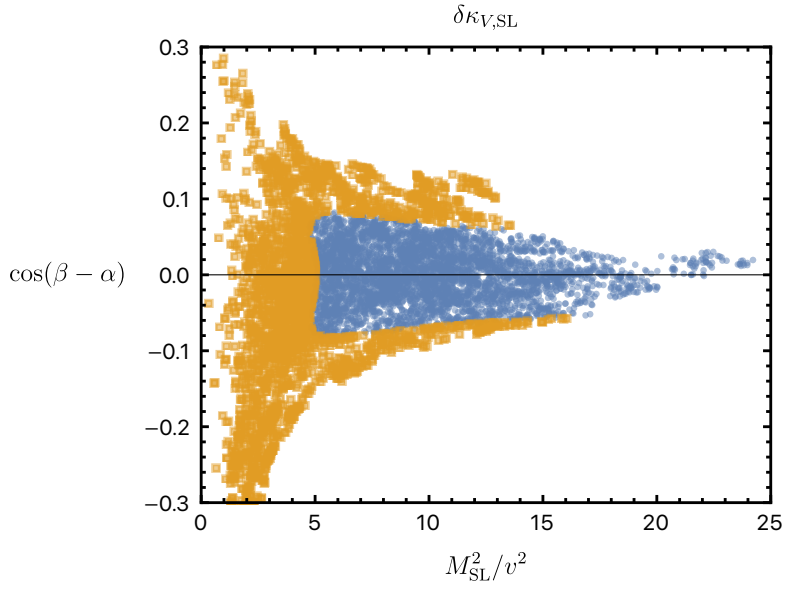

Figure 4.2: This figure shows for which models the SL basis EFT makes an accurate estimate of κ_V. Blue points are those for which $\delta\kappa_{V,\mathrm{SL}} < 0.1$ and orange points (shown on top of the blue points) are those for which $\delta\kappa_{V,\mathrm{SL}} > 0.1$.

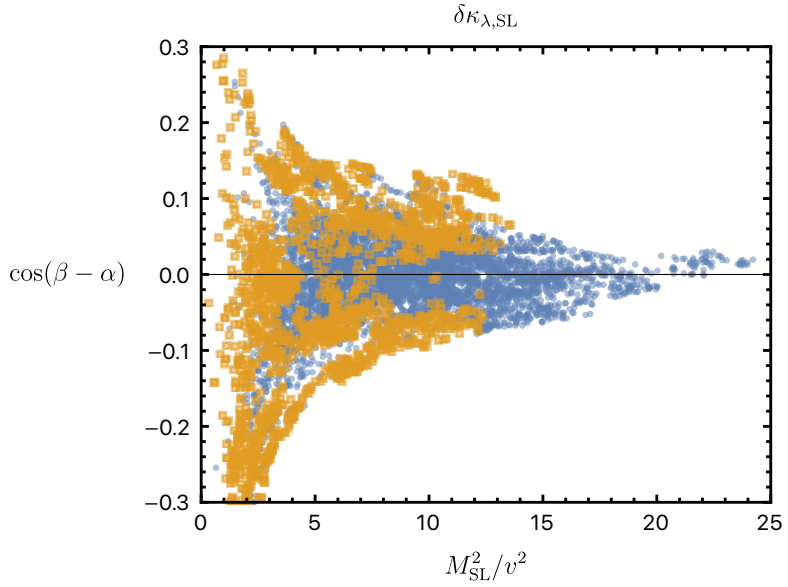

Figure 4.3: This figure shows for which models the SL basis EFT makes an accurate estimate of κ_λ. Blue points are those for which $\delta\kappa_{\lambda,\mathrm{SL}} < 0.1$ and orange points (shown on top of the blue points) are those for which $\delta\kappa_{\lambda,\mathrm{SL}} > 0.1$.

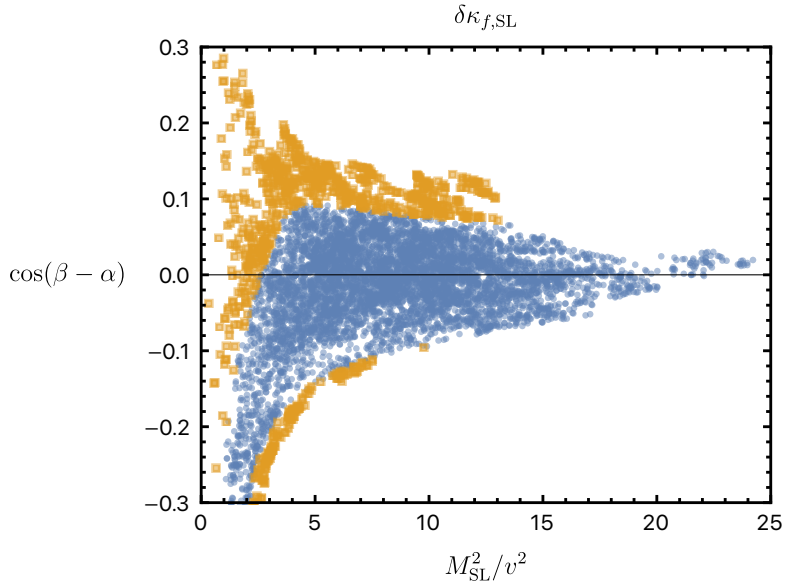

Figure 4.4: This figure shows for which models the SL basis EFT makes an accurate estimate of κ_f. We have taken the Yukawa couplings to the two Higgs doublets to be equal. Blue points are those for which $\delta\kappa_{f,\mathrm{SL}} < 0.1$ and orange points (shown on top of the blue points) are those for which $\delta\kappa_{f,\mathrm{SL}} > 0.1$. If the Yukawa couplings of the heavy doublet are instead set to zero, $\kappa_f = \kappa_V$.

where α is the Higgs mixing angle, $\beta = \arctan(v_2/v_1)$, and the combination $\cos(\alpha-\beta)$ is a measure of the alignment limit for the 2HDM. In the figures, we separate the points into those for which the fractional error is above or below 10% to provide a proxy for when the SL basis EFT prediction is accurate. As expected, we find better performance for larger values of M_{SL}. In addition, κ_V and κ_f are highly correlated with the measure of alignment; this is because $\kappa_{V,\mathrm{UV}}$ and $\kappa_{f,\mathrm{UV}}$ depend only on the alignment of the 2HDM (and, for κ_f, the Yukawa couplings of the Higgs doublets, which we have fixed). For κ_λ, the behavior is more complicated as a larger number of parameters affect the value of κ_λ.

A comparison of the performance for the SL basis EFT against the Higgs basis EFT is given in Figs. 4.5 to 4.7. The SL basis EFT typically outperforms the Higgs basis EFT by a significant margin (around 1-2 orders of magnitude smaller fractional error) for all three pseudo-observables; this is the case whether the SL basis EFT performs

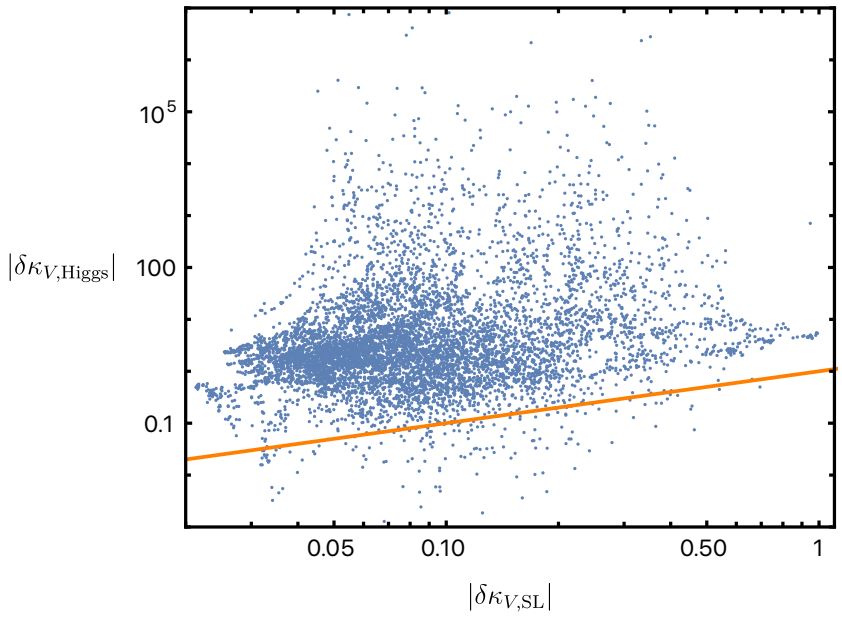

Figure 4.5: This figure shows the accuracy in computing κ_V for each of the EFTs. The straight orange line denotes equality between the accuracy of the two EFTs, with points above the line being those for which the SL basis EFT performs better than the Higgs basis EFT.

relatively well or relatively poorly. We do find parameter points for which the Higgs basis EFT outperforms the SL basis EFT, so the SL basis EFT is not universally better. In addition, for a significant minority of points the Higgs basis EFT catastrophically fails with a fractional error of several orders of magnitude; these catastrophic failures include many points on which the SL basis EFT performs quite well. By contrast, while points exist for which the SL basis EFT performs poorly, the Higgs basis tends to perform poorly as well, and none of the points included in our scan show a catastrophic failure of the SL basis.

The difference in performance of the two EFTs can be understood by looking at the mass scales involved in the power counting. As we saw in Eq. (4.76), higher-order corrections in the SL basis EFT are suppressed by powers of M_{SL}; this mass scale is comparable to the physical mass of the second Higgs doublet, so the EFT produces

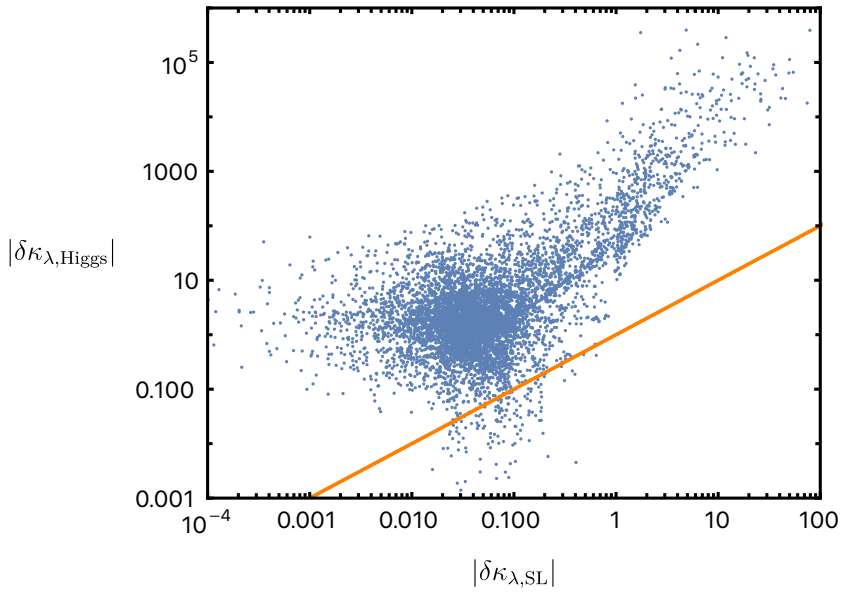

Figure 4.6: This figure shows the accuracy in computing κ_λ for each of the EFTs. The straight orange line denotes equality between the accuracy of the two EFTs, with points above the line being those for which the SL basis EFT performs better than the Higgs basis EFT.

reliable results when the second Higgs doublet is heavy. The higher-order corrections in the Higgs basis EFT are suppressed by powers of $Y_{\dot{2}\dot{2}}$. If the second Higgs doublet receives a large contribution to its mass from the vev, then $Y_{\dot{2}\dot{2}}$ can be significantly smaller than the mass of the second Higgs. We show how the relative performance of the two EFTs depends on the ratio of their respective mass scales in Figs. 4.8 to 4.10. We indeed see that when the mass scale of the Higgs basis EFT is significantly smaller than that of the SL basis EFT, the Higgs basis EFT is significantly less accurate. In addition, for all those points on which the Higgs basis EFT is more accurate than the SL basis EFT, the mass scales of the two EFTs are comparable, as expected.

Finally, we remark on the decoupling limit where the extra Higgs bosons are very heavy. As the quartic couplings of the 2HDM are constrained by perturbative unitarity to be $\mathrm{O}(8\pi)$, this requires taking the quadratic couplings large, namely, in the Higgs basis, $Y_{\dot{2}\dot{2}} \to \infty$ with $Y_{\dot{1}\dot{1}}, Y_{\dot{1}\dot{2}}$ fixed (see [159] for a recent discussion). By Eqs. (4.55)

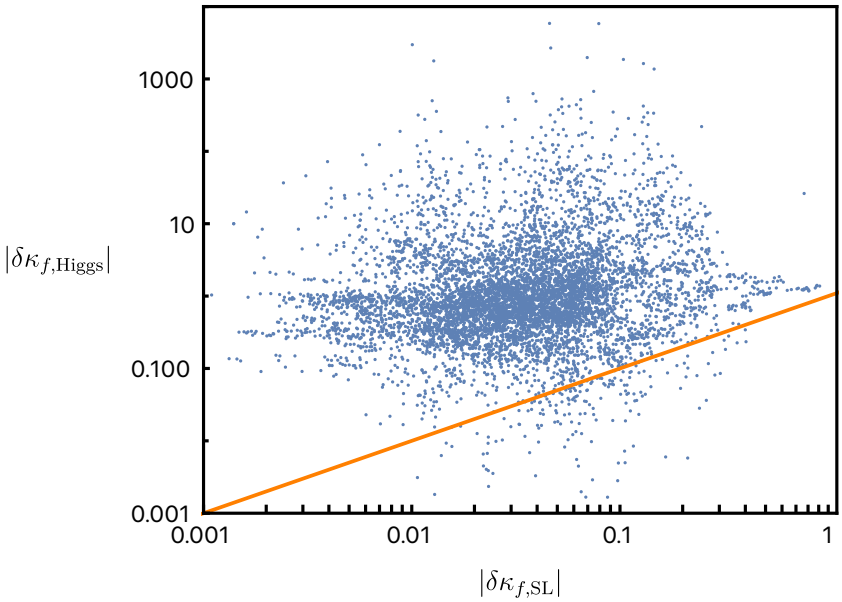

Figure 4.7: This figure shows the accuracy in computing κ_f. We have taken the Yukawa couplings to the two Higgs doublets to be equal. The straight orange line denotes equality between the accuracy of the two EFTs, with points above the line being those for which the SL basis EFT performs better than the Higgs basis EFT. If the Yukawa couplings of the heavy doublet are instead set to zero, $\kappa_f = \kappa_V$.

and (B.1a), this means both $\hat{Y}_{22}$ and M^2_{SL} in the SL basis approach the value of $Y_{\dot{2}\dot{2}}$. In App. C, we show that the SL basis EFT can be expanded in this limit to reproduce known results.

4.4 Conclusions

In this chapter, we have derived the tree-level matching coefficients by integrating out the BSM states in the 2HDM. The novel aspect of this work is the introduction of the SL basis, which is an optimal choice for performing the matching calculation. Working with the SL basis allows us to match a far broader parameter space of 2HDM models onto SMEFT and to resum all orders of the light Higgs field into the EFT Wilson coefficients in a systematic way. This leads to significantly improved predictions when compared to

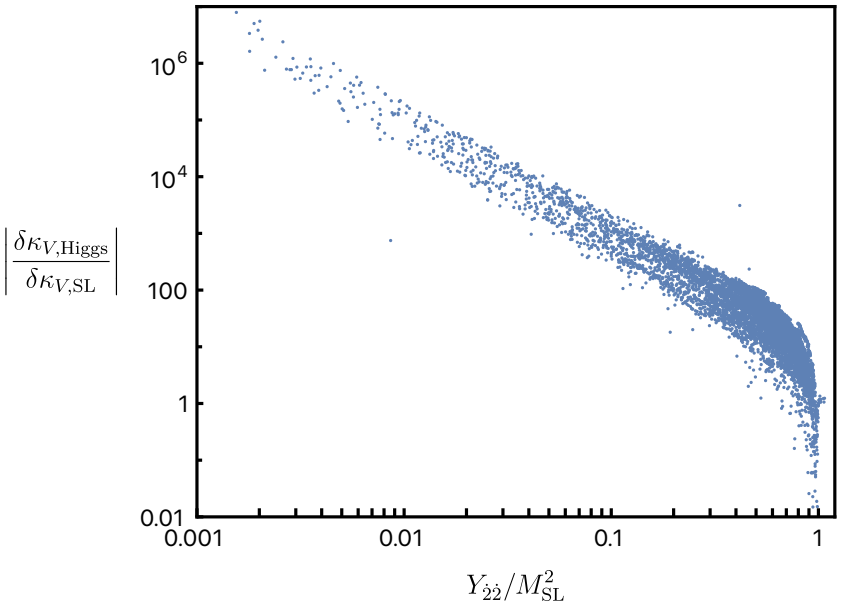

Figure 4.8: This figure shows how the performance of the SL basis EFT and the Higgs basis EFT prediction for κ_V depends on the ratio of the mass scales in the two EFTs.

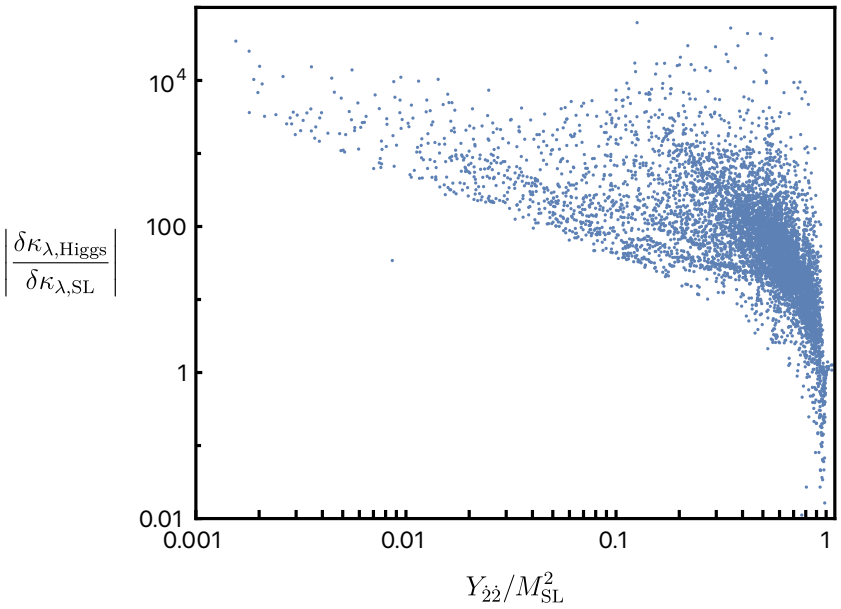

Figure 4.9: This figure shows how the performance of the SL basis EFT and the Higgs basis EFT prediction for κ_λ depends on the ratio of the mass scales in the two EFTs.

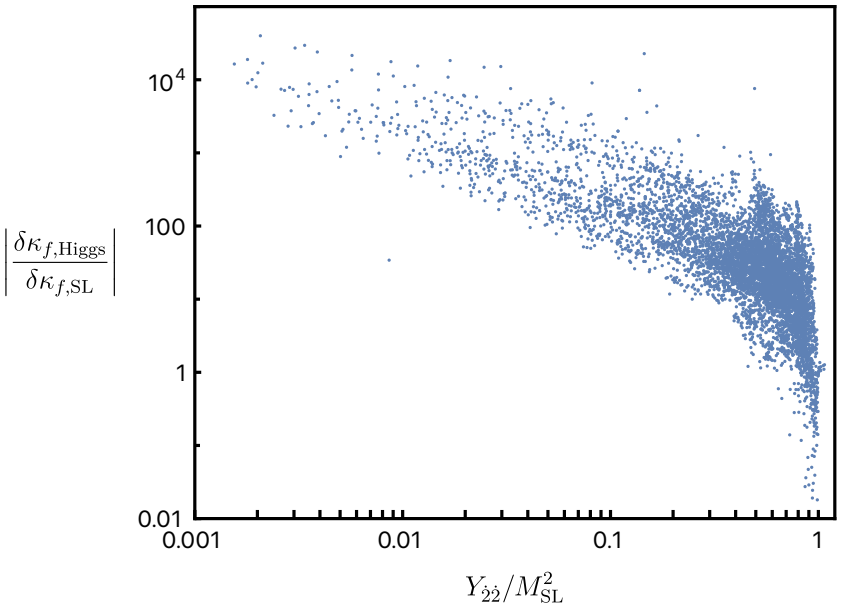

Figure 4.10: This figure shows how the performance of the SL basis EFT and the Higgs basis EFT prediction for κ_f depends on the ratio of the mass scales in the two EFTs. We have taken the Yukawa couplings to the two Higgs doublets to be equal. If the Yukawa couplings of the heavy doublet are instead set to zero, $\kappa_f = \kappa_V$.

the computation performed using the Higgs basis in the UV across most of the 2HDM parameter space. This demonstrates the utility of the EFT derived using the SL basis. In particular, this is the basis to use if one is interested in exploring the EFT predictions for the 2HDM for models that have alignment away from the decoupling limit. This brings the 2HDM fully into the EFT fold, extending the validity of EFT interpretations of Higgs coupling measurements across a wider range of 2HDMs.

There are many future directions to explore. As we have worked strictly at tree level, extending the SL basis EFT matching calculation to loop level (potentially with functional matching techniques) is a natural next step. Although we have focused our numerical studies on CP-conserving 2HDM, the SL basis is applicable in the fully general CP-violating 2HDMs, where further numerical studies are likely to be informative. It would also be instructive to extend the SL basis to models with extra scalar fields beyond the 2HDM.

There are also more phenomenological studies that could be done. Our expressions shed light on the physical combinations of parameters that can appear in the low energy virtual effects of the heavy doublet. However, since we only explored the properties of pseudo-observables here, it would be important to compute a set of full LHC observables which would serve as inputs to provide constraints on the 2HDM parameter space. It is possible that one could then identify novel indirect searches that could be performed which would be particularly sensitive to the effects of the 2HDM. And in the event that an indirect signal of BSM physics would be discovered, the results here would facilitate our ability to interpret such a signal in terms of the 2HDM parameter space.

Chapter 5

Conclusions

Effective field theory is a crucial tool in the search for physics beyond the Standard Model. Like any other tool, it needs to be well understood in order to be properly deployed and work to its full potential. One must understand how the choices made in constructing an EFT affect the space of UV models the EFT could describe and how to most efficiently analyze particular UV models using effective field theory.

In this work we have examined these questions. Loryons provide a family of simple UV models which are nevertheless excluded *a priori* by using SMEFT as the EFT description of the Standard Model. We have seen that Loryons remain experimentally viable, and their sizable coupling to the Higgs gives them striking experimental signatures both at colliders and in cosmology. On the other side, we have shown that an EFT description for the two Higgs doublet model is of significantly varying utility depending on the basis choice made in the UV. These results emphasize the need to think carefully about how to use EFT in order not to make mistakes and to derive the maximum benefit.

It's an exciting time in particle physics; there are physics phenomena in need of explanations, new discoveries in the heavens, and future colliders on the horizon. May it continue to produce wonder and joy as we learn more about the universe.

Appendix A

Effective Lagrangian from Loryons

In this Appendix, we calculate the mass spectra of scalar and fermionic Loryons in arbitrary custodial representations, as well as their one-loop corrections to the Higgs effective Lagrangian.

A.1 Scalars

In unitary gauge, Eq. (2.2), $\mathrm{tr}\left[T_2^a H T_2^{\dot{a}} H^\dagger\right] = \frac{1}{4}(v+h)^2\delta^{a\dot{a}}$. The part of the Lagrangian that is quadratic order in Φ can be written[1]

$$\mathcal{L}_{\rm quad} = -\frac{1}{2^\rho}\,\mathrm{tr}\left[\Phi^\dagger\left(D^2 + \frac{1}{2}\lambda_{\rm ex}v^2 + \frac{1}{2}\lambda_{h\Phi}(v+h)^2\right)\Phi + \lambda'_{h\Phi}(v+h)^2\,\Phi^\dagger T_L^a \Phi T_R^a\right]\,, \quad \text{(A.1)}$$

where D_μ is the covariant derivative.

To elucidate the mass spectrum, we decompose the matrix representation Φ of the custodial group $SU(2)_L \times SU(2)_R$ into irreps ϕ_V of its diagonal subgroup $SU(2)_V$. Here ϕ_V are V-dimensional vectors built out of linear combinations of the matrix elements

[1] This is built from pieces Eqs. (2.1), (2.3) and (2.4), plus a canonically normalized kinetic term.

$\Phi_{\alpha\dot{\alpha}}$:

$$\mathrm{tr}\left(U^i\Phi\right) = \left[\bigoplus_V \phi_V\right]^i, \tag{A.2}$$

with

$$V \in \mathcal{V} = \Big\{L+R-1\ ,\ L+R-3\ ,\ \cdots\ ,\ |L-R|+1\Big\}. \tag{A.3}$$

The explicit coefficients $U^i_{\dot{\alpha}\alpha}$ are given by the appropriate Clebsch-Gordan coefficients. U satisfies the resolution of the identity

$$\left(U^i_{\dot{\beta}\beta}\right)^* U^i_{\dot{\alpha}\alpha} = \delta_{\alpha\beta}\delta_{\dot{\alpha}\dot{\beta}}\,, \tag{A.4}$$

and U is also covariant under arbitrary transformations under the diagonal subgroup,

$$\mathrm{tr}\left[U\Phi'\right] = \bigoplus_V \phi'_V \quad \Rightarrow \quad \mathrm{tr}\left[U\exp(i\epsilon^a T^a_L)\,\Phi\,\exp\big(-i\epsilon^b T^b_R\big)\right] = \bigoplus_V \exp(i\epsilon^a T^a_V)\,\phi_V\,, \tag{A.5}$$

for ϵ^a arbitrary. Finding the second order variation of Eq. (A.5) with respect to ϵ^a yields

$$\mathrm{tr}\left[UT^{(a}_L T^{b)}_L\Phi + U\Phi T^{(a}_R T^{b)}_R - 2UT^{(a}_L\Phi T^{b)}_R\right] = \bigoplus_V T^{(a}_V T^{b)}_V\phi_V\,; \tag{A.6}$$

contracting with δ^{ab}, and using the fact that $T^a_L T^a_L = C_2(L)\mathbb{1}_L$ in any irrep L then gives

$$\mathrm{tr}\left[UT^a_L\Phi T^a_R\right] = \bigoplus_V \frac{1}{2}\Big[C_2(L)+C_2(R)-C_2(V)\Big]\phi_V\,. \tag{A.7}$$

Now inserting a resolution of the identity in Eq. (A.4), we get

$$\begin{aligned}\mathrm{tr}\left(\Phi^\dagger T^a_L\Phi T^a_R\right) &= \left[\mathrm{tr}\,(U\Phi)\right]^*\ \mathrm{tr}\left(UT^a_L\Phi T^a_R\right)\,,\\ &= \sum_V \phi^\dagger_V\frac{1}{2}\Big[C_2(L)+C_2(R)-C_2(V)\Big]\phi_V\,.\end{aligned} \tag{A.8}$$

Therefore, the Lagrangian in Eq. (A.1) decomposes into the sum

$$\mathcal{L}_{\rm quad} = -\frac{1}{2^\rho}\sum_V \phi_V^\dagger \left(D^2 + \frac{1}{2}\lambda_{\rm ex} v^2 + \frac{1}{2}\lambda_V (v+h)^2 \right) \phi_V \,, \tag{A.9}$$

where we have defined

$$\lambda_V = \lambda_{h\Phi} + \lambda'_{h\Phi}\Big[C_2(L) + C_2(R) - C_2(V) \Big] \,. \tag{A.10}$$

Note that we only retain the strong and electromagnetic interactions in the covariant derivative D in Eq. (A.9); weak interactions generically couple different irreps of $\mathcal{V}$.

Eq. (A.9) generates one-loop corrections to the Higgs Lagrangian, which we calculate up to two derivative order using (D.21) of [11],

$$\begin{aligned}
\mathcal{L}_{\rm eff} = \frac{1}{2^\rho (4\pi)^2}\sum_V V \Bigg\{ & \frac{1}{2}\left[\frac{1}{2}\lambda_{\rm ex} v^2 + \frac{1}{2}\lambda_V (v+h)^2 \right]^2 \left[\ln \frac{2\mu^2}{\lambda_{\rm ex} v^2 + \lambda_V (v+h)^2} + \frac{3}{2} \right] \\
& + \frac{1}{24}\frac{\lambda_V^2}{\lambda_{\rm ex} v^2 + \lambda_V (v+h)^2} \left[\partial (v+h)^2 \right]^2 + \mathcal{O}(\partial^4) \Bigg\} \\
\to \frac{1}{2^\rho (4\pi)^2}\sum_V V \Bigg\{ & \frac{1}{2}\left(\frac{1}{2}\lambda_{\rm ex} v^2 + \lambda_V |H|^2 \right)^2 \left(\ln \frac{2\mu^2}{\lambda_{\rm ex} v^2 + 2\lambda_V |H|^2} + \frac{3}{2} \right) \\
& + \frac{1}{3}\frac{\lambda_V^2}{\lambda_{\rm ex} v^2 + 2\lambda_V |H|^2} \frac{\left[\partial |H|^2 \right]^2}{2} \Bigg\} + \mathcal{O}(\partial^4) \,,
\end{aligned} \tag{A.11}$$

where we return to a general gauge by the substitution $(v+h)^2 \to 2|H|^2$.

A.2 Fermions

The most general quadratic Lagrangian for a pair of Dirac fermions Ψ_1, Ψ_2, transforming under $[L_1, R_1] \equiv [2l_1+1, 2r_1+1]$ and $[L_2, R_2] \equiv [2l_2+1, 2r_2+1]$ respectively, is

$$\mathcal{L}_{\text{quad}} = \text{tr}\left[\overline{\Psi}_1(i\not{D} - M_1)\Psi_1\right] + \text{tr}\left[\overline{\Psi}_2(i\not{D} - M_2)\Psi_2\right] - (\mathcal{L}_{\text{Yuk}} + \text{h.c.}) \ . \tag{A.12}$$

We assume w.l.o.g. that $M_1, M_2 > 0$. In the Yukawa term, one needs to contract the indices of fields properly to yield a custodial singlet,

$$\mathcal{L}_{\text{Yuk}} = y_{12}\overline{\Psi}_{1\alpha\dot{\alpha}}H_{\beta\dot{\beta}}\Psi_{2\gamma\dot{\gamma}}\left\langle \frac{1}{2}\beta; l_2\gamma \middle| l_1\alpha \right\rangle \left\langle r_1\dot{\alpha} \middle| \frac{1}{2}\dot{\beta}; r_2\dot{\gamma} \right\rangle \ . \tag{A.13}$$

Here we have shifted all the indices such that α runs in $[-l_1, l_1]$ (instead of $[1, 2l_1 + 1]$) and so on. This way we can identify the proper contraction coefficients as the standard Clebsch-Gordan coefficients, written in bra-ket notation.

As in the scalar case, we decompose fermionic matrix fields Ψ_1, Ψ_2 into their respective irreps under the diagonal subgroup $SU(2)_V \subset SU(2)_L \times SU(2)_R$:

$$\Psi_1 \to \bigoplus_{V_1} \psi_{1,V_1} \ , \qquad \Psi_2 \to \bigoplus_{V_2} \psi_{2,V_2} \ , \tag{A.14}$$

where $\psi_{1,V_1}(\psi_{2,V_2})$ are $V_1(V_2)$-dimensional vectors whose components are explicitly given by

$$\Psi_{1\mu\dot{\mu}} = \sqrt{\frac{V_1}{L_1}}\,\langle l_1\mu | j_1 m_1; r_1\dot{\mu}\rangle\, \psi^{m_1}_{1,V_1} \ , \tag{A.15a}$$

$$\Psi_{2\nu\dot{\nu}} = \sqrt{\frac{V_2}{L_2}}\,\langle l_2\nu | j_2 m_2; r_2\dot{\nu}\rangle\, \psi^{m_2}_{2,V_2} \ . \tag{A.15b}$$

In Eq. (A.15), the sums over the diagonal subgroup indices are

$$2j_1 + 1 = V_1 \quad \in \quad \mathcal{V}_1 = \Big\{ L_1 + R_1 - 1 \ , \ L_1 + R_1 - 3 \ , \ \cdots \ , \ |L_1 - R_1| + 1 \Big\} \, ,$$
$$\text{with} \quad -j_1 \leq m_1 \leq j_1 \, , \tag{A.16a}$$

$$2j_2+1=V_2 \quad \in \quad \mathcal{V}_2=\Big\{L_2+R_2-1\ ,\ L_2+R_2-3\ ,\ \cdots\ ,\ |L_2-R_2|+1\Big\}\,,$$
$$\text{with} \quad -j_2\le m_2\le j_2\,. \tag{A.16b}$$

Using Eq. (A.15), we write the Yukawa piece of the Lagrangian Eq. (A.13) in terms of ψ_{1,V_1} and ψ_{2,V_2}, in unitary gauge ($H_{\beta\dot\beta}=\frac{1}{\sqrt2}(v+h)\delta_{\beta\dot\beta}$):

$$\begin{aligned}\mathcal{L}_{\rm Yuk}=y_{12}\frac{1}{\sqrt2}(v+h)\,\overline\psi_{1,V_1}^{m_1}\psi_{2,V_2}^{m_2}\times\sqrt{\frac{V_1}{L_1}}\sqrt{\frac{V_2}{L_2}}\\ \times\langle l_1\alpha|j_1m_1;r_1\dot\alpha\rangle\,\langle j_2m_2;r_2\dot\gamma|l_2\gamma\rangle\left\langle\frac12\beta;l_2\gamma\middle|l_1\alpha\right\rangle\left\langle r_1\dot\alpha\middle|\frac12\beta;r_2\dot\gamma\right\rangle\,.\end{aligned} \tag{A.17}$$

Summing over the Greek indices, the product of Clebsch-Gordan coefficients evaluates to a Wigner 6j symbol [160, §12.1.4],

$$\begin{aligned}&\sqrt{\frac{V_1}{L_1}}\sqrt{\frac{V_2}{L_2}}\times\langle l_1\alpha|j_1m_1;r_1\dot\alpha\rangle\,\langle j_2m_2;r_2\dot\gamma|l_2\gamma\rangle\left\langle\frac12\beta;l_2\gamma\middle|l_1\alpha\right\rangle\left\langle r_1\dot\alpha\middle|\frac12\beta;r_2\dot\gamma\right\rangle\\ &=(-1)^{j_1+r_1+l_2+\frac12}\times\sqrt{L_1R_1}\times\delta_{j_1,j_2}\delta_{m_1,m_2}\times\begin{Bmatrix}r_2&l_2&j_1\\ l_1&r_1&\frac12\end{Bmatrix}\,,\end{aligned} \tag{A.18}$$

so the Lagrangian Eq. (A.12) decomposes as

$$\begin{aligned}\mathcal{L}_{\rm quad}=&\sum_{V\in\mathcal{V}_1-\mathcal{V}_2}\overline\psi_{1,V}\left(i\not\partial-M_1\right)\psi_{1,V}+\sum_{V\in\mathcal{V}_2-\mathcal{V}_1}\overline\psi_{2,V}\left(i\not\partial-M_2\right)\psi_{2,V}\\ &+\sum_{V\in\mathcal{V}_1\cap\mathcal{V}_2}\begin{pmatrix}\overline\psi_{1,V}&\overline\psi_{2,V}\end{pmatrix}\left[i\not\partial-\begin{pmatrix}M_1&\frac{1}{\sqrt2}y_V(v+h)\\ \frac{1}{\sqrt2}y_V^*(v+h)&M_2\end{pmatrix}\right]\begin{pmatrix}\psi_{1,V}\\ \psi_{2,V}\end{pmatrix}\,,\end{aligned} \tag{A.19}$$

where

$$y_V=(-1)^{j_1+r_1+l_2+\frac12}\,y_{12}\times\sqrt{L_1R_1}\times\begin{Bmatrix}r_2&l_2&j_1\\ l_1&r_1&\frac12\end{Bmatrix}\,. \tag{A.20}$$

To integrate out the above quadratic piece, we use the machinery from §6.3 of [11]. Up to two derivative order,

$$\begin{aligned}\mathcal{L}_{\text{eff}} = -\frac{1}{16\pi^2}\Bigg[\sum_{V\in\mathcal{V}_1-\mathcal{V}_2} V M_1^4\left(\ln\frac{\mu^2}{M_1^2}+\frac{3}{2}\right)+\sum_{V\in\mathcal{V}_2-\mathcal{V}_1} V M_2^4\left(\ln\frac{\mu^2}{M_2^2}+\frac{3}{2}\right)\Bigg]\\ -\frac{1}{16\pi^2}\sum_{V\in\mathcal{V}_1\cap\mathcal{V}_2} V\Bigg\{\sum_{M=M_\pm}\left(M^4+\frac{1}{2}|y_V|^2(\partial h)^2\right)\left(\ln\frac{\mu^2}{M^2}+\frac{3}{2}\right)\\ +\frac{4|y_V|^4(v+h)^2(\partial h)^2}{3(M_+-M_-)^2}\\ +M_+M_-\left[\frac{(M_+^2+M_-^2)}{(M_+^2-M_-^2)^2}-\frac{2M_+^2M_-^2}{(M_+^2-M_-^2)^3}\ln\frac{M_+^2}{M_-^2}\right]\\ \times\left[|y_V|^2(\partial h)^2-\frac{4|y_V|^4(v+h)^2(\partial h)^2}{(M_+-M_-)^2}\right]\Bigg\},\end{aligned} \tag{A.21}$$

where

$$M_\pm = \frac{1}{2}(M_1+M_2)\pm\frac{1}{2}\sqrt{(M_1-M_2)^2+2|y_V|^2(v+h)^2}\,. \tag{A.22}$$

Appendix B

Mapping EFT Quantities from SL to Higgs Basis

Using Eqs. (4.20), (4.21) and (4.23), quantities appearing in the EFT derived using the SL basis can be written in terms of Higgs basis parameters as

$$\begin{aligned}
\hat{Y}_{22} = (1+|k|^2)Y_{22} &= Y_{\dot{2}\dot{2}} + k^* Y_{\dot{2}\mathrm{i}} + k Y_{\mathrm{i}\dot{2}} + |k|^2 Y_{\mathrm{ii}} \\
&= Y_{\dot{2}\dot{2}} - \frac{|Y_{\mathrm{i}\dot{2}}|^2}{Y_{\mathrm{ii}}} = Y_{\dot{2}\dot{2}} - |k|^2 Y_{\mathrm{ii}}\,, \qquad \text{(B.1a)} \\
Z_1 = (1+|k|^2)Z_{\mathrm{i}\dot{2}\mathrm{i}2} & \\
&= Z_{\mathrm{i}\dot{2}\mathrm{i}\dot{2}} - \frac{Z^2_{\mathrm{ii}\mathrm{i}\dot{2}}}{Z_{\mathrm{iii}\mathrm{i}}} = Z_{\mathrm{i}\dot{2}\mathrm{i}\dot{2}} - (k^*)^2 Z_{\mathrm{iii}\mathrm{i}}\,, \qquad \text{(B.1b)} \\
Z_2 = (1+|k|^2)Z_{\mathrm{ii}2\mathrm{i}} & \\
&= Z_{\mathrm{ii}\dot{2}\dot{2}} - \frac{|Z_{\mathrm{ii}\mathrm{i}\dot{2}}|^2}{Z_{\mathrm{iii}\mathrm{i}}} = Z_{\mathrm{ii}\dot{2}\dot{2}} - |k|^2 Z_{\mathrm{iii}\mathrm{i}}\,, \qquad \text{(B.1c)} \\
Z_3 = (1+|k|^2)Z_{\mathrm{i}2\mathrm{i}\mathrm{i}} &
\end{aligned}$$

$$= Z_{\dot{1}2\dot{2}1} - \frac{|Z_{111\dot{2}}|^2}{Z_{1111}} = Z_{\dot{1}2\dot{2}1} - |k|^2 Z_{1111}\,, \tag{B.1d}$$

$$Z_4 = \sqrt{1+|k|^2}Z_{\dot{1}222}$$

$$= \frac{2|k|^2 Z_{11\dot{1}\dot{2}} + k^* Z_{\dot{1}2\dot{2}1} + k^* Z_{1\dot{1}2\dot{2}} + k Z_{\dot{1}2\dot{1}2} + Z_{\dot{1}2\dot{2}\dot{2}}}{1+|k|^2}\,, \tag{B.1e}$$

$$m_{\text{eff}}^2 = Y_{11}\,, \tag{B.1f}$$

$$\lambda_{\text{eff}} = Z_{1111}\,. \tag{B.1g}$$

In terms of the more conventional 2HDM parameters in Higgs basis (see Eq. (4.3)), the map is given by

$$k = -\frac{\lambda_6^*}{\lambda_1}\,, \tag{B.2a}$$

$$\hat{Y}_{22} = m_2^2 - |k|^2 m_1^2\,, \tag{B.2b}$$

$$Z_1 = \lambda_5 - (k^*)^2\lambda_1\,, \tag{B.2c}$$

$$Z_2 = \lambda_3 - |k|^2\lambda_1\,, \tag{B.2d}$$

$$Z_3 = \lambda_4 - |k|^2\lambda_1\,, \tag{B.2e}$$

$$Z_4 = \frac{2|k|^2\lambda_6 + k^*\lambda_3 + k^*\lambda_4 + k\lambda_5 + \lambda_7}{1+|k|^2} \tag{B.2f}$$

$$m_{\text{eff}}^2 = m_1^2\,, \tag{B.2g}$$

$$\lambda_{\text{eff}} = \lambda_1\,. \tag{B.2h}$$

Armed with these expressions, we can expand our expressions for our pseudo-observables in the SL basis EFT and check that they agree with the Higgs basis EFT. The Higgs basis EFT is an expansion in inverse powers of m_2^2; from Eq. (B.2b), we see that this

is equivalent to an expansion in inverse powers of $\hat{Y}_{22}$ (to leading order), so we should expand our expressions for $\kappa_V, \kappa_\lambda, \kappa_f$ in the SL basis EFT to leading order in $\hat{Y}_{22}$ and then convert to Higgs basis quantities. We have

$$b_4 \simeq \frac{1}{\hat{Y}_{22}} |k|^2 \,, \tag{B.3}$$

$$b_6 \simeq \frac{1}{\hat{Y}_{22}^2} |k|^2 (1 + |k|^2) \,, \tag{B.4}$$

$$c_4 \simeq -v \frac{1}{\hat{Y}_{22}^2} \left[|k|^2 (Z_2 + Z_3) + \mathrm{Re}\left(k^2 Z_1\right) \right] , \tag{B.5}$$

which gives

$$\kappa_{V,\mathrm{SL}} = 1 - \frac{1}{2}\left(b_6 - b_4^2\right) m_h^4 \simeq 1 - \frac{1}{2}\frac{|k|^2 \lambda_{\mathrm{eff}}^2 v^4}{\hat{Y}_{22}^2} \simeq 1 - \frac{1}{2}\frac{|\lambda_6|^2 v^4}{m_2^4} \,, \tag{B.6}$$

$$\kappa_{f,\mathrm{SL}} = 1 + \frac{b_4}{k} m_h^2 \simeq 1 + \frac{k^*}{\hat{Y}_{22}} \lambda_{\mathrm{eff}} v^2 \simeq 1 - \frac{\lambda_6 v^2}{m_2^2} \,, \tag{B.7}$$

$$\kappa_{\lambda,\mathrm{SL}} = 1 - 2 b_4 m_h^2 - c_4 v m_h^2 \simeq 1 - 2\frac{|k|^2 \lambda_{\mathrm{eff}} v^2}{\hat{Y}_{22}} = 1 - 2\frac{|k|^2 \lambda_{\mathrm{eff}}^2 v^4}{\hat{Y}_{22} m_h^2} \simeq 1 - 2\frac{|\lambda_6|^2 v^4}{m_2^2 m_h^2} \,, \tag{B.8}$$

all of which agree with the corresponding Higgs basis EFT expressions in Ref. [137].

Appendix C

Equivalence of Decoupling-Limit SL and Higgs Basis EFTs

The SL basis and Higgs basis EFTs are generally two different EFTs, equipped with their own power counting, and regimes of validity. However, in the decoupling limit, we can expand in inverse powers of large $Y_{\dot{2}\dot{2}} \equiv m_2^2$ to reproduce the same effects.

At the Lagrangian level this manifests as a field redefinition equivalence between the two EFTs. Whereas the two bases are related by a simple non-derivative field redefinition in the UV, in the EFT this requires a more complicated field redefinition with derivatives [**?**]. Here, we show the equivalence explicitly within the scalar parts of the two EFTs, working in the custodial limit and up to dimension 8 order, *i.e.*, $O(1/m_2^4)$.

Expanding the SL Basis EFT Eq. (4.47) in the custodial limit, we find

$$\begin{aligned}\mathcal{L} = &- H^\dagger D^2 H - m_1^2|H|^2 - \frac{1}{2}\lambda_1|H|^4 + \left(\frac{k^2}{m_2^2} + \frac{k^4 m_1^2}{m_2^4}\right)\left|D^2 H\right|^2 - \frac{k^2 Z_2}{m_2^4}|H|^2\left|D^2 H\right|^2 \\ &- \frac{k^2 Z_1}{2m_2^4}\left(H^\dagger D^2 H + \text{h.c.}\right)^2 - \frac{k^2(1+k^2)}{m_2^4}\left(D^2 H^\dagger\right)\left(D^4 H\right) \ . \end{aligned} \tag{C.1}$$

We have used Eq. (B.2) to convert the Wilson coefficients to Higgs basis parameters.

Under the substitution

$$
\begin{aligned}
H \to H &+ \left\{ -\frac{k^2\lambda_1}{2m_2^2} + \frac{k^2 m_1^2}{4m_2^4}\Big[4Z_1 + 2Z_2 - (4-k^2)\lambda_1\Big] \right\} |H|^2 H \\
&+ \frac{k^2\lambda_1}{8m_2^4}\Big[8Z_1 + 4Z_2 - (4-9k^2)\lambda_1\Big]|H|^4 H \\
&+ \left[\frac{k^2}{2m_2^2} + \frac{k^2(1+k^2)m_1^2}{2m_2^4}\right](D^2 H) - \frac{k^2}{4m_2^4}\Big[2Z_2 - (2-k^2)\lambda_1\Big]|H|^2 (D^2 H) \\
&+ \frac{k^2(4Z_1 + k^2\lambda_1)}{4m_2^4}|D_\mu H|^2 H - \frac{k^2}{4m_2^4}\Big[2Z_1 - (2-k^2)\lambda_1\Big]\left(D^2|H|^2\right) H \\
&+ \frac{k^2\lambda_1(4-k^2)}{4m_2^4}\left(D_\mu|H|^2\right)(D^\mu H) - \frac{k^2(4+k^2)}{8m_2^4}(D^4 H)\,,
\end{aligned}
\tag{C.2}
$$

and with the use of the identity

$$
2|D_\mu H|^2 = D^2|H|^2 - \left(H^\dagger D^2 H + \text{h.c.}\right) \tag{C.3}
$$

and the integration-by-parts relations

$$
-2\,|H|^2\left(D_\mu|H|^2\right)\left(D^\mu|H|^2\right) = |H|^4\left(D^2|H|^2\right)\,, \tag{C.4a}
$$

$$
2\,|H|^2 H^\dagger D^2\left(|H|^2 H\right) = |H|^4\left(H^\dagger D^2 H + \text{h.c.}\right) + |H|^4\left(D^2|H|^2\right)\,, \tag{C.4b}
$$

$$
\begin{aligned}
\left(D_\mu|H|^2\right)\Big[(D^\mu H)^\dagger\left(D^2 H\right) + \text{h.c.}\Big] &= -2|H|^2\left|D^2 H\right|^2 \\
&\quad - |H|^2\Big[(D_\mu H)^\dagger\left(D^\mu D^2 H\right) + \text{h.c.}\Big]\,,
\end{aligned}
\tag{C.4c}
$$

$$
\begin{aligned}
\left(D^2|H|^2\right)\left(H^\dagger D^2 H + \text{h.c.}\right) &= 2|H|^2\left|D^2 H\right|^2 \\
&\quad + 2|H|^2\Big[(D_\mu H)^\dagger\left(D^\mu D^2 H\right) + \text{h.c.}\Big] \\
&\quad + |H|^2\left(H^\dagger D^4 H + \text{h.c.}\right)\,,
\end{aligned}
\tag{C.4d}
$$

together with the subsequent rescaling

$$H \to H\left[1 - \frac{k^2 m_1^2}{2m_2^2} - \frac{k^2 m_1^4 (4+k^2)}{8m_2^4}\right], \tag{C.5}$$

the expanded SL Basis EFT in Eq. (C.1) can be reduced to

$$\begin{aligned}\mathcal{L} = &-H^\dagger D^2 H - \frac{k^2\lambda_1^2}{2m_2^4}|H|^4\left(D^2|H|^2\right) - \left(m_1^2 - k^2\frac{m_1^4}{m_2^2} - k^2\frac{m_1^6}{m_2^4}\right)|H|^2 \\ &- \frac{1}{2}\left[\lambda_1 - 4k^2\lambda_1\frac{m_1^2}{m_2^2} + 2k^2\frac{m_1^4}{m_2^4}\left(2\lambda_4+\lambda_3-3\lambda_1\right)\right]|H|^4 \\ &+ \left[k^2\frac{\lambda_1^2}{m_2^2} - k^2\lambda_1\frac{m_1^2}{m_2^4}\left(4\lambda_4+2\lambda_3-3\lambda_1\right)\right]|H|^6 - k^2\frac{\lambda_1^2}{m_2^4}\left(2\lambda_4+\lambda_3-\lambda_1\right)|H|^8 .\end{aligned} \tag{C.6}$$

We have used Eq. (B.2) again to write $Z_1 = Z_3 = \lambda_4 - k^2\lambda_1$ and $Z_2 = \lambda_3 - k^2\lambda_1$ in the custodial limit.

We can compare Eq. (C.6) to known results in the Higgs basis EFT. Assuming custodial symmetry, the scalar sector of the general results in [137] reduce to

$$\begin{aligned}\mathcal{L} = &\left(1 + \frac{m_{12}^4}{m_2^4}\right)|D_\mu H|^2 + \frac{2m_{12}^2\lambda_6}{m_2^4}\left[\frac{1}{2}\left(\partial_\mu|H|^2\right)\left(\partial^\mu|H|^2\right) + |H|^2|D_\mu H|^2\right] \\ &+ \frac{\lambda_6^2}{m_2^4}\left[2|H|^2\left(\partial_\mu|H|^2\right)\left(\partial^\mu|H|^2\right) + |H|^4|D_\mu H|^2\right] \\ &- \left(m_1^2 - \frac{m_{12}^4}{m_2^2}\right)|H|^2 - \frac{1}{2}\left[\lambda_1 - \frac{4m_{12}^2\lambda_6}{m_2^2} + \frac{2(\lambda_3+2\lambda_4)m_{12}^4}{m_2^4}\right]|H|^4 \\ &+ \left[\frac{\lambda_6^2}{m_2^2} - \frac{2(\lambda_3+2\lambda_4)m_{12}^2\lambda_6}{m_2^4}\right]|H|^6 - \frac{(\lambda_3+2\lambda_4)\lambda_6^2}{m_2^4}|H|^8 .\end{aligned} \tag{C.7}$$

This can be canonically normalized to $O\left(1/m_2^4\right)$ to give

$$\mathcal{L} = |D_\mu H|^2 + \frac{2m_{12}^2\lambda_6}{m_2^4}\left[\frac{1}{2}\left(\partial_\mu|H|^2\right)\left(\partial^\mu|H|^2\right) + |H|^2|D_\mu H|^2\right]$$

$$
\begin{aligned}
&+\frac{\lambda_6^2}{m_2^4}\left[2\left|H\right|^2\left(\partial_\mu|H|^2\right)\left(\partial^\mu|H|^2\right)+|H|^4|D_\mu H|^2\right]\\
&-\left(m_1^2-\frac{m_{12}^4}{m_2^2}-\frac{m_{12}^4m_1^2}{m_2^4}\right)|H|^2-\frac{1}{2}\left[\lambda_1-\frac{4m_{12}^2\lambda_6}{m_2^2}+\frac{2(\lambda_3+2\lambda_4-\lambda_1)m_{12}^4}{m_2^4}\right]|H|^4\\
&+\left[\frac{\lambda_6^2}{m_2^2}-\frac{2(\lambda_3+2\lambda_4)m_{12}^2\lambda_6}{m_2^4}\right]|H|^6-\frac{(\lambda_3+2\lambda_4)\lambda_6^2}{m_2^4}|H|^8\,. \qquad \text{(C.8)}
\end{aligned}
$$

Using IBPs and the field redefinition

$$
H\to H-\frac{m_{12}^2\lambda_6}{m_2^4}\left|H\right|^2H-\frac{\lambda_6^2}{2m_2^4}\left|H\right|^4H\,, \qquad \text{(C.9)}
$$

we obtain

$$
\begin{aligned}
\mathcal{L}=&|D_\mu H|^2-\frac{\lambda_6^2}{2m_2^4}|H|^4\left(D^2|H|^2\right)-\left(m_1^2-\frac{m_{12}^4}{m_2^2}-\frac{m_{12}^4m_1^2}{m_2^4}\right)|H|^2\\
&-\frac{1}{2}\left[\lambda_1-\frac{4m_{12}^2\lambda_6}{m_2^2}+\frac{2(\lambda_3+2\lambda_4-3\lambda_1)m_{12}^4}{m_2^4}\right]|H|^4\\
&+\left[\frac{\lambda_6^2}{m_2^2}-\frac{(2\lambda_3+4\lambda_4-3\lambda_1)m_{12}^2\lambda_6}{m_2^4}\right]|H|^6-\frac{(\lambda_3+2\lambda_4-\lambda_1)\lambda_6^2}{m_2^4}|H|^8\,, \qquad \text{(C.10)}
\end{aligned}
$$

where we have used $m_1^2\lambda_6=m_{12}^2\lambda_1$ (a consequence of the vev condition in the Higgs basis). As both $k\lambda_1=-\lambda_6$ and $km_1^2=-m_{12}^2$ (in the custodial limit), we see Eq. (C.10) and Eq. (C.6) are equivalent.

Bibliography

[1] I. Banta, T. Cai, N. Craig, and Z. Zhang, *Structures of Neural Network Effective Theories*, arXiv:2305.0233.

[2] I. Banta, T. Cohen, N. Craig, X. Lu, and D. Sutherland, *Effective field theory of the two Higgs doublet model*, *JHEP* **06** (2023) 150, [arXiv:2304.0988].

[3] I. Banta, *A strongly first-order electroweak phase transition from Loryons*, *JHEP* **06** (2022) 099, [arXiv:2202.0460].

[4] I. Banta, T. Cohen, N. Craig, X. Lu, and D. Sutherland, *Non-decoupling new particles*, *JHEP* **02** (2022) 029, [arXiv:2110.0296].

[5] H. Al Ali *et. al.*, *The muon Smasher's guide*, *Rept. Prog. Phys.* **85** (2022), no. 8 084201, [arXiv:2103.1404].

[6] A. Friedlander, I. Banta, J. M. Cline, and D. Tucker-Smith, *Wall speed and shape in singlet-assisted strong electroweak phase transitions*, *Phys. Rev. D* **103** (2021), no. 5 055020, [arXiv:2009.1429].

[7] S. Weinberg, *Effective Gauge Theories*, *Phys. Lett. B* **91** (1980) 51–55.

[8] J. Ellis, M. Madigan, K. Mimasu, V. Sanz, and T. You, *Top, Higgs, Diboson and Electroweak Fit to the Standard Model Effective Field Theory*, *JHEP* **04** (2021) 279, [arXiv:2012.0277].

[9] **SMEFiT** Collaboration, J. J. Ethier, G. Magni, F. Maltoni, L. Mantani, E. R. Nocera, J. Rojo, E. Slade, E. Vryonidou, and C. Zhang, *Combined SMEFT interpretation of Higgs, diboson, and top quark data from the LHC*, *JHEP* **11** (2021) 089, [arXiv:2105.0000].

[10] I. Brivio and M. Trott, *The Standard Model as an Effective Field Theory*, *Phys. Rept.* **793** (2019) 1–98, [arXiv:1706.0894].

[11] T. Cohen, N. Craig, X. Lu, and D. Sutherland, *Is SMEFT Enough?*, *JHEP* **03** (2021) 237, [arXiv:2008.0859].

[12] R. Alonso, E. E. Jenkins, and A. V. Manohar, *A Geometric Formulation of Higgs Effective Field Theory: Measuring the Curvature of Scalar Field Space*, *Phys. Lett. B* **754** (2016) 335–342, [arXiv:1511.0072].

[13] R. Alonso, E. E. Jenkins, and A. V. Manohar, *Geometry of the Scalar Sector*, *JHEP* **08** (2016) 101, [arXiv:1605.0360].

[14] A. Falkowski and R. Rattazzi, *Which EFT*, *JHEP* **10** (2019) 255, [arXiv:1902.0593].

[15] C. Cheung and Y. Nomura, *Higgs Descendants*, *Phys. Rev. D* **86** (2012) 015004, [arXiv:1112.3043].

[16] A. Djouadi and A. Lenz, *Sealing the fate of a fourth generation of fermions*, *Phys. Lett. B* **715** (2012) 310–314, [arXiv:1204.1252].

[17] E. Kuflik, Y. Nir, and T. Volansky, *Implications of Higgs searches on the four generation standard model*, *Phys. Rev. Lett.* **110** (2013), no. 9 091801, [arXiv:1204.1975].

[18] Q. Bonnefoy, L. Di Luzio, C. Grojean, A. Paul, and A. N. Rossia, *The anomalous case of axion EFTs and massive chiral gauge fields*, *JHEP* **07** (2021) 189, [arXiv:2011.1002].

[19] J. de Blas, J. C. Criado, M. Perez-Victoria, and J. Santiago, *Effective description of general extensions of the Standard Model: the complete tree-level dictionary*, *JHEP* **03** (2018) 109, [arXiv:1711.1039].

[20] T. Cohen, N. Craig, X. Lu, and D. Sutherland, *Unitarity Violation and the Geometry of Higgs EFTs*, arXiv:2108.0324.

[21] R. Alonso and M. West, *On the road(s) to the Standard Model*, arXiv:2109.1329.

[22] M. Jacob and G. C. Wick, *On the General Theory of Collisions for Particles with Spin*, *Annals Phys.* **7** (1959) 404–428.

[23] M. D. Goodsell and F. Staub, *Unitarity constraints on general scalar couplings with SARAH*, *Eur. Phys. J. C* **78** (2018), no. 8 649, [arXiv:1805.0730].

[24] J. F. Gunion, H. E. Haber, G. L. Kane, and S. Dawson, *The Higgs Hunter's Guide*, vol. 80. 2000.

[25] D. Carmi, A. Falkowski, E. Kuflik, T. Volansky, and J. Zupan, *Higgs After the Discovery: A Status Report*, *JHEP* **10** (2012) 196, [arXiv:1207.1718].

[26] **ATLAS** Collaboration, G. Aad *et. al.*, *Combined measurements of Higgs boson production and decay using up to* 80 fb^{-1} *of proton-proton collision data at* $\sqrt{s} =$ *13 TeV collected with the ATLAS experiment*, *Phys. Rev. D* **101** (2020), no. 1 012002, [arXiv:1909.0284].

[27] **CMS** Collaboration, A. M. Sirunyan *et. al.*, *Combined measurements of Higgs boson couplings in proton–proton collisions at* $\sqrt{s} = 13$ *TeV*, *Eur. Phys. J. C* **79** (2019), no. 5 421, [arXiv:1809.1073].

[28] B. W. Lynn, M. E. Peskin, and R. G. Stuart, *RADIATIVE CORRECTIONS IN SU(2) x U(1): LEP / SLC*, 7, 1985.

[29] M. E. Peskin and T. Takeuchi, *Estimation of oblique electroweak corrections*, *Phys. Rev. D* **46** (1992) 381–409.

[30] I. Maksymyk, C. P. Burgess, and D. London, *Beyond S, T and U*, *Phys. Rev. D* **50** (1994) 529–535, [hep-ph/9306267].

[31] C. P. Burgess, S. Godfrey, H. Konig, D. London, and I. Maksymyk, *A Global fit to extended oblique parameters*, *Phys. Lett. B* **326** (1994) 276–281, [hep-ph/9307337].

[32] A. Kundu and P. Roy, *A General treatment of oblique parameters*, *Int. J. Mod. Phys. A* **12** (1997) 1511–1530, [hep-ph/9603323].

[33] R. Barbieri, A. Pomarol, R. Rattazzi, and A. Strumia, *Electroweak symmetry breaking after LEP-1 and LEP-2*, *Nucl. Phys. B* **703** (2004) 127–146, [hep-ph/0405040].

[34] M. Farina, G. Panico, D. Pappadopulo, J. T. Ruderman, R. Torre, and A. Wulzer, *Energy helps accuracy: electroweak precision tests at hadron colliders*, *Phys. Lett. B* **772** (2017) 210–215, [arXiv:1609.0815].

[35] **Particle Data Group** Collaboration, M. Tanabashi *et. al.*, *Review of Particle Physics*, *Phys. Rev. D* **98** (2018), no. 3 030001.

[36] **CMS** Collaboration, V. Khachatryan *et. al.*, *Search for long-lived charged particles in proton-proton collisions at* $\sqrt{s} =$ *13 TeV*, *Phys. Rev. D* **94** (2016), no. 11 112004, [arXiv:1609.0838].

[37] **ATLAS** Collaboration, M. Aaboud *et. al.*, *Search for heavy charged long-lived particles in proton-proton collisions at* $\sqrt{s} = 13$ *TeV using an ionisation measurement with the ATLAS detector*, *Phys. Lett. B* **788** (2019) 96–116, [arXiv:1808.0409].

[38] **ATLAS** Collaboration, M. Aaboud *et. al.*, *Search for heavy charged long-lived particles in the ATLAS detector in 36.1* fb^{-1} *of proton-proton collision data at* $\sqrt{s} = 13$ *TeV*, *Phys. Rev. D* **99** (2019), no. 9 092007, [arXiv:1902.0163].

[39] J. Fan, M. Reece, and J. T. Ruderman, *Stealth Supersymmetry*, *JHEP* **11** (2011) 012, [arXiv:1105.5135].

[40] N. Craig, H. K. Lou, M. McCullough, and A. Thalapillil, *The Higgs Portal Above Threshold*, *JHEP* **02** (2016) 127, [arXiv:1412.0258].

[41] A. Crivellin, F. Kirk, C. A. Manzari, and L. Panizzi, *Searching for lepton flavor universality violation and collider signals from a singly charged scalar singlet*, *Phys. Rev. D* **103** (2021), no. 7 073002, [arXiv:2012.0984].

[42] **CMS** Collaboration, A. M. Sirunyan *et. al.*, *Search for pair-produced resonances decaying to quark pairs in proton-proton collisions at* $\sqrt{s} = 13$ *TeV*, *Phys. Rev. D* **98** (2018), no. 11 112014, [arXiv:1808.0312].

[43] D. Dercks and T. Robens, *Constraining the Inert Doublet Model using Vector Boson Fusion*, *Eur. Phys. J. C* **79** (2019), no. 11 924, [arXiv:1812.0791].

[44] N. F. Bell, M. J. Dolan, L. S. Friedrich, M. J. Ramsey-Musolf, and R. R. Volkas, *Two-Step Electroweak Symmetry-Breaking: Theory Meets Experiment*, *JHEP* **05** (2020) 050, [arXiv:2001.0533].

[45] C.-W. Chiang, G. Cottin, Y. Du, K. Fuyuto, and M. J. Ramsey-Musolf, *Collider Probes of Real Triplet Scalar Dark Matter*, *JHEP* **01** (2021) 198, [arXiv:2003.0786].

[46] **ALEPH, DELPHI, L3, OPAL, LEP** Collaboration, G. Abbiendi *et. al.*, *Search for Charged Higgs bosons: Combined Results Using LEP Data*, *Eur. Phys. J. C* **73** (2013) 2463, [arXiv:1301.6065].

[47] **ATLAS** Collaboration, G. Aad *et. al.*, *Search for doubly and singly charged Higgs bosons decaying into vector bosons in multi-lepton final states with the ATLAS detector using proton-proton collisions at* $\sqrt{s} = 13$ *TeV*, arXiv:2101.1196.

[48] **ATLAS** Collaboration, G. Aad *et. al.*, *Search for electroweak production of charginos and sleptons decaying into final states with two leptons and missing transverse momentum in* $\sqrt{s} = 13$ *TeV pp collisions using the ATLAS detector*, *Eur. Phys. J. C* **80** (2020), no. 2 123, [arXiv:1908.0821].

[49] **ATLAS** Collaboration, M. Aaboud *et. al.*, *Search for the direct production of charginos and neutralinos in final states with tau leptons in* $\sqrt{s} = 13$ *TeV pp collisions with the ATLAS detector*, *Eur. Phys. J. C* **78** (2018), no. 2 154, [arXiv:1708.0787].

[50] **CMS** Collaboration, A. M. Sirunyan *et. al.*, *Search for electroweak production of charginos and neutralinos in multilepton final states in proton-proton collisions at* $\sqrt{s} = 13$ *TeV*, *JHEP* **03** (2018) 166, [arXiv:1709.0540].

[51] **ATLAS** Collaboration, M. Aaboud *et. al.*, *Search for long-lived charginos based on a disappearing-track signature in pp collisions at* $\sqrt{s} = 13$ *TeV with the ATLAS detector*, *JHEP* **06** (2018) 022, [arXiv:1712.0211].

[52] V. Rentala, W. Shepherd, and S. Su, *A Simplified Model Approach to Same-sign Dilepton Resonances*, *Phys. Rev. D* **84** (2011) 035004, [arXiv:1105.1379].

[53] **ATLAS** Collaboration, M. Aaboud *et. al.*, *Search for doubly charged Higgs boson production in multi-lepton final states with the ATLAS detector using proton–proton collisions at* $\sqrt{s} = 13$ *TeV*, *Eur. Phys. J. C* **78** (2018), no. 3 199, [arXiv:1710.0974].

[54] **CMS** Collaboration, A. M. Sirunyan *et. al.*, *Search for supersymmetry in final states with two oppositely charged same-flavor leptons and missing transverse momentum in proton-proton collisions at* $\sqrt{s} = 13$ *TeV*, *JHEP* **04** (2021) 123, [arXiv:2012.0860].

[55] **ATLAS** Collaboration, G. Aad *et. al.*, *Search for chargino-neutralino production with mass splittings near the electroweak scale in three-lepton final states in* $\sqrt{s}$*=13 TeV pp collisions with the ATLAS detector*, *Phys. Rev. D* **101** (2020), no. 7 072001, [arXiv:1912.0847].

[56] **ATLAS** Collaboration, G. Aad *et. al.*, *Search for direct production of electroweakinos in final states with one lepton, missing transverse momentum and a Higgs boson decaying into two b-jets in pp collisions at* $\sqrt{s} = 13$ *TeV with the ATLAS detector*, *Eur. Phys. J. C* **80** (2020), no. 8 691, [arXiv:1909.0922].

[57] **CMS** Collaboration, *Search for chargino-neutralino production in final states with a Higgs boson and a W boson*, CMS-PAS-SUS-20-003, 2021.

[58] **CMS** Collaboration, A. M. Sirunyan *et. al.*, *Search for physics beyond the standard model in multilepton final states in proton-proton collisions at* $\sqrt{s} = 13$ *TeV*, *JHEP* **03** (2020) 051, [arXiv:1911.0496].

[59] **ATLAS** Collaboration, *Search for new phenomena in three- or four-lepton events in pp collisions at* $\sqrt{s} = 13$ *TeV with the ATLAS detector*, ATLAS-CONF-2021-011, 2021.

[60] S. D. Thomas and J. D. Wells, *Phenomenology of Massive Vectorlike Doublet Leptons*, *Phys. Rev. Lett.* **81** (1998) 34–37, [hep-ph/9804359].

[61] M. Cirelli, N. Fornengo, and A. Strumia, *Minimal dark matter*, *Nucl. Phys. B* **753** (2006) 178–194, [hep-ph/0512090].

[62] **ATLAS** Collaboration, *Search for long-lived charginos based on a disappearing-track signature using 136* fb^{-1} *of pp collisions at* $\sqrt{s} = 13$ *TeV with the ATLAS detector*, ATLAS-CONF-2021-015, 2021.

[63] A. Alloul, N. D. Christensen, C. Degrande, C. Duhr, and B. Fuks, *FeynRules 2.0 - A complete toolbox for tree-level phenomenology*, *Comput. Phys. Commun.* **185** (2014) 2250–2300, [arXiv:1310.1921].

[64] T. Hahn, *Generating Feynman diagrams and amplitudes with FeynArts 3*, *Comput. Phys. Commun.* **140** (2001) 418–431, [hep-ph/0012260].

[65] T. Hahn and M. Perez-Victoria, *Automatized one loop calculations in four-dimensions and D-dimensions*, *Comput. Phys. Commun.* **118** (1999) 153–165, [hep-ph/9807565].

[66] T. Hahn, S. Paßehr, and C. Schappacher, *FormCalc 9 and Extensions*, *PoS* **LL2016** (2016) 068, [arXiv:1604.0461].

[67] **LEPSUSYWG, ALEPH, DELPHI, L3 and OPAL** Collaboration, *Combined lep chargino results, up to 208 gev for low dm*, `http://lepsusy.web.cern.ch/lepsusy/www/inoslowdmsummer02/charginolowdm_pub.html`, 2002.

[68] D. Egana-Ugrinovic, M. Low, and J. T. Ruderman, *Charged Fermions Below 100 GeV*, *JHEP* **05** (2018) 012, [arXiv:1801.0543].

[69] M. Cepeda *et. al.*, *Report from Working Group 2: Higgs Physics at the HL-LHC and HE-LHC*, *CERN Yellow Rep. Monogr.* **7** (2019) 221–584, [arXiv:1902.0013].

[70] B. Henning, D. Lombardo, M. Riembau, and F. Riva, *Measuring Higgs Couplings without Higgs Bosons*, *Phys. Rev. Lett.* **123** (2019), no. 18 181801, [arXiv:1812.0929].

[71] V. Silveira and A. Zee, *Scalar Phantoms*, *Phys. Lett. B* **161** (1985) 136–140.

[72] J. McDonald, *Gauge singlet scalars as cold dark matter*, *Phys. Rev. D* **50** (1994) 3637–3649, [hep-ph/0702143].

[73] C. P. Burgess, M. Pospelov, and T. ter Veldhuis, *The Minimal model of nonbaryonic dark matter: A Singlet scalar*, *Nucl. Phys. B* **619** (2001) 709–728, [hep-ph/0011335].

[74] T. Cohen, J. Kearney, A. Pierce, and D. Tucker-Smith, *Singlet-Doublet Dark Matter*, *Phys. Rev. D* **85** (2012) 075003, [arXiv:1109.2604].

[75] V. A. Kuzmin, V. A. Rubakov, and M. E. Shaposhnikov, *On the Anomalous Electroweak Baryon Number Nonconservation in the Early Universe*, *Phys. Lett. B* **155** (1985) 36.

[76] M. E. Shaposhnikov, *Baryon Asymmetry of the Universe in Standard Electroweak Theory*, *Nucl. Phys. B* **287** (1987) 757–775.

[77] J. M. Cline, *Baryogenesis*, in *Les Houches Summer School - Session 86: Particle Physics and Cosmology: The Fabric of Spacetime*, 9, 2006. hep-ph/0609145.

[78] D. E. Morrissey and M. J. Ramsey-Musolf, *Electroweak baryogenesis*, *New J. Phys.* **14** (2012) 125003, [arXiv:1206.2942].

[79] A. D. Sakharov, *Violation of CP Invariance, C asymmetry, and baryon asymmetry of the universe*, *Pisma Zh. Eksp. Teor. Fiz.* **5** (1967) 32–35.

[80] C. Caprini *et. al.*, *Science with the space-based interferometer eLISA. II: Gravitational waves from cosmological phase transitions*, *JCAP* **04** (2016) 001, [arXiv:1512.0623].

[81] C. Caprini *et. al.*, *Detecting gravitational waves from cosmological phase transitions with LISA: an update*, *JCAP* **03** (2020) 024, [arXiv:1910.1312].

[82] J. Crowder and N. J. Cornish, *Beyond LISA: Exploring future gravitational wave missions*, *Phys. Rev. D* **72** (2005) 083005, [gr-qc/0506015].

[83] N. Seto, S. Kawamura, and T. Nakamura, *Possibility of direct measurement of the acceleration of the universe using 0.1-Hz band laser interferometer gravitational wave antenna in space*, *Phys. Rev. Lett.* **87** (2001) 221103, [astro-ph/0108011].

[84] K. Kajantie, M. Laine, K. Rummukainen, and M. E. Shaposhnikov, *The Electroweak phase transition: A Nonperturbative analysis*, *Nucl. Phys. B* **466** (1996) 189–258, [hep-lat/9510020].

[85] A. Katz and M. Perelstein, *Higgs Couplings and Electroweak Phase Transition*, *JHEP* **07** (2014) 108, [arXiv:1401.1827].

[86] M. J. Ramsey-Musolf, *The electroweak phase transition: a collider target*, *JHEP* **09** (2020) 179, [arXiv:1912.0718].

[87] J. R. Espinosa and M. Quiros, *The Electroweak phase transition with a singlet*, *Phys. Lett. B* **305** (1993) 98–105, [hep-ph/9301285].

[88] V. Barger, P. Langacker, M. McCaskey, M. Ramsey-Musolf, and G. Shaughnessy, *Complex Singlet Extension of the Standard Model*, *Phys. Rev. D* **79** (2009) 015018, [arXiv:0811.0393].

[89] A. Ashoorioon and T. Konstandin, *Strong electroweak phase transitions without collider traces*, *JHEP* **07** (2009) 086, [arXiv:0904.0353].

[90] T. Cohen, D. E. Morrissey, and A. Pierce, *Electroweak Baryogenesis and Higgs Signatures*, *Phys. Rev. D* **86** (2012) 013009, [arXiv:1203.2924].

[91] H. H. Patel and M. J. Ramsey-Musolf, *Stepping Into Electroweak Symmetry Breaking: Phase Transitions and Higgs Phenomenology*, *Phys. Rev. D* **88** (2013) 035013, [arXiv:1212.5652].

[92] S. Profumo, M. J. Ramsey-Musolf, C. L. Wainwright, and P. Winslow, *Singlet-catalyzed electroweak phase transitions and precision Higgs boson studies*, *Phys. Rev. D* **91** (2015), no. 3 035018, [arXiv:1407.5342].

[93] D. Curtin, P. Meade, and C.-T. Yu, *Testing Electroweak Baryogenesis with Future Colliders*, *JHEP* **11** (2014) 127, [arXiv:1409.0005].

[94] M. Jiang, L. Bian, W. Huang, and J. Shu, *Impact of a complex singlet: Electroweak baryogenesis and dark matter*, *Phys. Rev. D* **93** (2016), no. 6 065032, [arXiv:1502.0757].

[95] A. V. Kotwal, M. J. Ramsey-Musolf, J. M. No, and P. Winslow, *Singlet-catalyzed electroweak phase transitions in the 100 TeV frontier*, *Phys. Rev. D* **94** (2016), no. 3 035022, [arXiv:1605.0612].

[96] P. Huang, A. J. Long, and L.-T. Wang, *Probing the Electroweak Phase Transition with Higgs Factories and Gravitational Waves*, *Phys. Rev. D* **94** (2016), no. 7 075008, [arXiv:1608.0661].

[97] V. Vaskonen, *Electroweak baryogenesis and gravitational waves from a real scalar singlet*, *Phys. Rev. D* **95** (2017), no. 12 123515, [arXiv:1611.0207].

[98] G. C. Dorsch, S. J. Huber, T. Konstandin, and J. M. No, *A Second Higgs Doublet in the Early Universe: Baryogenesis and Gravitational Waves*, *JCAP* **05** (2017) 052, [arXiv:1611.0587].

[99] A. Beniwal, M. Lewicki, J. D. Wells, M. White, and A. G. Williams, *Gravitational wave, collider and dark matter signals from a scalar singlet electroweak baryogenesis*, *JHEP* **08** (2017) 108, [arXiv:1702.0612].

[100] G. Kurup and M. Perelstein, *Dynamics of Electroweak Phase Transition In Singlet-Scalar Extension of the Standard Model*, *Phys. Rev. D* **96** (2017), no. 1 015036, [arXiv:1704.0338].

[101] C.-W. Chiang, M. J. Ramsey-Musolf, and E. Senaha, *Standard Model with a Complex Scalar Singlet: Cosmological Implications and Theoretical Considerations*, *Phys. Rev. D* **97** (2018), no. 1 015005, [arXiv:1707.0996].

[102] L. Niemi, H. H. Patel, M. J. Ramsey-Musolf, T. V. I. Tenkanen, and D. J. Weir, *Electroweak phase transition in the real triplet extension of the SM: Dimensional reduction*, *Phys. Rev. D* **100** (2019), no. 3 035002, [arXiv:1802.1050].

[103] A. Beniwal, M. Lewicki, M. White, and A. G. Williams, *Gravitational waves and electroweak baryogenesis in a global study of the extended scalar singlet model*, *JHEP* **02** (2019) 183, [arXiv:1810.0238].

[104] N. F. Bell, M. J. Dolan, L. S. Friedrich, M. J. Ramsey-Musolf, and R. R. Volkas, *Electroweak Baryogenesis with Vector-like Leptons and Scalar Singlets*, *JHEP* **09** (2019) 012, [arXiv:1903.1125].

[105] J. Kozaczuk, M. J. Ramsey-Musolf, and J. Shelton, *Exotic Higgs boson decays and the electroweak phase transition*, *Phys. Rev. D* **101** (2020), no. 11 115035, [arXiv:1911.1021].

[106] S. Baum, M. Carena, N. R. Shah, C. E. M. Wagner, and Y. Wang, *Nucleation is more than critical: A case study of the electroweak phase transition in the NMSSM*, *JHEP* **03** (2021) 055, [arXiv:2009.1074].

[107] N. F. Bell, M. J. Dolan, L. S. Friedrich, M. J. Ramsey-Musolf, and R. R. Volkas, *A Real Triplet-Singlet Extended Standard Model: Dark Matter and Collider Phenomenology*, *JHEP* **21** (2020) 098, [arXiv:2010.1337].

[108] J. M. Cline, A. Friedlander, D.-M. He, K. Kainulainen, B. Laurent, and D. Tucker-Smith, *Baryogenesis and gravity waves from a UV-completed electroweak phase transition*, *Phys. Rev. D* **103** (2021), no. 12 123529, [arXiv:2102.1249].

[109] P. M. Schicho, T. V. I. Tenkanen, and J. Österman, *Robust approach to thermal resummation: Standard Model meets a singlet*, *JHEP* **06** (2021) 130, [arXiv:2102.1114].

[110] L. Niemi, P. Schicho, and T. V. I. Tenkanen, *Singlet-assisted electroweak phase transition at two loops*, *Phys. Rev. D* **103** (2021), no. 11 115035, [arXiv:2103.0746].

[111] A. D. Linde, *Infrared Problem in Thermodynamics of the Yang-Mills Gas*, *Phys. Lett. B* **96** (1980) 289–292.

[112] D. J. Gross, R. D. Pisarski, and L. G. Yaffe, *QCD and Instantons at Finite Temperature*, *Rev. Mod. Phys.* **53** (1981) 43.

[113] H. H. Patel and M. J. Ramsey-Musolf, *Baryon Washout, Electroweak Phase Transition, and Perturbation Theory*, *JHEP* **07** (2011) 029, [arXiv:1101.4665].

[114] M. Garny and T. Konstandin, *On the gauge dependence of vacuum transitions at finite temperature*, *JHEP* **07** (2012) 189, [arXiv:1205.3392].

[115] J. Löfgren, M. J. Ramsey-Musolf, P. Schicho, and T. V. I. Tenkanen, *Nucleation at finite temperature: a gauge-invariant, perturbative framework*, arXiv:2112.0547.

[116] J. Hirvonen, J. Löfgren, M. J. Ramsey-Musolf, P. Schicho, and T. V. I. Tenkanen, *Computing the gauge-invariant bubble nucleation rate in finite temperature effective field theory*, arXiv:2112.0891.

[117] M. Quiros, *Finite temperature field theory and phase transitions*, in *ICTP Summer School in High-Energy Physics and Cosmology*, pp. 187–259, 1, 1999. hep-ph/9901312.

[118] R. R. Parwani, *Resummation in a hot scalar field theory*, *Phys. Rev. D* **45** (1992) 4695, [hep-ph/9204216]. [Erratum: Phys.Rev.D 48, 5965 (1993)].

[119] D. Comelli and J. R. Espinosa, *Bosonic thermal masses in supersymmetry*, *Phys. Rev. D* **55** (1997) 6253–6263, [hep-ph/9606438].

[120] D. Croon, O. Gould, P. Schicho, T. V. I. Tenkanen, and G. White, *Theoretical uncertainties for cosmological first-order phase transitions*, *JHEP* **04** (2021) 055, [arXiv:2009.1008].

[121] T. Cohen and A. Pierce, *Electroweak Baryogenesis and Colored Scalars*, *Phys. Rev. D* **85** (2012) 033006, [arXiv:1110.0482].

[122] O. Gould and T. V. I. Tenkanen, *On the perturbative expansion at high temperature and implications for cosmological phase transitions*, *JHEP* **06** (2021) 069, [arXiv:2104.0439].

[123] G. D. Moore and T. Prokopec, *How fast can the wall move? A Study of the electroweak phase transition dynamics*, *Phys. Rev. D* **52** (1995) 7182–7204, [hep-ph/9506475].

[124] C. L. Wainwright, *CosmoTransitions: Computing Cosmological Phase Transition Temperatures and Bubble Profiles with Multiple Fields*, *Comput. Phys. Commun.* **183** (2012) 2006–2013, [arXiv:1109.4189].

[125] C. Wainwright, S. Profumo, and M. J. Ramsey-Musolf, *Gravity Waves from a Cosmological Phase Transition: Gauge Artifacts and Daisy Resummations*, *Phys. Rev. D* **84** (2011) 023521, [arXiv:1104.5487].

[126] M. Breitbach, J. Kopp, E. Madge, T. Opferkuch, and P. Schwaller, *Dark, Cold, and Noisy: Constraining Secluded Hidden Sectors with Gravitational Waves*, *JCAP* **07** (2019) 007, [arXiv:1811.1117].

[127] O. Gould, J. Kozaczuk, L. Niemi, M. J. Ramsey-Musolf, T. V. I. Tenkanen, and D. J. Weir, *Nonperturbative analysis of the gravitational waves from a first-order electroweak phase transition*, *Phys. Rev. D* **100** (2019), no. 11 115024, [arXiv:1903.1160].

[128] T. Alanne, T. Hugle, M. Platscher, and K. Schmitz, *A fresh look at the gravitational-wave signal from cosmological phase transitions*, *JHEP* **03** (2020) 004, [arXiv:1909.1135].

[129] X. Wang, F. P. Huang, and X. Zhang, *Phase transition dynamics and gravitational wave spectra of strong first-order phase transition in supercooled universe*, *JCAP* **05** (2020) 045, [arXiv:2003.0889].

[130] N. Bizot and M. Frigerio, *Fermionic extensions of the Standard Model in light of the Higgs couplings*, *JHEP* **01** (2016) 036, [arXiv:1508.0164].

[131] J. de Blas *et. al.*, *Higgs Boson Studies at Future Particle Colliders*, *JHEP* **01** (2020) 139, [arXiv:1905.0376].

[132] T. D. Lee, *A Theory of Spontaneous T Violation*, *Phys. Rev. D* **8** (1973) 1226–1239.

[133] S. Weinberg, *Gauge Theory of CP Violation*, *Phys. Rev. Lett.* **37** (1976) 657.

[134] G. C. Branco, P. M. Ferreira, L. Lavoura, M. N. Rebelo, M. Sher, and J. P. Silva, *Theory and phenomenology of two-Higgs-doublet models*, *Phys. Rept.* **516** (2012) 1–102, [arXiv:1106.0034].

[135] M. Gorbahn, J. M. No, and V. Sanz, *Benchmarks for Higgs Effective Theory: Extended Higgs Sectors*, *JHEP* **10** (2015) 036, [arXiv:1502.0735].

[136] J. Brehmer, A. Freitas, D. Lopez-Val, and T. Plehn, *Pushing Higgs Effective Theory to its Limits*, *Phys. Rev. D* **93** (2016), no. 7 075014, [arXiv:1510.0344].

[137] D. Egana-Ugrinovic and S. Thomas, *Effective Theory of Higgs Sector Vacuum States*, arXiv:1512.0014.

[138] H. Bélusca-Maïto, A. Falkowski, D. Fontes, J. C. Romão, and J. a. P. Silva, *Higgs EFT for 2HDM and beyond*, *Eur. Phys. J. C* **77** (2017), no. 3 176, [arXiv:1611.0111].

[139] S. Dawson and C. W. Murphy, *Standard Model EFT and Extended Scalar Sectors*, *Phys. Rev. D* **96** (2017), no. 1 015041, [arXiv:1704.0785].

[140] S. Dawson, D. Fontes, S. Homiller, and M. Sullivan, *Beyond 6: the role of dimension-8 operators in an EFT for the 2HDM*, arXiv:2205.0156.

[141] H. Georgi and D. V. Nanopoulos, *Suppression of Flavor Changing Effects From Neutral Spinless Meson Exchange in Gauge Theories*, *Phys. Lett. B* **82** (1979) 95–96.

[142] H. E. Haber and Y. Nir, *Multiscalar Models With a High-energy Scale*, *Nucl. Phys. B* **335** (1990) 363–394.

[143] H. E. Haber, *Nonminimal Higgs sectors: The Decoupling limit and its phenomenological implications*, in *Joint U.S.-Polish Workshop on Physics from Planck Scale to Electro-Weak Scale (SUSY 94)*, 12, 1994. hep-ph/9501320.

[144] A. Helset, A. Martin, and M. Trott, *The Geometric Standard Model Effective Field Theory*, *JHEP* **03** (2020) 163, [arXiv:2001.0145].

[145] G. C. Branco, L. Lavoura, and J. P. Silva, *CP Violation*, vol. 103. 1999.

[146] S. Davidson and H. E. Haber, *Basis-independent methods for the two-Higgs-doublet model*, *Phys. Rev. D* **72** (2005) 035004, [hep-ph/0504050]. [Erratum: Phys.Rev.D 72, 099902 (2005)].

[147] A. Trautner, *Systematic construction of basis invariants in the 2HDM*, *JHEP* **05** (2019) 208, [arXiv:1812.0261].

[148] J. F. Gunion and H. E. Haber, *Conditions for CP-violation in the general two-Higgs-doublet model*, *Phys. Rev. D* **72** (2005) 095002, [hep-ph/0506227].

[149] H. E. Haber and D. O'Neil, *Basis-independent methods for the two-Higgs-doublet model III: The CP-conserving limit, custodial symmetry, and the oblique parameters S, T, U*, *Phys. Rev. D* **83** (2011) 055017, [arXiv:1011.6188].

[150] A. Pomarol and R. Vega, *Constraints on CP violation in the Higgs sector from the rho parameter*, *Nucl. Phys. B* **413** (1994) 3–15, [hep-ph/9305272].

[151] P. M. Ferreira, R. Santos, and A. Barroso, *Stability of the tree-level vacuum in two Higgs doublet models against charge or CP spontaneous violation*, *Phys. Lett. B* **603** (2004) 219–229, [hep-ph/0406231]. [Erratum: Phys.Lett.B 629, 114–114 (2005)].

[152] A. Barroso, P. M. Ferreira, and R. Santos, *Charge and CP symmetry breaking in two Higgs doublet models*, *Phys. Lett. B* **632** (2006) 684–687, [hep-ph/0507224].

[153] T. Cohen, X. Lu, and Z. Zhang, *Snowmass White Paper: Effective Field Theory Matching and Applications*, in *Snowmass 2021*, 3, 2022. arXiv:2203.0733.

[154] S. Dawson *et. al.*, *LHC EFT WG Note: Precision matching of microscopic physics to the Standard Model Effective Field Theory (SMEFT)*, arXiv:2212.0290.

[155] S. L. Glashow and S. Weinberg, *Natural Conservation Laws for Neutral Currents*, *Phys. Rev. D* **15** (1977) 1958.

[156] **ATLAS** Collaboration, *A detailed map of Higgs boson interactions by the ATLAS experiment ten years after the discovery*, *Nature* **607** (2022), no. 7917 52–59, [arXiv:2207.0009]. [Erratum: Nature 612, E24 (2022)].

[157] **CMS** Collaboration, A. Tumasyan *et. al.*, *A portrait of the Higgs boson by the CMS experiment ten years after the discovery*, *Nature* **607** (2022), no. 7917 60–68, [arXiv:2207.0004].

[158] I. F. Ginzburg and I. P. Ivanov, *Tree-level unitarity constraints in the most general 2HDM*, *Phys. Rev. D* **72** (2005) 115010, [hep-ph/0508020].

[159] S. Dawson, D. Fontes, C. Quezada-Calonge, and J. J. Sanz-Cillero, *Matching the 2HDM to the HEFT and the SMEFT: Decoupling and Perturbativity*, arXiv:2305.0768.

[160] V. Khersonskii, A. Moskalev, and D. Varshalovich, *Quantum Theory Of Angular Momemtum*. World Scientific Publishing Company, 1988.